Ring-opening photochemistry in cyclohexadiene derivatives:

Ultrafast dynamics in solution and model membranes

by

Brenden C. Arruda

A dissertation submitted in partial fulfillment
of the requirements for the degree of
Doctor of Philosophy
(Chemistry)
in The University of Michigan
2015

Doctoral Committee:
Professor Roseanne J. Sension, Chair
Professor Zhan Chen
Professor Eitan Geva
Professor Jennifer Ogilvie

Dedication

To my parents, Ann Marie Matthes and Edward Charles Arruda

Acknowledgements

I would like to give special thanks to my mother, father, and sister who have selflessly offered their support to me throughout my life. I could not have persevered through graduate school without your hospitality and support. You have helped me to become the best person I can be, and for that I cannot thank you enough.

I must also thank the members of the Sension Group who have contributed greatly to my knowledge and success. Thank you to Broc Smith for teaching me the ways of the laser when I joined, Ted Wiley for years of interesting conversations and speculation in lab, and Nicholas Miller for offering a helping hand whenever you saw that I needed it. I must also thank my peers outside of lab; Jessica Gagnon especially, who shared her love and support throughout my entire graduate experience.

Thank you to my committee; Prof. Julie Biteen, Prof. Jennifer Ogilvie, Prof. Zhan Chen, and Prof. Eitan Geva. Your guidance helped shape the outcome of this thesis, and guided my thinking when I needed it. Thank you to Prof. Kenneth Spears for teaching me to "do the right thing the first time." A special thank you to Prof. Roseanne Sension for showing me how to become a scientist and teaching me how to think about hard problems. I owe the success of my academic career to you.

Finally thank you to all of the support staff from 1500 that have helped me figure out what I am doing along the way. There were many of you throughout the years, and I appreciate all of the help that you offered.

TABLE OF CONTENTS

LIST OF FIGURES

LIST OF TABLES

Chapter 1

Introduction

(Text adapted from Arruda, B. C., Sension, R. J., *Phys*. *Chem*. *Chem*. *Phys*., **16**, 4439-4455)

Photochemical transformations of polyenes are ubiquitous in photobiology and are utilized in the engineering of molecular switches, molecular motors, and nanomechanical actuators.[1-6] In this introduction, we will explore a subset of photoactive polyenes based on the 1,3-cyclohexadiene (CHD) chromophore and examine the recent advances in understanding the ultrafast ring-opening and closing dynamics of systems containing this fundamental building block. Introduction of the basic structure and advances in understanding the dynamics of the CHD chromophore will lay the foundation for the thesis work presented in later chapters.

We will begin our discussion with a look at the isolated cyclohexadiene chromophore. Much theoretical and experimental work has concentrated on this simple molecule, both in solution and in the gas phase. We will then move on to consider the substituted derivatives, α-terpinene (α-TP) and α-phellandrene (α-PH), the topics of discussion in chapters 3 and 4. These molecules are studied to probe steric effects on the CHD chromophore. Finally, the biological aspects of cyclohexadiene ring-opening will be discussed in the context of 7-dehydrocholesterol (DHC) photochemistry. The light-initiated ring-opening reaction that CHD undergoes is the reaction scheme responsible for the biological synthesis of vitamin D_3 in the skin from its diene-precursor, DHC. This will lay the foundation for the experiments discussed in chapters 3 and 5. These molecules are shown in Figure 1.1.

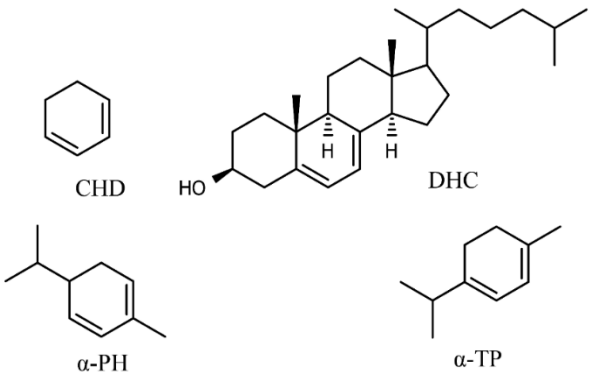

Figure 1.1: Structures of the dienes under investigation in this thesis; 1,3-cyclohexadiene (CHD), α-phellandrene (α-PH), α-terpinene (α-TP), and 7-dehydrocholesterol (DHC).

Structure and spectra of 1,3-cyclohexadiene and 1,3,5-hexatriene

The absorption spectrum of CHD shows a broad absorption peak in the UV (250 nm in gas phase and 258 nm in n-hexane) with a maximum extinction coefficient of ~3800 M^{-1} cm^{-1} in the gas phase.[7,8] Additional structure below 210 nm is characteristic of molecules containing this chromophore, but largely irrelevant to the experiments presented in later chapters of this thesis. The solution phase spectrum of CHD as well as the other compounds discussed below are shown in Figure 1.2, as all of the work presented will be in solution. Changes in the absorption maxima and peak centers with respect to the gas phase are present, but minor. McDiarmid and coworkers conducted a combined experimental and theoretical comparative investigation that showed most of the oscillator strength in the UV absorption band at 250 nm originates from the strongly allowed HOMO → LUMO excitation from the π-bonding to π *-antibonding orbital of the diene.[9,10]

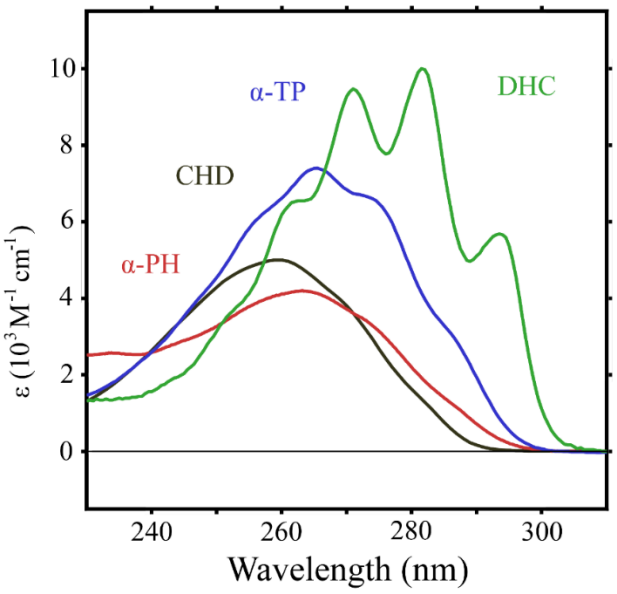

Figure 1.2: UV-Visible spectra of the dienes under consideration here. The oscillator strength of the ππ* transition is strongly dependent on the substitution on the CHD backbone. In addition, the vibronic structure in the electronic absorption is correlated with the rigidity of the chromphore and the lifetime of the S_1 state.

Excitation of CHD in the π - π * band leads to an electrocyclic ring-opening reaction, forming a HT photoproduct. The spectrum of 1,3,5-hexatriene (HT) is blue shifted with respect to CHD, and shows significant vibronic structure corresponding to the C=C stretches of the triene backbone. The potential energy surfaces that dictate the trajectory of this reaction can be described in qualitative terms using the Woodward-Hoffman rules governing the conservation of orbital symmetry, where the CHD → HT reaction represents a textbook example for the application of these rules. The participation of the dark 2A state in the ring opening was brought to light by van der Lugt and Oosterhoff, who extended the Woodward Hoffman rules to account for surface crossings.[11-14] The basic picture presented by these models is still used today to explain the progression of the CHD electrocyclic ring opening. The actual reaction coordinate, however, is somewhat more complex.

Theoretical studies have been conducted with ab initio[15,16] and complete active space self-consistent field (CASSCF)[17-21] quantum chemical methods, density functional theory5, 34[22-24] and

semiclassical[25] and quantum wavepacket dynamics[26-30] to address various aspects of the CHD excited state. A cartoon depiction derived from this body of work shows the potential energy surfaces involved in the ring-opening and ground state photoproduct in Figure 1.3. The reaction proceeds via excitation to a 1B state followed by ultrafast relaxation through a 2A dark state back to the ground state. As the molecule approaches the conical intersection leading back to the ground state, it reaches a branching point where it can either relax unreacted back to CHD, or react into the gauche-Z-gauche (gZg) hexatriene moiety as shown.

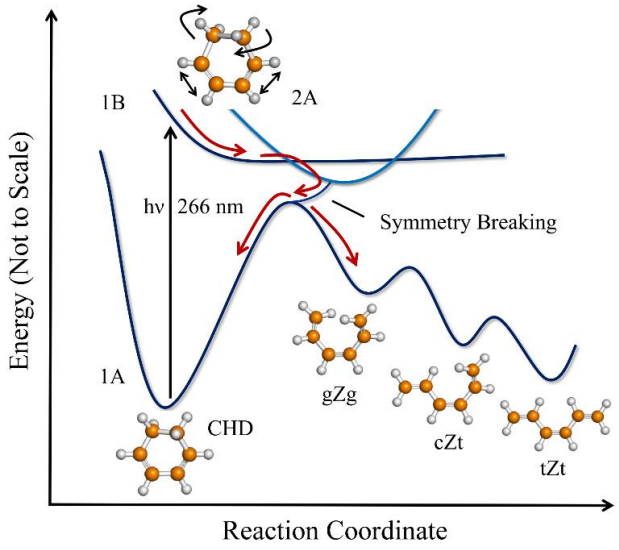

Figure 1.3: Cartoon depicting the potential energy surface for the cyclohexadiene ring-opening and the hexatriene isomerization. The excited state undergoes an ultrafast relaxation through two conical intersections on a sub 150 fs timescale.

Time-resolved studies

A variety of time-resolved spectroscopic methods have been used to study the excited state dynamics following the initial excitation into the 1B state. The fluorescence of CHD is extremely weak, with a measured quantum yield of ca. 10^{-6} in cyclohexane.[31-33] This quantum yield suggests that the excited CHD molecule remains in the Franck-Condon region of the excited state for no more than 10-20 fs. Intensity analysis of steady state resonance Raman spectra also predicts a ca.

10 fs depopulation of the initial excited state.[33,34] Experiments conducted after the development of ultrafast lasers support these early observations.

Excited state dynamics

Much of the pioneering work elucidating the time dependent decay of the CHD excited state in the gas phase comes from the transient ionization experiments of Fuss, Schmid, and Trushin in the 2000's, culminating with their most sophisticated experiment in 2009 which utilized a hollow-core argon filled fiber to generate the pump pulses, yielding 13 fs time resolution.[35-38] These measurements further refined and isolated each step in the ultrafast relaxation pathway.

Absorption of a photon at 266 nm excites the molecule from the 1A state and creates a wavepacket on the bright 1B state. This wavepacket experiences a steep potential slope on this $\pi\pi^*$ surface, and quickly decays with two distinct time constants of 21 and 35 fs. The first corresponds to the rapid movement out of the Franck-Condon region along a symmetric C=C stretch and C-C stretch, while the latter corresponds to the intersystem crossing from 1B to 2A accompanied by a ring puckering motion.[38] These assignments are based on CASSCF calculations, and are consistent with the ultrafast data. It is also possible that the time constants correspond to a different mechanism proposed by Tapavicza et al., which is discussed below.[22] This pathway is in agreement with much of the computational work, and fits with the description of the excited state shown in Figure 1.3.

Kuthirummal et al. used photoelectron spectroscopy to assign a 55 fs rise time for the 2A state, in good agreement with the results of Kosma et al.[39] Recent work by Kim et al. demonstrated the temporal location of the intersection between the 1B and 2A states effectively by utilizing light-induced conical intersections (a pump-dump technique) to modulate the ring-opening quantum yield.[18] Transitions between the ground state CHD and the 2A state are forbidden for a

one-photon interaction. Thus the time scale for effective "dumping" is also a measure of the lifetime of the 1B state. The optimum time delay of 50 fs for the 800 nm dump pulse further supports the sub-80 fs lifetime of the 1B state.

Relaxation to the 2A minimum proceeds along the C_2 symmetry-breaking coordinate through a low frequency ring-deformation mode, allowing the wavepacket to move ballistically through the 2A/1A conical intersection on an 80 fs timescale.[38-41] Such a rapid decay implies that the lifetime of the 2A state is shorter than the vibrational period of the principle vibration involved. Thus, the intersystem crossing occurs on the first pass of the wavepacket.[35] In the Landau-Zenner model[42] this would mean that the probability of crossing from the upper to lower state approaches 100%, and thus the energy gap between the states must approach $\Delta E = 0$. The presence of this crossing is predicted unambiguously by theory, and the experimental evidence lends strong support to the existence of this conical intersection.

While the probability of crossing through the conical intersection to the ground state from the 2A state in such a ballistic model would approach 100%, the branching ratio of reactive vs. unreactive trajectories in gas-phase CHD has been a subject of some controversy. According to studies by Ruan et al.[43] and by Dudek and Weber,[44] the gas phase generation of HT following excitation of CHD as observed by transient electron diffraction appears to occur with unit quantum yield. The primary evidence for this is the absence of signatures of vibrationally hot CHD. A subsequent study by Rudakov and Weber using a structure-sensitive photoionization-photoelectron technique also reports near unit quantum yield for the ring-opening reaction.[45] The technique used in this later study is blind to vibrational excitation, but the magnitude of the CHD depletion is in agreement with the expected excitation of CHD (21%) based on laser power, beam size, sample density, and the extinction coefficient.

These reports of essentially unit quantum yield for the ring-opening reaction are in contrast to most theoretical work that predicts a ca. 50% branching ratio of reactive and unreactive trajectories, [17,22,24] and with quantum yield measurements in pentane solution.[8] There is no evidence that the time scale for the ring-opening reaction is substantially different in gas and solution phases. Thus it is surprising that the solution would have such a significant influence on the reaction coordinate.

In more recent experiments, the Weber group used femtosecond hard x-ray scattering experiments to analyze the ring-opening process with both time and structure sensitivity.[46] These measurements point to the formation of E-hexatriene ca. 100 fs after excitation, which implies that the internal energy in the molecule is enough to allow for rotation about the central double bond when returning to the ground state. No measurement of direct formation of E-hexatriene has been done in solution, and UV-visible spectroscopy methods are unable to distinguish between the E and Z isomers. This experiment also revealed a quantum yield for ring-opening of less than 100%.

White et al. used a simplex-based "spectral unmixing" technique that relies on principle component analysis to identify the multiphoton time-of-flight (TOF) spectra of species present in a sample of CHD before and after femtosecond excitation at 267 nm.[47] The transient ion TOF spectra were decomposed into "endmember" spectra corresponding to CHD, CHD+ and HT with time-varying amplitudes. These results are consistent with a ca. 50% yield for HT formation. However, there is ambiguity in the analysis and unit quantum yield for HT at the longest time delay (600 fs) cannot be ruled out.

In yet another experiment that addresses the question of the quantum yield for the gas phase ring opening reaction, Kotur et al. used a closed-loop learning algorithm and UV pulse shaping to modify the yield of HT production following excitation of CHD at 260 nm.[48] The probe was

multiphoton ionization of HT 1.8 ps after the excitation pulse. This time delay avoided the influence of transients on the product signal. While it was not possible to determine absolute yields in this experiment, a ~37% increase in yield was observed for shaped excitation pulses, and sets an apparent upper limit of 73% for the quantum yield. If the initial quantum yield was near unity it would be hard to explain this increase.

Ground state relaxation

Returning to the ground state in a reactive trajectory as the HT photoproduct is not the end of the relaxation process resulting from the ultrafast ring-opening. This species reaches the ground state with a surplus of vibrational energy amounting to an internal temperature of ca. 2200 K.[49] There are three distinct conformations that the molecule can adopt. As indicated in Figure 1.3, these local minima on the HT ground state potential are identified according to the conformation about the two single bonds (cis, gauche, or trans, c, g, or t) and the central double bond (Z or E). Thus the initial photoproduct is gZg-HT according to the principle of least motion.[50] We emphasize that the initial conformation is gauche rather than cis due to steric hindrance which prevents a totally planar conformation. The gZg-HT product is helical with an angle of ca. 40° as a result of the steric interaction.[51,52] The excess vibrational energy present in HT following return to the ground state results in a highly fluxional species with rapid interchange between the various accessible conformations, as observed with time-resolved Rydberg electron binding energy spectroscopy and transient x-ray fragmentation.[41,43-45,53]

The first femtosecond time-resolved studies of CHD and HT in solution were reported by Pullen and Anderson et al., by Lochbrunner et al. and by Ohta et al. in a series of concurrent papers.[51,52,54-59] Most of these experiments used tunable single wavelength probes to span the product spectrum, although broadband spectra obtained using a UV continuum generated in

sapphire were used to calibrate the single wavelength measurements of Pullen et al. and Anderson et al.[52,54,55] Solution phase measurements have thus far been blind to the excited state dynamics of CHD as no unambiguous excited state absorption signal has been identified, and the phtoproduct absorption assigned to the gZg-HT conformer appears within an instrument limited 200 fs timescale. This is in contrast to some of the other substituted CHD molecules discussed in later chapters.

The ring-opening occurs in solution with a ca. 40% quantum yield,[8] and the vibrationally hot gZg-HT undergoes rotational isomerization from the sterically crowded gZg form to a quasi-equilibrium distribution of gZg-, cZt-, and tZt-HT. Unlike in the gas phase, HT also transfers energy to the surrounding solvent, and reaches thermal equilibrium on a picosecond time scale. As the molecule cools, the barriers become more important to the conformational distribution, and the population tends toward the most stable tZt conformer dominant at equilibrium. This vibrational cooling and thermal equilibration occurs on a solvent dependent time scale ranging from ca. 10 – 30 ps. These measurements also demonstrate that a small population of HT (~7-15%) remains kinetically trapped in the cZt form followed by relaxation to tZt-HT by a thermally activated barrier crossing on a much longer time scale of hundreds of picoseconds.[54,58,59]

Photochemistry of natural product CHD derivatives

Overview

The technical introduction to CHD and its photoproduct isomerization establishes the groundwork for many of the experiments carried out on more complicated molecules containing the CHD chromophore. The effect of steric substitution can have profound effects on the equilibrium distribution of photoproducts and the excited state pathway in many cases. This becomes relevant when trying to model more complex processes such as those found in biology

and materials science using conclusions drawn from CHD photochemistry. It is desirable from a physical chemistry perspective to have small molecule analogs that will still be amenable to advanced computational techniques while offering only minor perturbations to the dynamics of the chromophore. Model systems like this can help to guide the thinking for larger systems where other factors may confound experimental or theoretical progress. The small cyclic monoterpenes α-terpinene (α-TP) and α-phellandrene (α-PH) both contain the 1,3-cyclohexadiene chromophore, and thus their practical application in consumer products is limited by their light sensitivity and autooxidation properties. Additionally, from a physical chemistry perspective, they serve as excellent probes of the effect of steric substitution on the CHD chromophore. The alkyl groups are not extremely large (they both differ from CHD by a methyl and isopropyl group) and are situated in different locations on the ring (α-TP is 1,4- disubstituted and α-PH is 2,5- disubstituted). Because of this, the electronic structure of the CHD excited states is not greatly perturbed, but the ground state dynamics are significantly altered.

α-Terpinene and α-phellandrene photochemistry

A comprehensive study of the ground-state isomerization energetics of α-TP and its photoproduct, (Z)-2-isopropyl-5-methyl-1,3,5-hexatriene (IPMHT), has recently been undertaken by Marzec et al.[60] In this experiment, a dilute mixture of α-TP and either argon or xenon was prepared and deposited to create a cryogenic temperature (10 – 30 K) solid matrix with isolated α-TP molecules that interact solely with the host matrix atoms. The matrix was then irradiated with a UV light source to induce photochemistry in the α-TP molecules. The photoproducts were probed by steady state FTIR spectroscopy and compared with density functional theory calculations. This allowed for identification of individual conformations and rotamers of the IPMHT photoproduct.

As with CHD and HT, the ring opening of α-TP proceeds initially to the gZg conformation of IPMHT which can undergo single bond rotation to more sterically and energetically favorable conformations. Due to the presence of the bulky isopropyl group on one of the rotable bonds, the isomerization in low temperature matrices proceeds predominantly from gZg- to tZg-IPMHT (rotation of the methyl bearing bond), a rearrangement that requires activation free energy of ca. 15 kJ/mol in gas phase, and little structural rearrangement of the inert matrix.[61] Rotating to this form stabilizes the IPMHT molecule by ~5 – 10 kJ/mol depending on the orientation of the isopropyl group and the skew of the methylene groups.[60] However, the steric hindrance in the backbone precludes occupation of a tZt type arrangement for IPMHT.

A similar study was conducted on α-PH, which showed a ring-opening reaction to the photoproduct, (3Z,5E)-3,7-dimethylocta-1,3,5-triene (DOT).[62] The primary conformers found in the matrix isolated environment contained the gZg and tZg backbone, i.e., the conformations requiring the smallest changes in the DOT backbone and the local environment of the matrix itself. In a fluid environment or in the gas phase, however, the tZt-DOT isomer is expected to dominate the population, as it is the energetic minimum by ~10 – 20 kJ/mol. The calculated barrier for rotating the methylene group from gZg-DOT to tZg-DOT is only 5 kJ/mol, while the forward reaction of gZg to gZt or either intermediate isomer to the final tZt isomer are closer to 10 kJ/mol.[63]

The studies by Marzec et al. present the structural and thermodynamic properties of the open ring photoproducts, and use a conformation-sensitive analysis to show that the photochemistry of α-TP and α-PH consist exclusively of ring-opening, with no signatures of a "dewar" form that can be found in other ring-opening reactions, such as that of α-pyrone.[62,64] These studies also highlight the differences in the potential energy surfaces of the ground state

photoproducts. Due to the location of the steric groups, the α-PH photoproduct can isomerize to the tZt form (much like HT), while the α-TP photoproduct is sterically restricted to the tZg isomer.

Time resolved studies

Excited state dynamics

The first comparative study of the excited state ring-opening of CHD, α-TP, and α-PH was reported in 2001 by Garavelli et al.[36] Nonresonant multiphoton dissociative ionization was used to probe the excited state dynamics following excitation at 267 nm. Three time constants were identified for each species: 10 ± 5 fs, 43 ± 3 fs, and 77 ± 7 fs for CHD, 40 ± 5 fs, 59 ± 4 fs, and 86 ± 6 fs for α-TP, and 10 ± 5 fs, 66 ± 4 fs, and 97 ± 6 fs for α-PH. Subsequent work refined the time constants for CHD to 21 fs, 35 fs, and 80 fs.58 These times are interpreted as (1) movement out of the Franck-Condon region, (2) movement around the 1B/2A avoided crossing, and (3) movement through the 2A/1A conical intersection onto the ground state surface. The physical explanation of different time constants in the transient ionization work was assigned and justified by extensive CASSCF calculations on the excited state potential in order to describe the vibrational motion the chromophore undergoes to dissipate the excess energy from the absorbed photon.

The initial motion out of the Franck-Condon region is along a C=C stretch coordinate that incorporates the substituted 1 and 4 position carbons in α-TP. The four-fold increase in the lifetime of the Franck-Condon wavepacket was explained by a mass effect of the 1,4-subtituents on the CHD backbone. The substitution effectively increases the reduced mass for the vibrational mode carrying the wavepacket away from the initially prepared geometry. This also correlates with the observation of a stronger vibronic progression in the steady state UV-Vis of α-TP compared with CHD and α-PH. The large steroid ring in 7-dehydrocholesterol further rigidifies the chromophore

and slows the Franck-Condon dynamics, resulting in the most prominent vibronic structure as seen in Figure 1.2.

In support of this notion, the 2,5-disubstituted α-PH does not show any time lengthening relative to CHD in this observation window, indicating that the 2 and 5 positions in the ring are not significantly involved in the initial motion. However, in the subsequent step of breaking the C5-C6 σ-bond, α-PH has a time constant of 1.5 times that of CHD.[36] The mass effect can be used to explain this result as well, since α-PH has an isopropyl substitution on C5. It should be noted that this study provides some validity to the assumption that although alkyl substitution modulates the 1A/1B energy gap, it does not have a significant effect on the topology of the excited state surfaces. That is, the dynamics are governed by similar molecular motions and driving forces in all cases.

The photophysics of α-TP and α-PH have also been investigated in alkane and alcohol solvents. Moran and coworkers used ultrafast 2D spectroscopy in the UV to study the excited state dynamics of CHD and α-TP concurrently with the experiments described in this thesis.[65,66] Two dimensional photon echo (2DPE) spectroscopy provides all the time resolution of transient absorption measurements but with an additional dimension of resolution along the pump frequency. Correlating the excitation and detection frequencies in 2DUV is analogous to 2D nuclear magnetic resonance methods that have been used for decades.[67] Important technological hurdles including minimizing pulse duration and maximizing bandwidth have limited the use of 2DPE in the UV, but are recently being overcome with new methods for generating the UV pulses. The technique is only in its infancy, but has already provided some interesting new information on the CHD and α-TP ring-opening processes.

The anisotropy of the α-TP excited state measured by West et al. shows non-exponential behavior at short timescales (<150 fs).[66] This work shows the inseparability of the electronic and nuclear degrees of freedom in the evolution of the α-TP excited state. This non-exponential relaxation can also be isolated in the absorption spectrum by fitting the spectrum within the framework of optical response including vibronic transitions.[66,68,69]

West et al. point out that one should not expect dynamics occurring on such short timescales of a few hundred femtoseconds to be exponential. In fact, exponential relaxation is a consequence of assuming so-called "Markovian" dynamics in which the timescales of the bath in a quantum open system are much shorter than the timescales of the system.[68] Such is not the case for these excited state electrocyclic ring-opening reactions in solution in which the nuclei experience steep potential gradients and the electronic states exhibit multiple points of degeneracy (conical intersections) which guide the internal conversion and vibrational relaxation. A system of this type is governed by non-Markovian dynamics in which relaxation timescales are frequently inadequately described using exponentials.

These key works on α-TP and α-PH address both the excited state dynamics, and equilibrium thermodynamics of the photoproducts. They are complementary to the work presented in this thesis where different aspects of the excited state spectra are observed and the conformational dynamics of the ground state photoproducts are fully characterized.

Photochemistry of 7-dehydrocholesterol

A more complex and relevant compound that undergoes ring-opening is found in 7-dehydrocholesterol (DHC), a precursor in the biological synthesis of vitamin D_3. Polyene photochemistry of DHC has been well studied since the 1960's and Havinga's pioneering work on its photochemical interconversion with the various conformations of subsequent

photoproducts.[70,71] The primary photobiology of DHC is contained in the light-activated ring-opening reaction of the cyclohexadiene chromophore embedded in the steroid skeleton. Much like the development of the ring-opening of CHD, the understanding of DHC photochemistry has been aided immensely by ultrafast spectroscopic measurements and simulations with atomic level resolution.

Excited state properties of 7-dehydrocholesterol

Although the active chromophore of DHC is a substituted 1,3-cyclohexadiene ring, there are a number of features that contrast this molecule with the small molecules described up to this point. These include the presence of an OH group and the rigidity of the rings on either side of the CHD chromophore. The excited state lifetime of DHC is substantially longer than that of the isolated CHD molecule or either of the small substituted natural products a-TP or a-PH. Recent fluorescence measurements of DHC in room temperature solution reported a quantum yield of $(3 \pm 1) \times 10^{-4}$ in 2-butanol and $(2 \pm 1) \times 10^{-4}$ in heptane.[72,73] When the Strickler-Berg formula is used to estimate the radiative lifetime of DHC, these quantum yields are consistent with excited state lifetimes of 1 to 2 ps.[72]

Like α-TP, DHC exhibits a strong excited state absorption (ESA) in the visible region of the spectrum, though a clear contribution from ESA is also observed in the UV spectral region.[61,73-75] The most comprehensive experimental study on the excited state evolution of DHC was conducted by Tang et al. This study focused on the broad excited state absorption spanning the region from 400 nm to 800 nm, and implemented the first full spectral and temporal analysis of DHC.

The decay of the excited state absorption does not fit a single exponential, but is well modelled as a biexponential decay.[73] The time constants and amplitudes are weakly dependent on

the solvent with a fast component of ~0.4 to 0.65 ps and a slow component of 1.0 to 1.8 ps. Both components contribute significantly to the decay of the integrated intensity of the ESA band, ranging from ratios of 65:35 fast to slow in heptane to 30:70 in methanol. The other alcohols and alkanes investigated fall between these limits.

The ~1 ps timescale for ring-opening was recently corroborated by Meyer-Ilse et al. using ultrafast circular dichroism (CD) spectroscopy.[76] The ring-opening from DHC to previtamin D_3 (Pre) is accompanied by the loss of two chiral centers, resulting in a change in the magnitude of the circular dichroism signal. The transient CD probed at 285 and 300 nm shows an exponential timescale of 1–2 ps, in good agreement with the transient absorption measurements. Since the CD signal is a direct probe of the change from closed to open-ring form, this allows for a confident assignment of this time constant. The combination of time-resolved instrumentation with conformation and stereo-sensitive techniques is a powerful tool for the elucidation of reaction mechanisms in which the number of chiral centers in a molecule changes.

The weak dependence of the excited state decay on macroscopic properties such as shear viscosity or polarity and microscopic properties like hydrogen bonding capacity and solvent packing indicates only minor spatial rearrangement of the steroid skeleton on the excited electronic state. The temperature dependence of the decay was used to estimate effective barriers for internal conversion back to the ground state of ~4–10 kJ mol^{-1}.[73] Much of the barrier is solvent induced as initially proposed by Nakashima et al., but a ca. 2 kJ mol^{-1} intrinsic barrier remains after the influence of the environment is taken into account.[77]

The biexponential nature of the ESA decay can be explained within the context of two different models; sequential internal conversion between two distinct excited states, or rapid branching along two distinct pathways followed by parallel decay of these two populations. The

parallel model is more consistent with the experimental data,[73,78] and is supported by a recent computational study on Pro.[22,24]

Tapavicza et al. used a TD-DFT surface hopping method to study the excited state reaction progression and ground state photoproduct distribution for DHC. This comprehensive study represents one of the most sophisticated computational treatments of the DHC–Pre system.[22,24] The simulations of DHC suggest that reactive trajectories return to the ground state with a time constant of 267 fs while unreactive trajectories return to the ground state almost a factor of two slower (489 fs). The calculated quantum yield for the ring-opening reaction is 0.62, compared with the experimental value of 0.34 measured in ethanol.[79] Both reactive and unreactive trajectories in the simulation undergo an internal conversion from the bright 1B state to the dark 2A state, similar to the curves sketched in Figure 1.3**.**

Ground state isomerization and previtamin D_3 photochemistry

The triene previtamin D_3 (Pre) adopts two distinct conformations on the ground state potential consisting of gZg-Pre and tZg-Pre due to steric barriers similar to those in the α-TP photoproduct (IPMHT) discussed above. Upon reaching the ground state after photoexcitation, Pre can form solely in the gZg conformation. Relaxation from this hot photoproduct results in an equilibrium distribution dominated by the tZg-Pre rotamer. Tapavicza et al. demonstrate this in their ground state equilibrium distributions of Pre, showing multiple minima on the ground state potential.[22] The distribution at high temperature is somewhat delocalized around the gZg and tZg rotamers, and at lower temperatures, significantly favors tZg. These equilibrium distributions serve as a useful tool for interpreting much of the Pre experimental data, but powerful computational techniques and accelerated sampling molecular dynamics methods will be required

to fully understand the ground state hot photoproduct relaxation. These simulations provide corroborating evidence for the conclusions drawn from the experiments presented in chapter 3.

Acknowledgements

This work was supported in part by NSF Grants CHE-0718219 and CHE-1150660.

References

(1) Chopade, P. R.; Louie, J. *Advanced Synthesis & Catalysis* **2006**, *348*, 2307-2327.

(2) Milder, M. T. W.; Areephong, J.; Feringa, B. L.; Browne, W. R.; Herek, J. L. *Chem. Phys. Lett.* **2009**, *479*, 137-139.

(3) Conyard, J.; Addison, K.; Heisler, I. A.; Cnossen, A.; Browne, W. R.; Feringa, B. L.; Meech, S. R. *Nat. Chem.* **2012**, *4*, 547-551.

(4) Irie, M. *Chemical Reviews* **2000**, *100*, 1685-1716.

(5) Irie, M.; Kobatake, S.; Horichi, M. *Science* **2001**, *291*, 1769-1772.

(6) Kobatake, S.; Takami, S.; Muto, H.; Ishikawa, T.; Irie, M. *Nature* **2007**, *446*, 778-781.

(7) Minnaard, N. G.; Havinga, E. *Recueil Des Travaux Chimiques Des Pays-Bas-Journal of the Royal Netherlands Chemical Society* **1973**, *92*, 1179-1188.

(8) Minnaard, N. G.; Havinga, E. *Recueil Des Travaux Chimiques Des Pays-Bas-Journal of the Royal Netherlands Chemical Society* **1973**, *92*, 1315-1320.

(9) McDiarmid, R.; Sabljic, A.; Doering, J. P. *J. Chem. Phys.* **1985**, *83*, 2147-2152.

(10) Merchan, M.; Serrano-Andres, L.; Slater, L. S.; Roos, B. O.; McDiarmid, R.; Xing, Y. *J. Phys.Chem. A* **1999**, *103*, 5468-5476.

(11) Woodward, R. B.; Hoffmann, R. *Angew. Chem. Int. Ed.* **1969**, *8*, 781-853.

(12) Woodward, R. B.; Hoffman, R. *The Conservation of Orbital Symmetry*; VCH: Weinheim, 1970.

(13) van der Lugt, W. T. A. M.; Oosterhoff, L. J. *Chemical Communications (London)* **1968**, 1235-1236.

(14) Van der Lugt, W. T. A. M.; Oosterhoff, L. J. *J. Am. Chem. Soc.* **1969**, *91*, 6042-6049.

(15) Share, P. E.; Kompa, K. L.; Peyerimhoff, S. D.; Vanhemert, M. C. *Chem*. *Phys*. **1988**, *120*, 411-419.

(16) Tamura, H.; Nanbu, S.; Nakamura, H.; Ishida, T. *Chem*. *Phys*. *Lett*. **2005**, *401*, 487-491.

(17) Tamura, H.; Nanbu, S.; Ishida, T.; Nakamura, H. *J*. *Chem*. *Phys*. **2006**, *124*, 084313.

(18) Kim, J.; Tao, H. L.; White, J. L.; Petrovic, V. S.; Martinez, T. J.; Bucksbaum, P. H. *J*. *Phys*.*Chem*. *A* **2012**, *116*, 2758-2763.

(19) Celani, P.; Ottani, S.; Olivucci, M.; Bernardi, F.; Robb, M. A. *J*. *Am*. *Chem*. *Soc*. **1994**, *116*, 10141-10151.

(20) Celani, P.; Bernardi, F.; Robb, M. A.; Olivucci, M. *J*. *Phys*.*Chem*. **1996**, *100*, 19364-19366.

(21) Garavelli, M.; Celani, P.; Fato, M.; Bearpark, M. J.; Smith, B. R.; Olivucci, M.; Robb, M. A. *J*. *Phys*.*Chem*. *A* **1997**, *101*, 2023-2032.

(22) Tapavicza, E.; Meyer, A. M.; Furche, F. *Phys*. *Chem*. *Chem*. *Phys*. **2011**, *13*, 20986-20998.

(23) Wanko, M.; Garavelli, M.; Bernardi, F.; Niehaus, T. A.; Frauenheim, T.; Elstner, M. *J*. *Chem*. *Phys*. **2004**, *120*, 1674-1692.

(24) Tapavicza, E.; Bellchambers, G. D.; Vincent, J. C.; Furche, F. *Phys*. *Chem*. *Chem*. *Phys*. **2013**, *15*, 18336-18348.

(25) Li, A. Y.; Yuan, S. A.; Dou, Y. S.; Wang, Y. B.; Wen, Z. Y. *Chem*. *Phys*. *Lett*. **2009**, *478*, 28-32.

(26) Hofmann, A.; de Vivie-Riedle, R. *J*. *Chem*. *Phys*. **2000**, *112*, 5054-5059.

(27) Hofmann, A.; Kurtz, L.; de Vivie-Riedle, R. *Appl*. *Phys*. *B* **2000**, *71*, 391-396.

(28) Hofmann, A.; de Vivie-Riedle, R. *Chem*. *Phys*. *Lett*. **2001**, *346*, 299-304.

(29) Kurtz, L.; Hofmann, A.; de Vivie-Riedle, R. *J*. *Chem*. *Phys*. **2001**, *114*, 6151-6159.

(30) Schonborn, J. B.; Sielk, J.; Hartke, B. *J*. *Phys*.*Chem*. *A* **2010**, *114*, 4036-4044.

(31) Lawless, M. K.; Wickham, S. D.; Mathies, R. A. *Accounts of Chemical Research* **1995**, *28*, 493-502.

(32) Reid, P. J.; Lawless, M. K.; Wickham, S. D.; Mathies, R. A. *J*. *Phys*.*Chem*. **1994**, *98*, 5597-5606.

(33) Trulson, M. O.; Dollinger, G. D.; Mathies, R. A. *J*. *Am*. *Chem*. *Soc*. **1987**, *109*, 586-587.

(34) Trulson, M. O.; Dollinger, G. D.; Mathies, R. A. *J*. *Chem*. *Phys*. **1989**, *90*, 4274-4281.

(35) Fuss, W.; Schmid, W. E.; Trushin, S. A. *J*. *Chem*. *Phys*. **2000**, *112*, 8347-8362.

(36) Garavelli, M.; Page, C. S.; Celani, P.; Olivucci, M.; Schmid, W. E.; Trushin, S. A.; Fuss, W. *J*. *Phys*.*Chem*. *A* **2001**, *105*, 4458-4469.

(37) Fuss, W.; Schmid, W. E.; Trushin, S. A.; Billone, P. S.; Leigh, W. J. *Chemphyschem* **2007**, *8*, 592-598.

(38) Kosma, K.; Trushin, S. A.; Fuss, W.; Schmid, W. E. *Phys*. *Chem*. *Chem*. *Phys*. **2009**, *11*, 172-181.

(39) Kuthirummal, N.; Rudakov, F. M.; Evans, C. L.; Weber, P. M. *J*. *Chem*. *Phys*. **2006**, *125*.

(40) Bucksbaum, P. H.; Petrovic, V. *Farad*. *Disc*. **2013**, *In Press*.

(41) Petrovic, V. S.; Siano, M.; White, J. L.; Berrah, N.; Bostedt, C.; Bozek, J. D.; Broege, D.; Chalfin, M.; Coffee, R. N.; Cryan, J.; Fang, L.; Farrell, J. P.; Frasinski, L. J.; Glownia, J. M.; Guhr, M.; Hoener, M.; Holland, D. M. P.; Kim, J.; Marangos, J. P.; Martinez, T.; McFarland, B. K.; Minns, R. S.; Miyabe, S.; Schorb, S.; Sension, R. J.; Spector, L. S.; Squibb, R.; Tao, H.; Underwood, J. G.; Bucksbaum, P. H. *Physical Review Letters* **2012**, *108*.

(42) Klessinger, M.; Michl, J. *Excited states and photochemistry of organic molecules*; VCH: New York, 1995.

(43) Ruan, C. Y.; Lobastov, V. A.; Srinivasan, R.; Goodson, B. M.; Ihee, H.; Zewail, A. H. *Proc*. *Natl*. *Acad*. *Sci*. **2001**, *98*, 7117-7122.

(44) Dudek, R. C.; Weber, P. M. *J*. *Phys*.*Chem*. *A* **2001**, *105*, 4167-4171.

(45) Rudakov, F.; Weber, P. M. *Chem*. *Phys*. *Lett*. **2009**, *470*, 187-190.

(46) Minitti, M. P.; Budarz, J. M.; Kirrander, A.; Robinson, J. S.; Ratner, D.; Lane, T. J.; Zhu, D.; Glownia, J. M.; Kozina, M.; Lemke, H. T.; Sikorski, M.; Feng, Y.; Nelson, S.; Saita, K.; Stankus, B.; Northey, T.; Hastings, J. B.; Weber, P. M. *Physical Review Letters* **2015**, *114*.

(47) White, J. L.; Kim, J.; Petrovic, V. S.; Bucksbaum, P. H. *J*. *Chem*. *Phys*. **2012**, *136*, 054303.

(48) Kotur, M.; Weinacht, T.; Pearson, B. J.; Matsika, S. *J*. *Chem*. *Phys*. **2009**, *130*, 134311.

(49) Harris, D. A.; Orozco, M. B.; Sension, R. J. *J*. *Phys*.*Chem*. *A* **2006**, *110*, 9325-9333.

(50) Hine, J. *J*. *Org*. *Chem*. **1966**, *31*, 1236-&.

(51) Pullen, S.; Walker, L. A.; Donovan, B.; Sension, R. J. *Chem*. *Phys*. *Lett*. **1995**, *242*, 415-420.

(52) Pullen, S. H.; Anderson, N. A.; Walker, L. A.; Sension, R. J. *J*. *Chem*. *Phys*. **1997**, *107*, 4985-4993.

(53) Cardoza, J. D.; Dudek, R. C.; Mawhorter, R. J.; Weber, P. M. *Chem*. *Phys*. **2004**, *299*, 307-312.

(54) Anderson, N. A.; Pullen, S. H.; Walker, L. A.; Shiang, J. J.; Sension, R. J. *J*. *Phys*.*Chem*. *A* **1998**, *102*, 10588-10598.

(55) Pullen, S. H.; Anderson, N. A.; Walker, L. A.; Sension, R. J. *J*. *Chem*. *Phys*. **1998**, *108*, 556-563.

(56) Anderson, N. A.; Durfee, C. G.; Murnane, M. M.; Kapteyn, H. C.; Sension, R. J. *Chem*. *Phys*. *Lett*. **2000**, *323*, 365-371.

(57) Lochbrunner, S.; Fuss, W.; Schmid, W. E.; Kompa, K. L. *J*. *Phys*.*Chem*. *A* **1998**, *102*, 9334-9344.

(58) Ohta, K.; Naitoh, Y.; Saitow, K.; Tominaga, K.; Hirota, N.; Yoshihara, K. *Chem*. *Phys*. *Lett*. **1996**, *256*, 629-634.

(59) Ohta, K.; Naitoh, Y.; Tominaga, K.; Hirota, N.; Yoshihara, K. *J*. *Phys*.*Chem*. *A* **1998**, *102*, 35-44.

(60) Marzec, K. M.; Reva, I.; Fausto, R.; Malek, K.; Proniewicz, L. M. *J*. *Phys*.*Chem*. *A* **2010**, *114*, 5526-5536.

(61) Arruda, B. C.; Peng, J.; Smith, B.; Spears, K. G.; Sension, R. J. *J*. *Phys*.*Chem*. *B* **2013**, *117*, 4696-4704.

(62) Marzec, K. M.; Reva, I.; Fausto, R.; Proniewicz, L. M. *J*. *Phys*.*Chem*. *A* **2011**, *115*, 4342-4353.

(63) Arruda, B. C.; Smith, B.; Spears, K. G.; Sension, R. J. *Farad*. *Disc*. **2013**, *163*, 159-171.

(64) Breda, S.; Reva, I.; Lapinski, L.; Fausto, R. *Phys*. *Chem*. *Chem*. *Phys*. **2004**, *6*, 929-937.

(65) West, B. A.; Moran, A. M. *J*. *Phys*. *Chem*. *Lett*. **2012**, *3*, 2575-2581.

(66) West, B. A.; Molesky, B. P.; Montoni, N. P.; Moran, A. M. *New Journal of Physics* **2013**, *15*, 025007.

(67) Mukamel, S.; Abramavicius, D.; Yang, L.; Zhuang, W.; Schweigert, I. V.; Voronine, D. V. *Accounts of Chemical Research* **2009**, *42*, 553-562.

(68) Nitzan, A. *Chemical Dynamics in Condensed Phases: Relaxation, Transfer, and Reactions in ondensed Molecular Systems*; Oxford University Press Inc.: New York, 2006.

(69) Mukamel, S. *Principles of Nonlinear Optical Spectroscopy*; Oxford University Press Inc.: New York, 1999.

(70) Havinga, E.; Dekock, R. J.; Rappoldt, M. P. *Tetrahedron* **1960**, *11*, 276-284.

(71) Havinga, E.; Schlatmann, J. *Tetrahedron* **1961**, *16*, 146-&.

(72) Strickler, S. J.; Berg, R. A. *J*. *Chem*. *Phys*. **1962**, *37*, 814-822.

(73) Tang, K.-C.; Rury, A.; Orozco, M. B.; Egendorf, J.; Spears, K. G.; Sension, R. J. *J*. *Chem*. *Phys*. **2011**, *134*, 104503.

(74) Anderson, N. A.; Shiang, J. J.; Sension, R. J. *J*. *Phys*.*Chem*. *A* **1999**, *103*, 10730-10736.

(75) Anderson, N. A.; Sension, R. J. In *Liquid Dynamics: Experiment, Simulation, and Theory*; Fourkas, J. T., Ed.; American Chemical Society: Washington, D.C., 2002; Vol. 820, p 148-158.

(76) Meyer-Ilse, J.; Akimov, D.; Dietzek, B. *J*. *Phys*. *Chem*. *Lett*. **2012**, *3*, 182-185.

(77) Nakashima, N.; Meech, S. R.; Auty, A. R.; Jones, A. C.; Phillips, D. *J*. *Photochem*. **1985**, *30*, 207-214.

(78) Tang, K. C.; Sension, R. J. *Farad*. *Disc*. **2011**, *153*, 117-129.

(79) Jacobs, H. J. C.; Gielen, J. W. J.; Havinga, E. *Tetrahedron Letters* **1981**, *22*, 4013-4016.

Chapter 2

Experimental background

Ultrafast broadband UV-Visible transient absorption (TA) is the primary technique used to investigate the photochemical processes discussed in this thesis. This technique employs optically compressed amplified laser pulses which are used to both stimulate optical transitions and to probe the resulting chemical dynamics in a pump-probe geometry. The observable used to quantify these dynamics are changes in absorption (ΔA) of the probe between the steady state population and the pumped non-equilibrium ensemble. The quantity ΔA is given by

$$\Delta A = \log\left(\frac{I_{pump-on}}{I_0}\right) - \log\left(\frac{I_{pump-off}}{I_0}\right) \quad (1)$$

Where I_0 is the reference probe spectrum, $I_{pump\text{-}on}$ is the probe intensity after the sample with the pump pulse present, and $I_{pump\text{-}off}$ is the probe intensity without the pump pulse. Assuming that the reference spectrum I_0 is the same over the course of a spectrometer integration cycle, the equation can be reduced to

$$\Delta A = \log\left(\frac{I_{pump-on}}{I_{pump-off}}\right) \quad (2)$$

Multiple iterations of laser setups have been utilized to collect the data in the various experiments discussed herein, but the instrument capabilities as far as optical bandwidth and time resolution were similar.

Optics frontend and chirped pulse amplification

Ultrafast methods employing continuum generation and other high order non-linear processes require laser pulses with extremely high energy densities.[1] The optics chain begins with a titanium doped sapphire (Ti:Sapph) modelocked oscillator optimized to support laser modes centered at 800 nm with a full width at half maximum (FWHM) of 30nm. The repetition rate of this cavity when operating in pulsed mode is approximately 88 MHz, while the laser pulses can be < 50 fs. An optical stretcher imparts negative dispersion to the pulses, and stretches them in time to a duration of typically ~100 ps. Stretching the laser pulses is necessary for the ensuing amplification process so that the peak intensity does not reach the damage threshold of the amplification medium.

A Pockels cell, or pulse picker, is used to down-convert the repetition rate of the pulses from 88 MHz to 1 kHz to allow for synchronization with a flash lamp or diode YLF pump laser. The 527 nm YLF pumps a Ti:Sapph crystal into an excited electronic state. When the 800 nm seed beam is overlapped with the pump in space and time in the crystal, it can induce stimulated emission from the crystal, and produce gain in the seed pulse. The duration of the pump laser pulse (~ 250 ns) is enough to support 8 passes of the seed through the crystal, leading to gains as high as 10^9. These amplified pulses are recompressed in a grating compressor that counteracts the dispersion imparted by the stretcher and compensates for dispersive optics in the beam path of the experiment to minimize the pulse duration at the sample. A block diagram indicating the major changes to the laser pulse as it traverses these optical systems is shown in Figure 2.1.

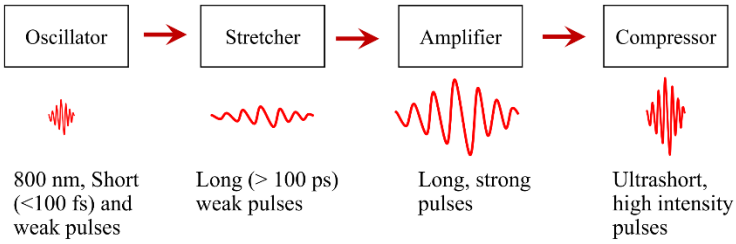

Figure 2.1: Block diagram depicting the general function of the components in the front end amplification systems.

Broadband transient absorption experiment

The pump and probe arm are treated separately, because they have different energy requirements and undergo different non-linear processes. The pump arm is frequency tripled to 266 nm in a series of second harmonic generation (SHG) followed by third harmonic generation (THG). This UV pulse typically arrives at the sample with a duration on the order of 100 – 200 fs depending on the dispersive optics between the 266 generation and the sample. These optics could include a half-wave plate for changing the polarization of the beam and a focusing lens.

The probe pulse is used to generate a white light continuum through self-phase modulation in a CaF_2 crystal.[2] When 800 nm light is used, the continuum can span ~330 nm to 900 nm. More typically, a usable spectrum from 360 nm to 750 nm was achievable. In order to span the UV part of the spectrum (270 – 650 nm), the 800 nm pulses can be frequency doubled prior to continuum generation. Typically the higher frequency portion of the continuum is more stable, but because the two continuua contain a large region of overlap, experiments using the different setups can be scaled and combined when there are overlapping signals.

Time dynamics are acquired by delaying the probe pulses with respect to the pump. The probe beam is incident on an uncoated gold retro-reflector mounted on a Newport ILS150PP translational stage. The time delay between the pump and probe pulses can be changed by varying the path-length of the probe with a minimum delay time of 13 fs. A full data set is a 3

dimensional construct with time points along one axis and wavelength along the other. The values in this grid correspond to the difference in absorption of the probe when the pump is present vs. when it is blocked by an optical chopper. The experimental portion of the TA system is depicted in Figure 2.2 below.

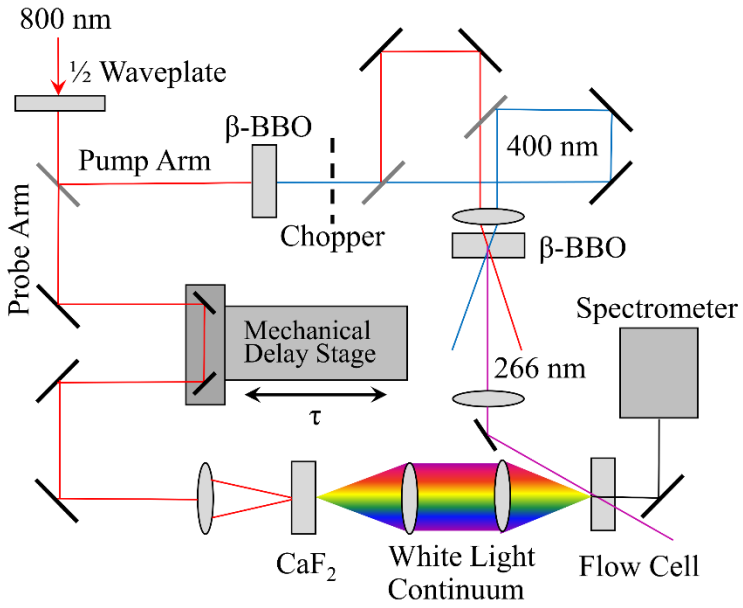

Figure 2.2: Cartoon diagram of the experimental setup. The pump-arm consists of the frequency tripled 266 nm pulse, while the probe is a white light continuum.

Electronics and triggering

The core of the triggering that synchronizes the electronics with the laser pulses relies on the mode-locked operation of the oscillator. The 88 MHz beam irradiates a photodiode to produce an electronic pulse train that is converted to a 1 kHz master signal by a Medox Pockels Cell Timer and Driver. This 1 kHz trigger signal sets the absolute t_0 for a Stanford Research Systems DG535 four channel digital delay / pulse generator. In the frontend, the Stanford delay generator triggers the pockels cell and the YLF pump laser for the amplifier. The phase of the triggers are set so that the two laser pulses arrive in the gain medium synchronously.

Due to the digitization speed of the spectrometers used for the work summarized in chapters 3 and 4, the spectrometer had to integrate over three laser pulses per spectrum. This "3-on, 3-off" operational scheme added significant time to each experiment, operating at less than 1/3 of the theoretical TA data collection efficiency of a 1 kHz laser system. The fastest the laser system could operate is acquisition of 1 TA spectrum / 2 ms, but this is limited in this instance by the speed of the spectrometer (1 TA spectrum / 6 ms) and the USB transfer rate between spectrometer and computer. In order to achieve signal-to-noise of an acceptable level in a typical experiment, 400 difference spectra (800 total absorption spectra between pump-on and pump-off) are averaged, and ca. 300 individual time points are collected at various time delays that characterize the system. A sample would typically be exposed to the laser radiation for roughly 3 hours over the course of an experiment. Minimizing the exposure time is critical in the case of samples that undergo degradation over the timescale of hours such as the liposome samples discussed in Chapter 5.

The ideal operation of the laser system is "1-on, 1-off", where each of the 400 difference spectra at a time point consists of one probe spectrum with the pump on, and one probe spectrum with the pump off. In this mode of operation, a single pulse can saturate the spectrometer, and the contribution of shot-to-shot noise in the probe spectrum is reduced.[1-4] Referring back to equations 1 and 2, the best referencing is possible when $I_{pump\text{-}on}$ and $I_{pump\text{-}off}$ are acquired with a probe spectrum that is as similar as possible. Due to the high amount of correlation between successive pulses, this condition is achieved by constructing TA spectra using back-to-back laser shots.[1] In addition, the efficiency of the system can approach the theoretical maximum for the 1 kHz repetition rate. This mode of operation was implemented into the laser system with the purchase of an Avantes AvaSpec FAST spectrometer. Significant changes in the triggering

scheme and LabVIEW code for the experiment were made and are described below. Overall, these improvements and their compounding time-savings allow for an increase in the data collection rate of approximately 675%. Currently, the data collection rate is limited by the USB transfer rate between spectrometer and computer, and the delay stage movement speed.

In the previous experimental setup, the delay generator coordinated the acquisition of spectra by externally triggering the chopper. The optical chopper contains a photodiode in the base that is used to generate a 50:50 duty cycle square wave as the blade spins. The voltage corresponds to the chopper status; high for pump beam "unblocked" and low for "blocked." This trigger fed a frequency doubling circuit that converted the 166 Hz chopper output to a 333 Hz electronic pulse (2f pulse). The chopper status square wave was fed to a data acquisition (DAQ) card in the computer and saved as an array, while the 2f signal triggered the acquisition in the spectrometer. The spectrometer would integrate over 3 laser pulses, and the integrated intensity was stored to internal memory. Once the desired number of spectra was collected (800 total spectra), they were transferred via USB to the computer. The LabVIEW software would compare the chopper status array with the index of each spectrum to determine of it was taken with the pump on or off. This is the so-called "3-on, 3-off" chopping scheme, in which the digitization speed of the spectrometer limits the collection rate.

Implementation of the new spectrometer capable of 1 kHz digitization rate greatly streamlines the triggering and software. The chopper produces a 500 Hz square wave in this operation to trigger the spectrometer. Spectra are automatically recorded to internal memory at the laser repetition rate of 1 kHz. The integration cycle begins on the rising edge of the chopper status, and so the sorting of "pump-on" and "pump-off" probe spectra is automatic. No frequency doubling box or recording of the chopper status in software is necessary, eliminating

the need for a DAQ card. Using this "1-on, 1-off" chopping scheme allows for the rapid acquisition of data on precious or fragile samples. These upgrades were necessary for the experiments discussed in Chapter 5.

Sample preparation

The TA instrument operates with a flow cell apparatus for the sample reservoir. Flowing the sample can eliminate photoproduct buildup in the beam path that could contaminate the sample during long experiments. For bulk samples, the optical density at the pump wavelength should be maximized, while maintaining an excitation probability on the order of 10%. This reduces the magnitude of non-linear optical signals from sample interactions with the laser pulses. In general, 20 mL of sample volume is sufficient to eliminate photoproduct buildup.

Liposome samples discussed in Chapter 5 are created by a standard sonication preparation method.[5] The appropriate molar ratios of 1,2-dipalmitoyl-sn-glycero-3-phosphocholine (16:0 PC, DPPC) and sterol (7-dehydrocholesterol or cholesterol) are co-dissolved in a small volume of chloroform. The solvent is rotovaped off at 323 K, leaving a lipid film on the round bottom flask. Phosphate buffered saline (pH 7.4) is added at 323 K and the sample is agitated at this temperature (above the chain melting phase transition for DPPC[6]) for 1 hour. The final concentration of sterol is typically 2 – 3 mM depending on the desired loading. The rehydrated suspension consists of large multiwalled vesicles that are broken up into liposomes by sonication until the scattering background is minimized.

Steady state spectroscopy

Steady state photolysis experiments were conducted using the unfiltered output of a mercury arc lamp (7A, 125 V power supply) and a Shimadzu UV-2401pc UV-VIS spectrometer with a wavelength range of 190 nm to 1100 nm and a resolution of 0.1 nm. Fluorescence

measurements were performed using a Jasco FP-6500 Spectrofluoremeter at an optical density of < 0.4 in a 1 cm quartz cell.

Computational methods

Optimized structures and single point energies are calculated using a time-dependent density functional theory (TD-DFT) approach in the Gaussian03 software package.[7] All calculations discussed in this thesis employ the 6-311++G(d,p) basis set and the B3LYP density functional. Transition state optimizations are conducted using the Synchronous Transit-Guided Quasi-Newton (STQN) method.[8] The correct transition state is verified using the results of frequency calculations to ensure that only one imaginary (negative) frequency corresponding to the reactive coordinate is present. Unless otherwise noted, all calculations are done in the gas-phase, because the properties of the dienes studied in this thesis do not tend to depend on the solvent environment.

References

(1) Megerle, U.; Pugliesi, I.; Schriever, C.; Sailer, C. F.; Riedle, E. *Appl*. *Phys*. *B* **2009**, *96*, 215-231.

(2) Bradler, M.; Baum, P.; Riedle, E. *Appl*. *Phys*. *B* **2009**, *97*, 561-574.

(3) Schriever, C.; Lochbrunner, S.; Riedle, E.; Nesbitt, D. J. *Review of Scientific Instruments* **2008**, *79*.

(4) Vonderlinde, D. *Applied Physics B-Photophysics and Laser Chemistry* **1986**, *39*, 201-217.

(5) Pitcher, W. H.; Huestis, W. H. *Biochemical and Biophysical Research Communications* **2002**, *296*, 1352-1355.

(6) Bernsdorff, C.; Winter, R. *J*. *Phys*.*Chem*. *B* **2003**, *107*, 10658-10664.

(7) Frisch, M. J.; G. W. Trucks; Schlegel, H. B.; Scuseria, G. E.; Robb, M. A.; Cheeseman, J. R.; J. A. Montgomery, J.; Vreven, T.; Kudin, K. N.; Burant, J. C.; Millam, J. M.; Iyengar, S.; Tomasi, J.; Barone, V.; Mennucci, B.; Cossi, M.; Scalmani, G.; Rega, N.; Petersson, G. A.; Nakatsuji, H.; Hada, M.; Ehara, M.; Toyota, K.; Fukuda, R.; Hasegawa, J.; Ishida, M.; Nakajima, T.; Honda, Y.; Kitao, O.; Nakai, H.; Klene, M.; Li, X.; Knox, J. E.; Hratchian, H. P.; Cross, J. B.; Bakken, V.; Adamo, C.; Jaramillo, J.; Gomperts, R.; Stratmann, R. E.; Yazyev, O.; Austin, A. J.; Cammi, R.; Pomelli, C.; Ochterski, J. W.; Ayala, P. Y.; Morokuma, K.; Voth, G. A.; Salvador, P.; Dannenberg, J. J.; Zakrzewski, V. G.; Dapprich, S.; Daniels, A. D.; Strain, M. C.; Farkas, O.; Malick, D. K.; Rabuck, A. D.; Raghavachari, K.; Foresman, J. B.; Ortiz, J. V.; Cui, Q.; Baboul, A. G.; Clifford, S.; Cioslowski, J.; Stefanov, B. B.; Liu, G.; Liashenko, A.; Piskorz, P.; Komaromi, I.; Martin, R. L.; Fox, D. J.; Keith, T.; Al-Laham, M. A.; Peng, C. Y.; Nanayakkara, A.; Challacombe, M.; Gill, P. M. W.; Johnson, B.; Chen, W.; Wong, M. W.; Gonzalez, C.; Pople, J. A.

(8) Peng, C. Y.; Schlegel, H. B. *Isr*. *J*. *Chem*. **1993**, *33*, 449-454.

Chapter 3

Excited and ground state relaxation dynamics of α-terpinene and 7-dehydrocholesterol

(Text adapted from Arruda, B. C., et al., *J*. *Phys*. *Chem*. *B*., **2013**, *117*, 4696)

Introduction

Due to its efficacy as a model photo-switchable molecule, a coherent control candidate, and its interesting solute-solvent interactions, CHD and HT have been the focus of many steady state and ultrafast spectroscopic experiments[1-8] as well as high level calculations.[9-12] In addition, the CHD backbone is the photoactive chromophore in the biological synthesis of previtamin D_3 (Pre) and vitamin D_3 from 7-dehydrocholesterol (DHC).[13-16]

Recent non-adiabatic molecular dynamics simulations have explored both the excited state dynamics of CHD and DHC and the ground state conformational relaxation of Pre.[10] Low temperature excited state simulations indicate that both DHC and CHD undergo an initial rapid decrease in the length of the C6-C1 and C4-C5 single bonds, accompanied by an increase in the length of the C1=C2 and C3=C4 double bonds and decrease in the length of the C2-C3 single bond on a ca. 10 fs time scale. The bond lengths exhibit a very small oscillation in CHD and then relax monotonically to a structure with five equivalent bonds. In DHC the adjacent rings hinder the ring-opening reaction and a damped oscillation of the bond lengths is observed for more than 300 fs. The C5-C6 bond length increases monotonically for CHD from 0 to 200 fs, while an induction period of ca. 175 fs with only a slight increase in the bond length followed by a

monotonic increase from 175 fs to 370 fs is observed for DHC. The steric influence of the adjacent rings also influences the conformational relaxation process from the initial all cis photoproduct to the equilibrium rotamer distribution.

The cyclic monoterpene, α-terpinene (α-TP), bears similar substitution and steric restrictions to its conformational states as DHC / Pre (see Figure 3.1). This combined with its small size makes it an excellent candidate as a model to probe how steric substitution affects the dynamics and conformational relaxation of CHD-based molecules. The methyl and isopropyl groups on the CHD backbone in α-TP isolates the influence of C1, C4 substitution dynamics. In addition, the ground state steric interactions prevent formation of the tZt conformer, which is also inaccessible in Pre.

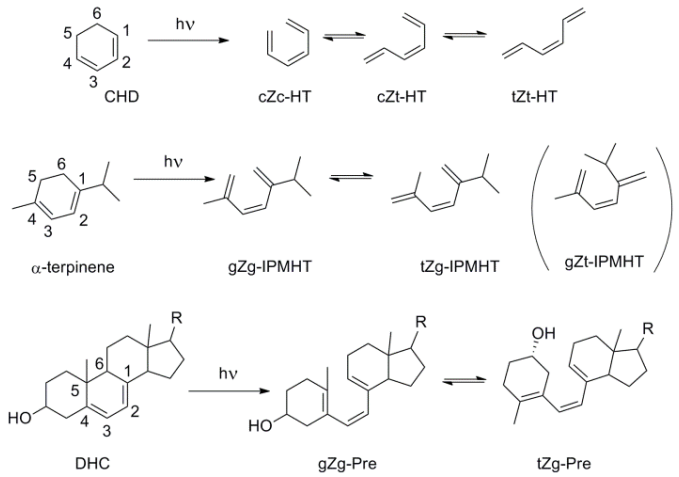

Figure 3.1: Photochemical ring opening reactions of cyclohexadiene (CHD), α-terpinene, and 7-dehydrocholesterol (DHC). The ring-numbering given in the figure, standard for CHD, is used for simplicity in the discussion of the ring-opening reaction for all compounds.

In a recent matrix isolation study, Marzec et al. used infrared spectroscopy combined with density functional calculations to show that upon UV irradiation, α-terpinene undergoes an electrocyclic ring opening reaction in an analogous manner to CHD and DHC forming the hexatriene product (Z)-2-isopropyl-5-methyl-1,3,5-hexatriene (IPMHT, See Figure 1).[17] As the

orientations around the single bonds in the "cis" configurations are helical with a significant distortion from planarity it is common to refer to this as gauche or gZg. This nomenclature is adopted for the substituted trienes studied here. Because of the variability in the orientation of the methyl and isopropyl groups, the gZg-IPMHT, tZg-IPMHT, and gZt-IPMHT conformers in Figure 1 each represent several different configurations. Marzec et al. include an analysis of all of these configurations in their calculations and in simulated IR spectra.[17] The equilibrium distribution of the α-terpinene photoproduct IPMHT consists predominantly of the tZg conformer in the gas phase. Similarly, the dominant conformer of Pre at equilibrium is the equivalent tZg conformer.[10]

In this chapter we report a study of the excited state dynamics of α-terpinene and compare these with the ring-opening reaction in DHC. We also investigate the ground state relaxation dynamics of gZg-Pre and the gZg-IPMHT photoproduct of α-terpinene using ultrafast broadband UV transient absorption spectroscopy. The transient absorption spectra are compared to quantum chemical calculations in an effort to better understand the absorption features. The relaxation dynamics were measured in both alcohols and alkanes spanning a range of viscosities. This is the first such experiment conducted on α-terpinene in solution with ultrafast time resolution. In addition, we report the first broadband UV detection of the DHC photoproduct, previtamin D_3, with ultrafast time resolution.

Results

Steady state photolysis and fluorescence of α-terpinene

The steady state absorption spectra of α-terpinene and its photoproducts at various UV irradiation times as well as the normalized, solvent-subtracted fluorescence spectrum are shown in Figure 3.2. α-TP exhibits a broad absorption band centered at 265.5 nm with a slight shoulder

around 286 nm and a peak extinction coefficient of 6620 ± 40 $M^{-1}cm^{-1}$. The evolution of the spectrum following UV irradiation is consistent with conversion of α-TP to the Z-type photoproduct at the shortest irradiation times. Longer irradiation times lead to reabsorption and the growth of the E-type isomer spectrum. This growth is gradual, and the assignment to a new photoproduct is evidenced by a shift in the zero-crossing point in the difference spectrum from 259 nm to 275 nm. The steady state spectra of both α-TP and its photoproducts are virtually identical in all solvents under investigation here.

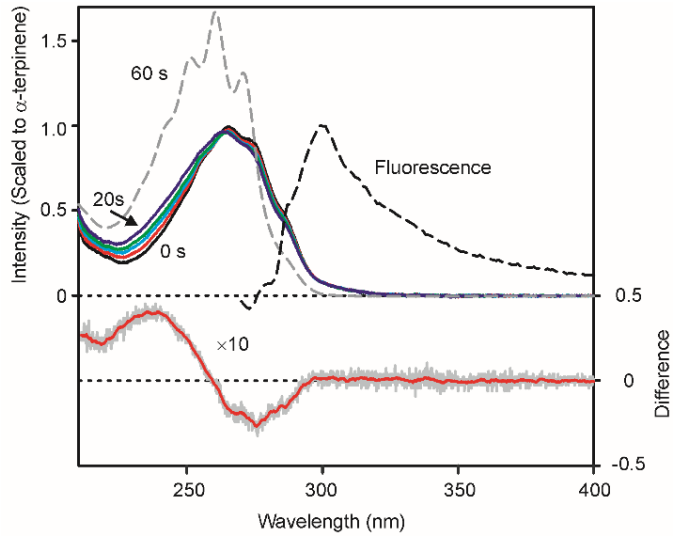

Figure 3.2: Steady state absorption spectra of α-terpinene and its photoproducts at various UV irradiation times (solid black - α-terpinene absorption spectrum, dashed black - α-terpinene fluorescence, red – 5 s, lt. blue – 10 s, green – 15 s, dk. blue – 20 s, dashed gray – 60 s). The difference curve is between α-terpinene and the 5 s photoproduct. This spectrum has been offset and multiplied by 10 for clarity. The grey line is the raw data while the red line has been smoothed with a 2 nm running average. This difference spectrum is consistent with the long-time difference spectrum in the ultrafast measurements.

Time integrated fluorescence measurements on α-TP in heptane showed a fluorescent band peaking at 300 nm. By comparison with the well characterized fluorescence spectrum for *trans*-stilbene, an estimate of the excited state lifetime of α-terpinene can be made. The fluorescence quantum yield for *trans*-stilbene in heptane is estimated to be 5.0×10^{-2}.[16,18] Using this value as a standard, a fluorescence quantum yield for α-terpinene is estimated as $\phi_f = \sim 2 \times$

10^{-5}. The Strickler-Berg Equation[19] can be used to estimate the radiative lifetime of α-terpinene in heptane solution with the approximation $n = n_D$:

$$k_r \cong \frac{8\pi n^2 2303}{N_a c^2} \left\langle \nu_f^3 \right\rangle \int \frac{\varepsilon(\nu_a)}{\nu_a} d\nu_a \qquad (1)$$

Using the Strickler-Berg equation, the radiative lifetime of α-TP is estimated to be on the order of 6 ns. Given both the fluorescence quantum yield and the radiative lifetime, the fluorescence lifetime of the excited state can be estimated as $(2\times10^{-5})(6\times10^{6}$ fs) = ~120 fs (±100 fs).

Transient absorption spectroscopy of α-terpinene

Time resolved transient absorption spectra (TA spectra) were obtained for α-TP in seven solvents to cover a wide range of solvent polarities and viscosities. All spectra show a spike at t = 0 ps corresponding to a two-photon absorption of the solvent and solute when there is maximum temporal overlap of the pump and probe pulses. Solvent scans yielded only minimal dynamics beyond this spike, which provides the cross-correlation of the pump and probe pulses. The solvent signal was subtracted in all of the spectra before analysis.

The early time UV-VIS transient absorption spectra of α-TP in hexane, 1-propanol and 1-butanol are plotted in Figure 3.3. The spectrum in 1-butanol was obtained with a continuum generated by focusing 800 nm in CaF_2 and the spectra in hexane and 1-propanol were obtained with a continuum generated by focusing 400 nm in CaF_2. At early times the spectra in the alcohols are characterized by a strong peak in the visible region with a maximum at ca. 470 nm. This absorption is similar to the visible absorption band observed following excitation of DHC. In contrast, no excited state absorption signal has been observed for CHD. The excited state absorption of α-TP decays with a lifetime of 0.16 ps in 1-butanol. In hexane the excited state absorption is red-shifted slightly, with a maximum at ~480 nm, and decays with a lifetime of 0.12 ps. The decay of the excited state absorption is consistent with the fluorescence lifetime

deduced from the quantum yield above and likely reflects decay of the strongly allowed state populated following electronic excitation.

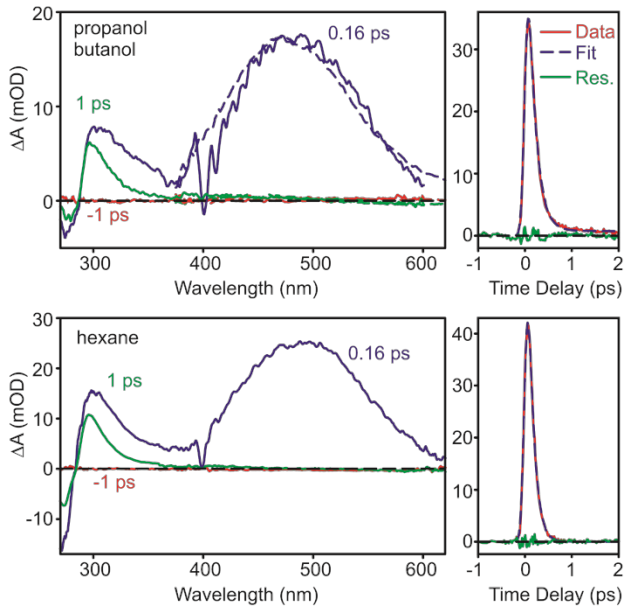

Figure 3.3: Excited state absorption of α-terpinene in 1-propanol (solid line), 1-butanol (dashed line) and n-hexane. The dip at ca. 400 nm is an artifact of residual 400 nm used to produce the continuum probe. There is a broad visible absorption band peaking at ca. 470 nm in the alcohols and 480 nm in hexane. The decay of the ESA between 470 nm and 475 nm in 1-butanol is plotted in the top right panel. The decay in hexane is plotted in the lower right panel.

The UV absorption band observed in the difference spectra decays on a much longer time scale. Difference spectra obtained following excitation of α-TP in hexane at 266 nm are shown in Figure 3.4 for time delays 0.5 – 100 ps and probe wavelengths between 270 nm and 370 nm. A negative signal corresponding to the ground state bleach of α-terpinene is seen at 270 - 290 nm. This bleach is present for all time delays following the initial 2-photon spike, indicating formation of a permanent photoproduct. A positive absorption peak is observed ranging from approximately 285 – 330 nm. TA spectra in all solvents studied here, hexane, decane, dodecane, hexadecane, cyclohexane, methanol, 1-propanol, and 1-butanol, behave similarly with little difference in the nature of the spectral or kinetic components.

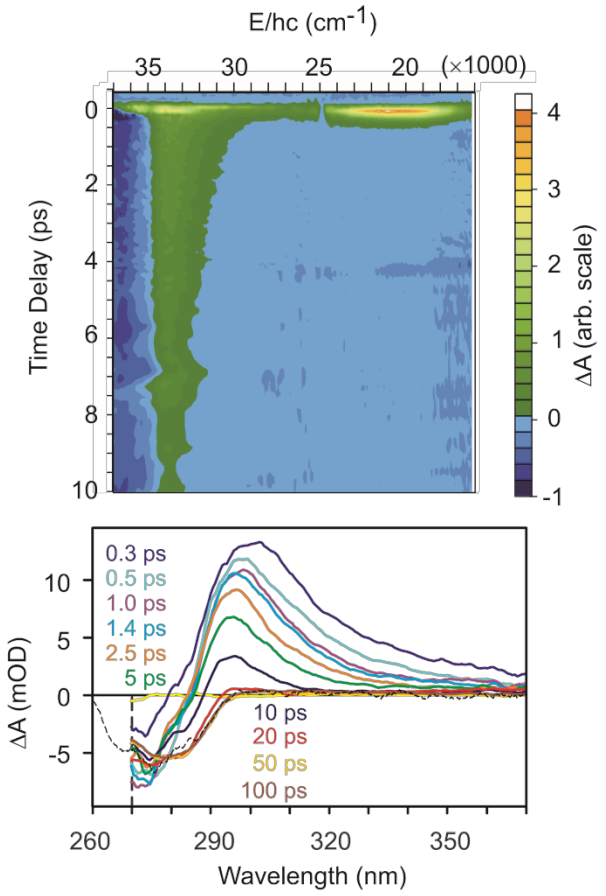

Figure 3.4: Top: Transient absorption spectra of α-terpinene in hexane at various time delays. The main spectral features are a bleach on the blue edge and a peak at 300 nm. The peak appears at early times and decays with a time constant around 6 ps in all solvents.

Kinetic traces of α-TP in dodecane at various wavelengths are shown in Figure 3.5. Best fit parameters were obtained using a multi-exponential fitting routine in a global analysis program. A multiexponential model was used because it captures the dynamics at all wavelengths while avoiding over-interpretation of the spectrum. Two exponentials are required to fit the data at all wavelengths. A third amplitude is required to account for permanent photoproduct formation. The need for two exponential decay components is most clearly demonstrated by the rise and decay at $\lambda = 280$ nm. Using fewer exponentials in the model led to a non-zero residual, while adding more exponentials did not improve the χ^2 value for the fit.

At 300 nm only one exponential is required to fit the data, 7.1 ps in dodecane. For wavelengths to the red of 300 nm the additional fitting parameter has a wavelength dependence as illustrated in the inset to Figure 5. By 360 nm this component is indistinguishable from the decay of the visible excited state absorption. For probe wavelengths between 270 nm and 300 nm the second exponential does not vary significantly with wavelength. The time constant of this component is 4.2 ps ± 0.2 ps in dodecane.

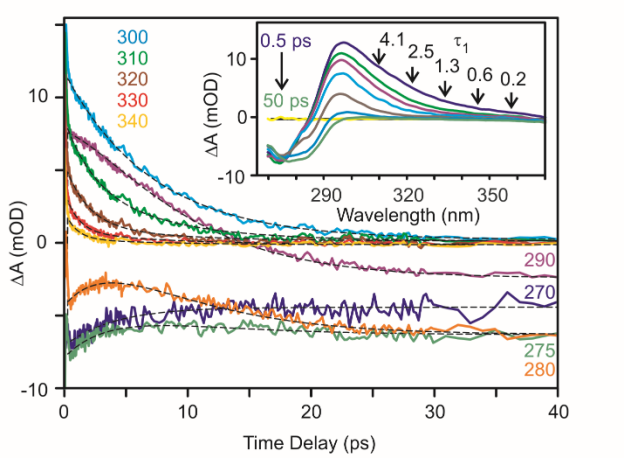

Figure 3.5: Kinetic traces (colored) and fits (black) of α-terpinene in dodecane at representative wavelengths indicated on the plot. The fits have residuals centered at 0 with no features other than noise. The inset shows the wavelength dependence of the fast component in the bi-exponential fit. The rate becomes faster (time constant becomes smaller) on the red edge of the absorption. The spectra are plotted for time delays of 0.5 ps, 1.4 ps, 2.5 ps, 5 ps, 10 ps, 20 ps, and 50 ps.

The data in the other alkane and alcohol solvents studied here are similar. The traces are well modeled by a biexponential decay at most wavelengths. The decay of the peak of the positive absorption signal around 300 nm requires only a single exponential ranging from 5.5 ps to 7.4 ps. The decay constants obtained from the fits are given in Table 3.1. There is no clear trend with macroscopic solvent properties, including solvent shear viscosity. The data, plotted in Figure 3.6 are scattered around a central value.

Table 3.1: Viscosities and the time constants from the exponential fits across the UV portion of the α-TP TA.

Solvent	η (mPa s)[a]	τ_1 (ps)[b]	τ_2 (ps)[c]
Hexane	0.300	2.8 ± .25[d]	6.7 ± .25
Decane	0.838	3.3 ± .25	7.3 ± .25
Dodecane	1.383	4.2 ± .20	7.1 ± .20
Hexadecane	3.032	1.7 ± .25	5.5 ± .25
Cyclohexane	0.894	3.7 ± .50	7.4 ± .50
Methanol	0.544	3.6 ± .35	5.9 ± .35
1-Propanol	1.945	2.9 ± .25	6.0 ± .25
1-Butanol	2.544	3.8 ± .27	6.3 ± .27

[a]Viscosities are reported for 25° C.[20]
[b]The fast component, τ_1 depends on solvent and wavelength. The values in the table are from the blue portion of the spectrum where τ_1 is constant across wavelength. For wavelengths >320, the rate of the fast component increases with wavelength.
[c]The time constant τ_2 characterizes the decay of the absorption peak at 300 nm.
[d]The error represents the range at which the χ^2 for the fit remains within 0.01 of the best fit.

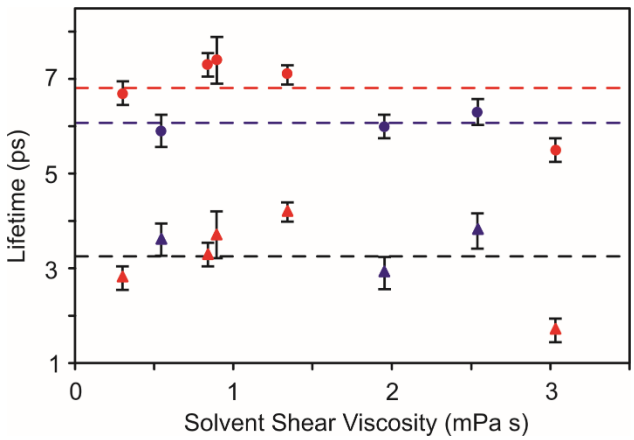

Figure 3.6: Lifetime of the fast (triangles) and slow (circles) components for the UV absorption following excitation of α-terpinene. The blue symbols are measurements in alcohols, the red symbols are measurements in alkanes.

Optimized structures of α-terpinene and the primary rotamers of its photoproducts were used for a set of excited state and ground state calculations. The calculated ground state single point energies, transition dipole moments, and energy differences between the ground and first singlet excited state are shown in Table 3.2. The ground state energies are in good agreement with the calculations conducted by Marzec et al.[17] The initial gZg conformation of the photoproduct is predicted to absorb to the red of α-terpinene while other conformations absorb to the blue of α-terpinene. In addition, frequency calculations on the gZg and tZg conformations as well as the transition state between the two were conducted in order to obtain free energies. These structures and values are shown in Figure 3.7. The Gibb's free energy of activation for the gZg to tZg interconversion is calculated to be 16.5 kJ/mol, while the enthalpy of activation is 9.9 kJ/mol. The calculated Gibb's free energy and enthalpy of reaction are -3.5 and -5.1 kJ/mol respectively.

Table 3.2: Excited state and single point ground state energies and oscillator strengths. Qualitatively the results agree well with experimental observations.

Conformer	Oscillator Strength	Singlet Transition (nm)	Ground State Energy (kJ/mol)
α-terpinene	0.2241	277.83	0
gZg-IPMHT	0.1168	282.4	100.4
tZg-IPMHT	0.3835	265.46	94.2
gZt-IPMHT	0.2500	268.74	99.1
tEt-IPMHT	0.8359	270.7	62.2

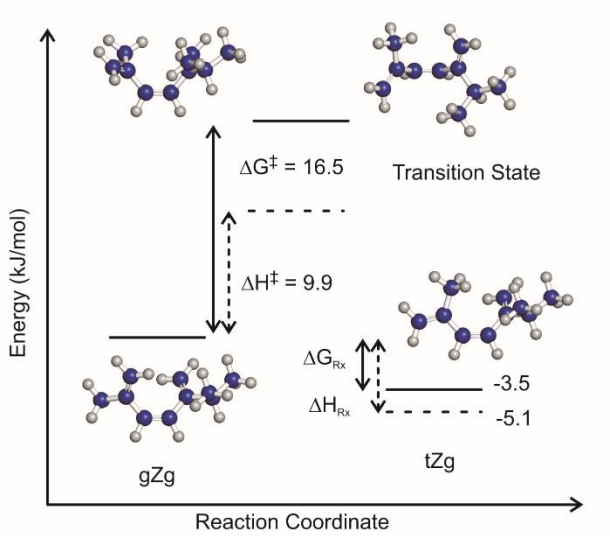

Figure 3.7: Thermodynamic quantities obtained from frequency calculations in the Gaussian 03 software package using the B3LYP density functional and the 6-311++G(d,p) basis set.[21,22] The free energy of activation has a large entropic component and the overall energy decreases as the photoproduct interconverts from gZg to tZg.

Steady-state and transient spectroscopy of 7-dehydrocholesterol

The steady state absorption spectra of DHC and its photoproducts at various UV irradiation times as well as the normalized, solvent-subtracted fluorescence spectrum of DHC are shown in Figure 3.8. The fluorescence spectrum is consistent with that reported earlier.[16] The zero-point crossings in the difference spectra obtained in the photolysis measurements are stable for the first 15 seconds and then begin to shift as additional photoproducts accumulate. The difference spectrum shown in Figure 8 is a weighted average of the difference at 5s (w=1), 10 s (w=.45) and 15 s (w=.32) scaled to the intensity of the 5 s difference.

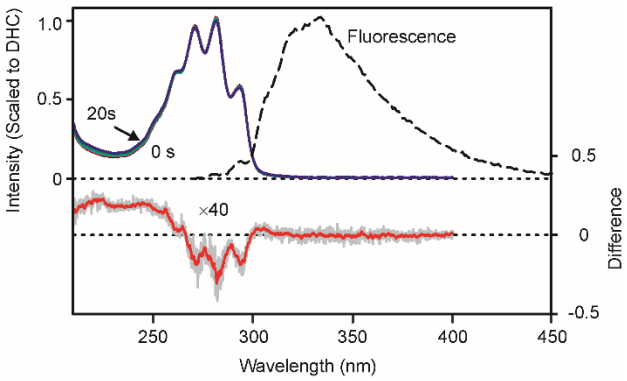

Figure 3.8: Steady state absorption spectra of DHC and its photoproducts in heptane at various UV irradiation times (solid black - DHC absorption spectrum, dashed black - DHC fluorescence, red – 5 s, lt. blue – 10 s, green – 15 s, dk. blue – 20 s). The difference curve is between DHC and the early time photoproduct observed between 5 and 15 s. This spectrum has been offset and multiplied by 40 for clarity. The grey line is the raw data while the red line has been smoothed with a 1 nm running average.

For comparison with the results reported above for α-terpinene, UV transient absorption spectra were obtained for DHC in n-heptane, dodecane, methanol, and 2-butanol. The UV-visible transient absorption spectrum of DHC in 2-butanol is plotted in Figure 3.9. The excited state absorption in the visible region is identical to that reported earlier.[16] The time-dependent difference spectra in the ultraviolet region are in reasonably good agreement with previous TA experiments which utilized selected single wavelength probes.[13-15] The current data sets, however, are more complete and provide a better overall picture of the relaxation dynamics of the pre-vitamin D_3 molecule formed following the excited state ring-opening reaction.

The main features in the UV difference spectra are a net bleaching signal observed between 270 nm and 295 nm and a broad net absorption peak around 305 nm. A global fitting algorithm was used to analyze the evolution of the difference spectrum. Contrary to the conclusions of earlier single wavelength measurements, the DHC fitting parameters show little wavelength dependence. The data is appropriately fit using two exponential decay components and a constant component representing formation of the long-lived photoproduct. The fast component (~1.1-1.8 ps) is in good agreement with the average decay of the visible absorption

and is assigned to the decay of the electronically excited state.[12,13,15,22] The longer time scale decay ranges from 5 ps in methanol and heptane to 8.5 ps in dodecane and represents the decay of a red-shifted absorption band. The assignment for this absorption will be considered in the discussion below. A summary of the time constants obtained for the four solvents studied here is provided in Table 3.3.

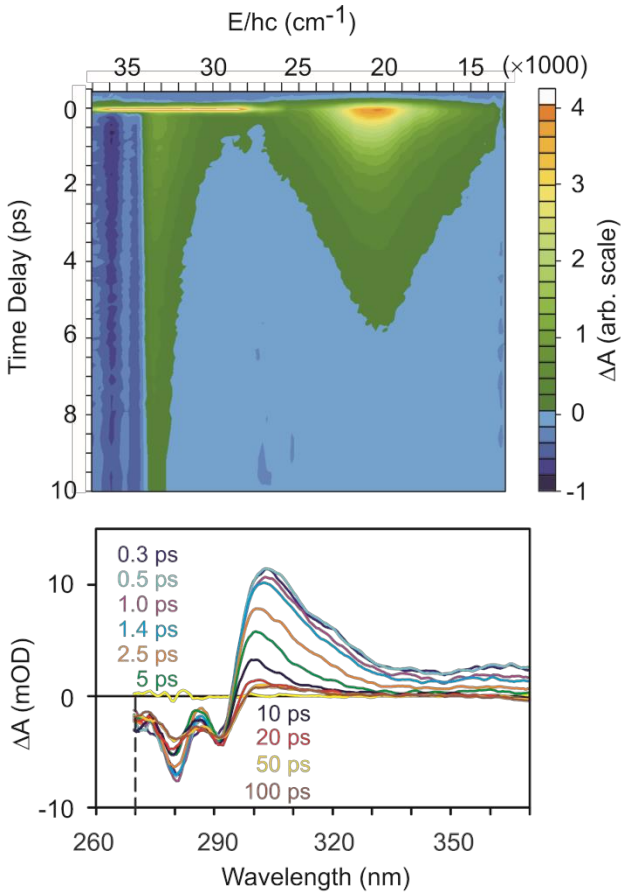

Figure 3.9: Transient absorption spectra of DHC at various time delays. The contour plot shows both the spectral behavior in the UV region as well as the excited state absorption in the visible. The plots here are for DHC in 2-butanol.

Table 3.3: Time constants obtained from global fits across a wavelength range in DHC of 275 – 370 nm. Viscosities are reported for 25° C.[20]

Solvent	η (mPa s)	τ_1 (ps)	τ_2 (ps)
Heptane	0.387	1.1 ± .45	5.1 ± .45
Dodecane	1.383	1.4 ± .45	8.5 ± .45
Methanol	0.544	1.5 ± .60	5.4 ± .60
2-Butanol	3.096	1.8 ± .25	6.2 ± .25

Discussion

Assignment of transient absorption features of α-terpinene

The qualitative features in the transient absorption spectra of α-terpinene are remarkably similar to the trends observed in DHC. There is a strong excited state absorption assigned to a transition from the initially excited state. The estimated fluorescence lifetime of the initially excited state is in very good agreement with the lifetime of the visible excited state absorption. The excited state decay in α-terpinene is approximately an order of magnitude faster than observed for DHC, on the same general time scale as the rapid non-adiabatic decay back to the ground state observed for CHD.[3,7,23] However, the presence of a fluorescence signal and an excited state absorption suggest that the electronic states involved in the ring-opening of α-terpinene are more similar to those of DHC than CHD.[16] CHD has a fluorescence lifetime of ca. 10 fs[24] and no excited state absorption is observed in the visible region of the spectrum. Control experiments using a dump pulse to control dynamics are consistent with the hypothesis that population on the optically allowed state persists for no longer than 50 fs.[7]

The solvent dependence of the excited state decay in DHC suggests the presence of both an intrinsic barrier of ca. 2 kJ/mole and a solvent induced barrier influenced by the solvent

viscosity.[16] There may be a small solvent dependence in the excited state decay of α-terpinene, similar to the dependence observed for DHC, but the overall effect is within the errors of the present measurement and would require better time resolution as a function of temperature to be fully characterized. The order of magnitude difference between the lifetime of the excited state in DHC and α-terpinene suggests that the intrinsic and environmental barriers for the excited state are much smaller than k_BT at room temperature for the α-terpinene molecule.

The features observed in the UV region of the difference spectrum obtained following excitation of α-terpinene reflect the vibrational cooling and conformational relaxation of the hexatriene product (IPMHT) formed following the photochemical ring-opening reaction. TD-DFT calculations predict that molecules in a gZg-IPMHT conformation will have an absorption band with approximately half the intensity, shifted approximately 5 nm to the red of the corresponding transition in α-terpinene. Molecules in a tZg-IPMHT conformation are predicted to absorb 12 nm to the blue, with an oscillator strength about 70% larger than the corresponding transition of α-terpinene. These observations are in qualitative agreement with the steady state photolysis and ultrafast transient absorption measurements.

Adding a scaled amount of the α-terpinene spectrum to the difference spectrum from Figure 2 allows for a rough estimate of the location and shape of the steady state IPMHT photoproduct spectrum (predominantly tZg-IPMHT). Varying the scale factor for the amount of α-terpinene spectrum to add to the difference spectrum sets the limits for the relative magnitude and peak shifts of the gZg-IPMHT and tZg-IPMHT spectra. The lower limit is set by the condition of having the estimated tZg spectrum be positive, while increasing the scale causes the tZg spectrum to approach the initial α-terpinene spectrum. The cartoon spectra shown in Figure 10 represent a reasonable estimate and help elucidate the key features in the transient absorption.

We stress however, that this is a qualitative treatment because the spectra for gZg and tZg-IPMHT are not known and likely contain asymmetries not captured by a Gaussian function.

The initial photoproduct is formed in a gZg conformation as is consistent with the principle of least motion.[17] The peak at ca. 300 nm in the ultrafast transient absorption measurements reflects the formation, thermalization, and conformational relaxation of this initial gZg-IPMHT photoproduct. The red-shift of the gZg-IPMHT spectrum in Figure 10 is ca. 8 nm, and the oscillator strength of the gZg-conformation appears to be comparable to that of α-terpinene. The dynamics in the transient absorption measurements represent a combination of spectral narrowing as the molecule cools and population decay as the gZg-IPMHT conformation decays to an equilibrium distribution of conformers dominated by tZg-IPMHT configurations.

The difference spectra obtained with time delays ≥50 ps and the initial steady state photolysis measurements are characterized by the bleach of the α-terpinene absorption and the appearance of an absorption peak to the blue of α-terpinene. The peak of this absorption falls outside of the spectral window of the ultrafast measurements, but is clearly seen in the steady state spectra. The estimate plotted in Figure 3.10 represents a 6 nm blue shift of the tZg spectrum with respect to α-terpinene and an oscillator strength comparable to that of both α-terpinene and the gZg conformer. This is a qualitative analysis and discrepancies in the magnitude of the peak shifts and peak heights are likely caused by limitations in the ability to extract the tZg and gZg spectra from the data as well as limitations in the accuracy of the calculations.

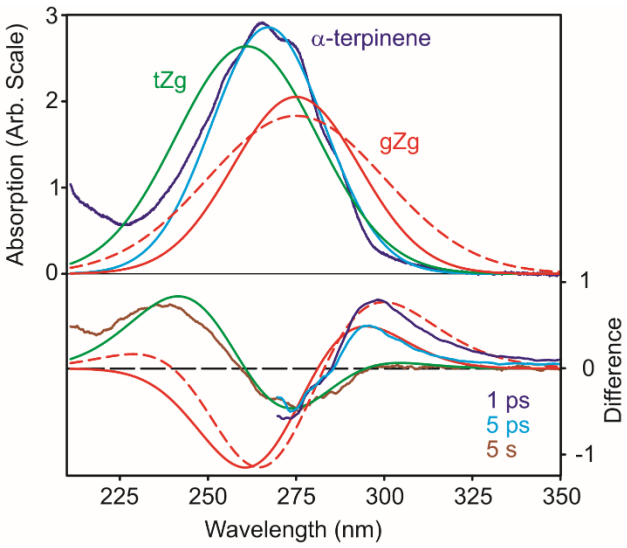

Figure 3.10: Cartoon spectra based on the calculated spectra for α-terpinene and IPMHT photoproducts. The dark blue spectrum in the top panel is the measured spectrum of α-terpinene. The light blue is a Gaussian fit to the α-terpinene spectrum. The green is an estimated spectrum of tZg-IPMHT. The red lines are estimated spectra of hot (dashed) and cool (solid) gZg-IPMHT. The bottom panel compared the difference spectra at 1 ps, 5 ps, and steady state (see Figure 4) with the difference spectra calculated from the Gaussian spectra plotted in the top panel.

As described above, the ultrafast spectral evolution of α-terpinene in solution can be fit well using a linear combination of two exponential terms with amplitude and decay constants as the fitting parameters and constant corresponding to the permanent photoproduct. The ca. 7 ps decay is associated with the depletion of red-absorbing gZg-IPMHT via conformer interconversion to tZg-IPMHT. The faster decay component is characterized by a wavelength dependent decay of the intensity on the red edge of the spectrum and an increase in the absorption intensity around the peak of the gZg-IPMHT transition. This component likely reflects the approach to thermal equilibrium with the surrounding solvent as the spectrum narrows and conformer interconversion occurs. The comparison of the dashed and solid red lines representing gZg-IPMHT in Figure 3.10 illustrate the expected influence of spectral narrowing on the time-resolved spectra.

Assignment of decay processes in 7-dehydrocholesterol.

The ultrafast excited state and ground state dynamical processes in DHC have been well characterized by a number of experimental studies and high level calculations.[10,13-16] Tang *et al*. used broadband visible transient absorption spectroscopy to demonstrate that the excited state decay is biexponential with time constants of 0.4 – 0.65 ps and 1.0 – 1.8 ps depending on solvent and the temperature.[16] The probable explanation for the biexponential decay behavior is a branching down different decay pathways with distinct populations on the excited state surface as the cyclohexadiene ring opens.[16,25] Meyer-Ilse *et al*. performed UV femtosecond time-resolved circular dichroism (TRCD) measurements that provide further support for a fast ring-opening reaction.[26] TRCD provides a unique probe for the ring opening process because it is sensitive to the change in chirality caused by the ring-opening reaction. The results of the TRCD measurements show a chirality change on a time scale of 1-2 ps. This allows for a confident assignment of the picosecond component to the ring opening process on the electronic excited state.

A comparison of the early (2.5 ps) and late (>100 ps) TA difference spectra obtained following excitation of DHC in methanol and heptane is shown in Figure 3.11. These difference spectra are compared with the steady state difference spectrum obtained after 5-10 s of UV photolysis (see Figure 3.8), the spectrum of DHC and the estimated spectrum of the Previtamin D_3 photoproduct. The photoproduct spectrum was obtained by adding the DHC spectrum to the 5s difference spectrum until the vibronic structure between 265 nm and 300 nm was minimized in the photoproduct spectrum. The Gaussian fit to the product spectrum in heptane peaks at ca. 260

nm with a FWHM of ca. 6500 cm^{-1}. In methanol the Gaussian fit peaks at 265 nm with a FWHM of ca. 6000 cm^{-1}. This is in reasonable agreement with the spectrum reported by Fuss *et. al.* in ethanol.[15]

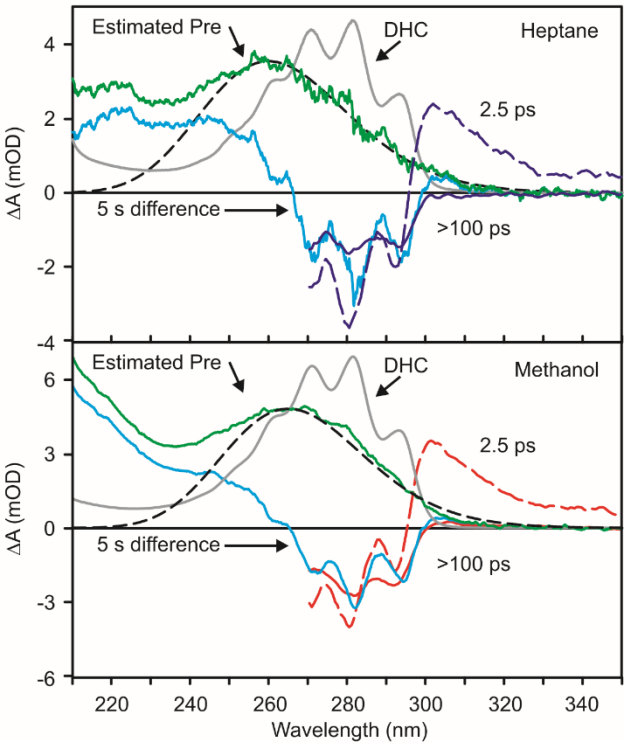

Figure 3.11: Comparison of the early (dashed, 2.5 ps) and late (solid >100 ps) difference spectra following photolysis of DHC in methanol (bottom, red) and heptane (top, blue). The steady state spectra of DHC (gray), the early steady state difference spectrum (lt. blue, see Fig. 8) and the estimated spectrum of Previtamin D_3 (green) are also shown for each solvent. The black dashed line is a Gaussian fit to the estimated spectrum of Previtamin D_3.

In previous work Anderson *et al.* assigned the 5 – 6 ps decay component observed in the UV to vibrational relaxation of the initial gZg-Pre photoproduct on the ground state and a long time decay of 100 ± 20 ps to the rotational isomerization on the ground state producing an equilibrium mixture of gZg and tZg conformers.[14] However, the 100 ps component was reported to have very low amplitude relative to the other components and is not observed in the data reported here when care is taken to account for and minimize contributions from multi-photon excitation of the solvent. The 5-8 ps component observed in DHC is likely associated, as in α-

terpinene, with the decay of the gZg conformer of Pre produced in the initial ring-opening process to a mixture of rotamers approaching that expected at thermal equilibrium. This 5-8 ps decay component in the transient spectrum may also contain a contribution due to vibrational relaxation of both gZg-Pre and DHC following ground state recovery.

Tapavicza *et al*. predicted using *ab initio* excited state non-adiabatic dynamics simulations of DHC and its photochemistry that, following relaxation to the ground state, Pre adopts the equilibrium distribution of rotamers within ~6 ps.[10] The present experiments are consistent with this simulation and suggest that for the hot gZg-Pre molecule there is a rapid ground state conformer interconversion to the tZg-Pre conformation. The interconversion depends only modestly on the solvent environment, with the relaxation in the more viscous alkane and alcohol solvents only slightly slower than in the less viscous solvents.

For time scales longer than 50 ps there is a small residual absorption on the red edge of the DHC spectrum in methanol and 2-butanol. This absorption is smaller in heptane or dodecane where the difference decays to zero on the red edge. The difference spectrum observed for time-delays greater than 50 ps is qualitatively similar to the steady state difference spectrum, but is not as structured (See Figure 11). This may reflect a limitation of the transient measurement, but more likely reflects continued conformational relaxation of Pre on the ground state surface. This complex molecule can adopt a wide range of similar configurations as Tapavicza et al. observe in their simulations.

We note, as well, that the distribution formed following the 6 ps relaxation in solution need not be the distribution of gZg-Pre and tZg-Pre expected at thermal equilibrium. Earlier measurements on hexatriene and cyclohexadiene demonstrated that ca. 5-7% was trapped in the higher energy tZc-HT conformation and underwent thermal relaxation to tZt-HT on a timescale

greater than 100 ps.[1,2] Likewise, single wavelength measurements by Fuss et al. on DHC in ethanol suggest that there is a ca. 100 ps decay component corresponding to thermal interconversion of gZg-Pre → tZg-Pre.[15] The temperature dependence of this component yielded an interconversion barrier of 15.5 ± 1 kJ/mol. Molecular dynamics simulations by Tapavicza *et al*. indicate a large accessible conformational space at 600 K spanning a number of conformations including gZg, and tZg, while cooling to room temperature greatly shifts the equilibrium towards the tZg conformation. It is possible that the ca. 100 ps component observed by Fuss *et al*. represents the final approach to equilibrium following trapping of a small excess of excited conformers as the initial hot photoproduct cools through energy transfer to the solvent. The probe wavelengths used in the single wavelength temperature dependent measurements of Fuss et al were near the zero-crossing point between 260 nm and 270 nm, outside the range of the present measurements. In this region the data will be more sensitive to small changes in the conformational populations than at the longer probe wavelengths used here.

Conclusion

The goal of this study was to characterize the photochemistry of α-terpinene and the structural dynamics of the IPMHT photoproduct following the ring-opening reaction. These measurements are compared with analogous experiments probing the photochemistry of 7-dehydrocholesterol and the subsequent relaxation of previtamin D_3. Quantum chemical calculations were used to justify the assignment of the absorption features of the gZg-IPMHT and tZg-IPMHT photoproducts in the steady state and ultrafast regimes.

Following UV excitation, both α-terpinene and DHC exhibit visible excited state absorption from the initially excited state. No such absorption is observed for CHD. The excited state absorption decays on a time scale of ~150 fs in α-terpinene and 1-2 ps in DHC.[16] The

fluorescence quantum yields and excited state lifetimes are in good agreement demonstrating that the initially excited state has a lifetime much longer than the corresponding state of CHD. The ring-opening reaction of both α-terpinene and DHC occurs on essentially the same time scale as the decay of the initially excited state.

The initial gZg-IPMHT triene photoproduct absorbs to the red of the α-terpinene ground state spectrum. Ultrafast UV transient absorption measurements show that conformer interconversion from the gZg-IPMHT triene photoproduct to tZg-IPMHT occurs on a 5.5 ps to 7.4 ps time scale with no systematic dependence on solvent polarity or viscosity. Thermalization occurs on a time scale of 2 – 4 ps depending on solvent, also with no particular trends within the solvent series. The UV transient spectrum of the gZg-Pre product formed following excitation of DHC is similar to that of gZg-IPMHT. This photoproduct is also characterized by a red-shifted absorption with a peak at ca. 300 nm in the ultrafast difference spectrum. The solvent dependence for the decay of gZg-Pre is somewhat larger than observed for gZg-IPMHT, ranging from 5.1 ps to 8.5 ps, but still relatively small. The similarity in time scales for gZg-IPMHT and gZg-Pre is surprising given the large size difference in the substitutions around the triene structure. Future studies of these ring-opening reactions and the relaxation of the resulting triene systems will involve using a shorter wavelength UV probe to characterize the formation of the photoproduct more completely along with molecular dynamics simulations in an attempt to understand the mechanism for the conformational relaxation and the reason for the small influence of solvent environment on the process.

Acknowledgements

This work was supported in part by NSF Grants CHE-0718219 and CHE-1150660.

References

(1) Anderson, N. A.; Pullen, S. H.; Walker, L. A.; Shiang, J. J.; Sension, R. J. *J*. *Phys*.*Chem*. *A* **1998**, *102*, 10588-10598.

(2) Harris, D. A.; Orozco, M. B.; Sension, R. J. *J*. *Phys*.*Chem*. *A* **2006**, *110*, 9325-9333.

(3) Kosma, K.; Trushin, S. A.; Fuss, W.; Schmid, W. E. *Phys*. *Chem*. *Chem*. *Phys*. **2009**, *11*, 172-181.

(4) White, J. L.; Kim, J.; Petrovic, V. S.; Bucksbaum, P. H. *J*. *Chem*. *Phys*. **2012**, *136*, 054303.

(5) Carroll, E. C.; Pearson, B. J.; Florean, A. C.; Bucksbaum, P. H.; Sension, R. J. *J*. *Chem*. *Phys*. **2006**, *124*, 114506.

(6) Carroll, E. C.; White, J. L.; Florean, A. C.; Bucksbaum, P. H.; Sension, R. J. *J*. *Phys*.*Chem*. *A* **2008**, *112*, 6811-6822.

(7) Kim, J.; Tao, H. L.; White, J. L.; Petrovic, V. S.; Martinez, T. J.; Bucksbaum, P. H. *J*. *Phys*.*Chem*. *A* **2012**, *116*, 2758-2763.

(8) Garavelli, M.; Page, C. S.; Celani, P.; Olivucci, M.; Schmid, W. E.; Trushin, S. A.; Fuss, W. *J*. *Phys*.*Chem*. *A* **2001**, *105*, 4458-4469.

(9) Schonborn, J. B.; Sielk, J.; Hartke, B. *J*. *Phys*.*Chem*. *A* **2010**, *114*, 4036-4044.

(10) Tapavicza, E.; Meyer, A. M.; Furche, F. *Phys*. *Chem*. *Chem*. *Phys*. **2011**, *13*, 20986-20998.

(11) Geppert, D.; Seyfarth, L.; de Vivie-Riedle, R. *Appl*. *Phys*. *B* **2004**, *79*, 987-992.

(12) Hofmann, A.; de Vivie-Riedle, R. *J*. *Chem*. *Phys*. **2000**, *112*, 5054-5059.

(13) Anderson, N. A.; Sension, R. J. In *Liquid Dynamics: Experiment, Simulation, and Theory*; Fourkas, J. T., Ed.; American Chemical Society: Washington, D.C., 2002; Vol. 820, p 148-158.

(14) Anderson, N. A.; Shiang, J. J.; Sension, R. J. *J*. *Phys*.*Chem*. *A* **1999**, *103*, 10730-10736.

(15) Fuss, W.; Hofer, T.; Hering, P.; Kompa, K. L.; Lochbrunner, S.; Schikarski, T.; Schmid, W. E. *J*. *Phys*.*Chem*. **1996**, *100*, 921-927.

(16) Tang, K.-C.; Rury, A.; Orozco, M. B.; Egendorf, J.; Spears, K. G.; Sension, R. J. *J*. *Chem*. *Phys*. **2011**, *134*, 104503.

(17) Marzec, K. M.; Reva, I.; Fausto, R.; Malek, K.; Proniewicz, L. M. *J*. *Phys*.*Chem*. *A* **2010**, *114*, 5526-5536.

(18) Saltiel, J.; Sun, Y. P. *J*. *Phys*.*Chem*. **1989**, *93*, 6246-6250.

(19) Strickler, S. J.; Berg, R. A. *J*. *Chem*. *Phys*. **1962**, *37*, 814-822.

(20) In *CRC Handbook of Chemistry and Physics*; 91st Edition (Internet Version 2011) ed.; Haynes, W. M., Ed.; CRC Press/Taylor and Francis: Boca Raton, FL.

(21) Version 1.2r3pre ed.; Schrodinger, LLC.

(22) Frisch, M. J.; G. W. Trucks; Schlegel, H. B.; Scuseria, G. E.; Robb, M. A.; Cheeseman, J. R.; J. A. Montgomery, J.; Vreven, T.; Kudin, K. N.; Burant, J. C.; Millam, J. M.; Iyengar, S.; Tomasi, J.; Barone, V.; Mennucci, B.; Cossi, M.; Scalmani, G.; Rega, N.; Petersson, G. A.; Nakatsuji, H.; Hada, M.; Ehara, M.; Toyota, K.; Fukuda, R.; Hasegawa, J.; Ishida, M.; Nakajima, T.; Honda, Y.; Kitao, O.; Nakai, H.; Klene, M.; Li, X.; Knox, J. E.; Hratchian, H. P.; Cross, J. B.; Bakken, V.; Adamo, C.; Jaramillo, J.; Gomperts, R.; Stratmann, R. E.; Yazyev, O.; Austin, A. J.; Cammi, R.; Pomelli, C.; Ochterski, J. W.; Ayala, P. Y.; Morokuma, K.; Voth, G. A.; Salvador, P.; Dannenberg, J. J.; Zakrzewski, V. G.; Dapprich, S.; Daniels, A. D.; Strain, M. C.; Farkas, O.; Malick, D. K.; Rabuck, A. D.; Raghavachari, K.; Foresman, J. B.; Ortiz, J. V.; Cui, Q.; Baboul, A. G.; Clifford, S.; Cioslowski, J.; Stefanov, B. B.; Liu, G.; Liashenko, A.; Piskorz, P.; Komaromi, I.; Martin, R. L.; Fox, D. J.; Keith, T.; Al-Laham, M. A.; Peng, C. Y.; Nanayakkara, A.; Challacombe, M.; Gill, P. M. W.; Johnson, B.; Chen, W.; Wong, M. W.; Gonzalez, C.; Pople, J. A.

(23) Deb, S.; Weber, P. M. *Ann*. *Rev*. *Phys*.*Chem*. **2011**, *62*, 19-39.

(24) Trulson, M. O.; Dollinger, G. D.; Mathies, R. A. *J*. *Chem*. *Phys*. **1989**, *90*, 4274-4281.

(25) Tang, K. C.; Sension, R. J. *Farad*. *Disc*. **2011**, *153*, 117-129.

(26) Meyer-Ilse, J.; Akimov, D.; Dietzek, B. *J*. *Phys*. *Chem*. *Lett*. **2012**, *3*, 182-185.

Chapter 4

A comparison of ring-opening dynamics in 1,3-cyclohexadiene and α-phellandrene with α-terpinene, and 7-dehydrocholesterol

(Some text adapted from Arruda, B. C. et al., *Farad*. *Disc*., **2013**, *163*, 159)

Introduction

Photochemical transformations in the condensed phase are at the forefront of physical chemistry and find application in molecular electronics, nano-scale optical switches[1,2], molecular motors[3], catalysis[4], and photobiology.[5-7] The 1,3-cyclohexadiene (CHD) chromophore is one of the most well characterized photochemically active molecules, with an enormous literature on its gas and solution phase dynamics in the electronically excited state and the ground state (see for instance[8,9] and the references therein). Substitution around the CHD backbone can alter the ground and excited state potential energy surfaces, but the photochemical transformation from diene to triene is pervasive (Figure 4.1A). A number of theoretical studies have targeted the excited state potentials and motions that drive the molecule as it traverses the electronic states involved in the nonadiabatic ring opening process.[10-13] The current model described in Chapter 1 is accepted due to the large body of experimental work supporting these predictions.[14-24]

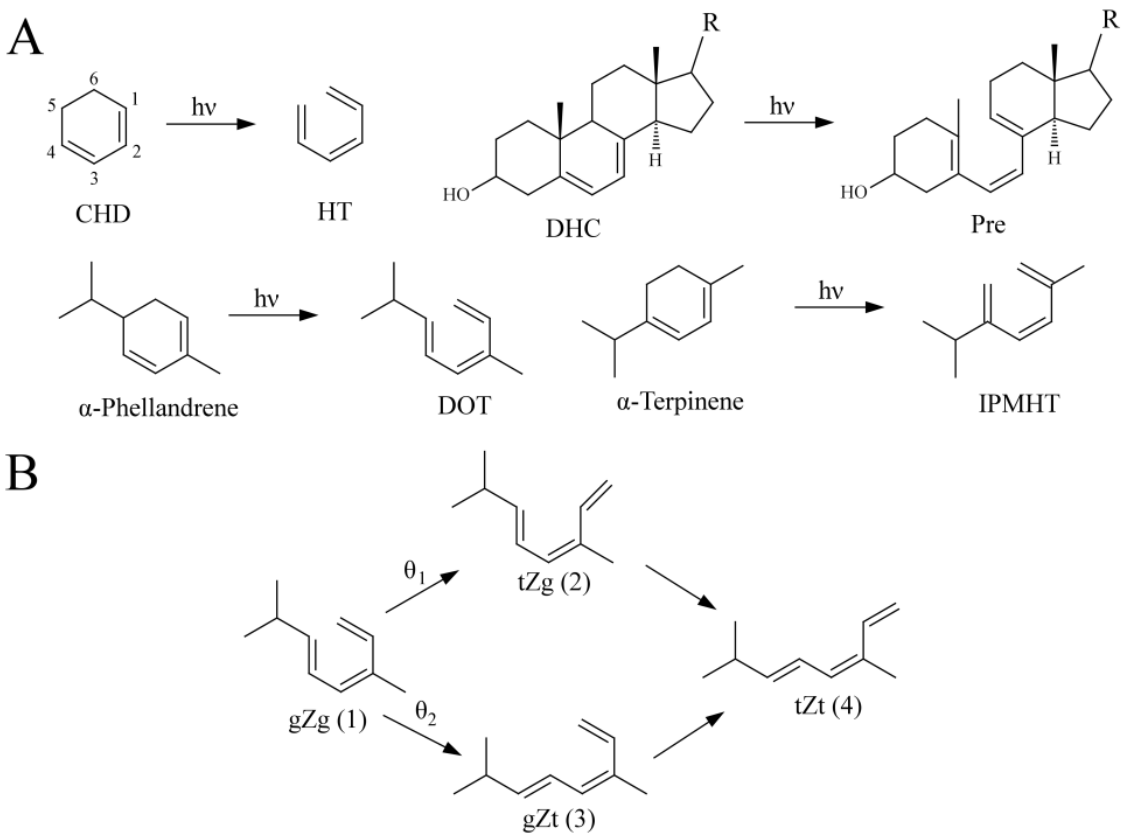

Figure 4.1: A - Photochemical transformations of the cyclohexadienes under investigation here. The numbers indicate the carbon number on the CHD backbone and the other structures are drawn to be consistent with this numbering scheme. B - The energetically distinct isomerization pathways for DOT following rotation around the dihedrals θ_1 and θ_2.

The all-cis hexatriene photoproduct is generated initially in agreement with the principle of least motion in solution, but is energetically less favourable than the "trans" rotamers. Approach to the equilibrium distribution for a HT population requires rotamer interconversion through the cZt intermediate to the tZt-HT conformation dominant at room temperature. The traditional naming scheme for the HT rotamers includes designations for the single and central double bonds, where the "c" and "t" index refer to the cis and trans orientations of the single bonds and "Z" or "E" refer to the orientation of the central double bond. Steric effects cause helicity in the cis forms, so when appropriate, gauche (g) is used instead of cis to describe the

single bond conformation. Previous studies in condensed phases have found the thermalization process for HT to occur on a picosecond timescale which depends only on solvent type (alcohols vs. alkanes) but not on specific solvents within a series.[16,19]

The photochemistry of α-TP and its photoproduct, IPMHT, are discussed in the previous chapter. Steric hindrance as a result of the bulky isopropyl substitution on the HT backbone prevents IPMHT from isomerizing to the tZt isomer. The isomerization from gZg – tZg is observed in the TA spectra presented previously. Marzec *et al*. used matrix isolation infrared spectroscopy and DFT calculations to show this result as well. In the condensed phase matrix, the tZg form dominates at equilibrium, and their quantum chemical calculations predict no stable conformation with a tZt geometry. For the α-phellandrene (α-PH) photoproduct, (3Z,5E)-3,7-dimethylocta-1,3,5-triene (DOT), Marzec *et al*. showed that in the matrix isolation environment, the tZg conformer once again dominates the equilibrium population.[25] However, for a non-static environment such as liquid solution, full exploration of the conformational space is expected, as the most energetically favorable minimum is found to be the tZt rotamer. Relaxation to this rotamer requires traversing one of two different reaction pathways which are energetically distinct (Figure 4.1B). For the ease of the reader, a list of acronyms and their definitions are provided in Table 4.1.

Table 4.1: Acronyms used in this manuscript and their corresponding definitions.[a]

Acronym	Definition
CHD	1,3-cyclohexadiene
HT	1,3,5-hexatriene
IPMHT	(Z)-2-isopropyl-5-methyl-1,3,5-hexatriene
DOT	(3Z,5E)-3,7-dimethylocta-1,3,5-triene
DHC	7-dehydrocholesterol, Provitamin D_3
Pre	Previtamin D_3

[a] See Figure 4.1A for structures corresponding to the compounds discussed here.

In the work presented in this chapter, we have used broadband femtosecond transient absorption spectroscopy (TA spectroscopy) in the UV-Visible spectral region to compare the excited and ground state dynamics of CHD, α-PH, α-TP, and DHC. The previous chapter examined the similarities and differences between α-terpinene and DHC photochemistry.[26] This chapter presents transient absorption measurements of α-PH and provides a global comparison of the ground and excited state behaviour of these four CHD containing compounds. Emphasis is placed on the effects of hydrocarbon substitution on the CHD backbone, which appears to play a major role in determining the excited state spectra and ground state dynamics. This work connects the femtosecond timescale excited state behaviour observed by Garavelli *et al*.[18] to the picosecond timescale ground state relaxation observed by Reid *et al*.[14] This is the first examination of the excited and ground state conformational relaxation of DOT in solution following photoexcitation of α-phellandrene with femtosecond time resolution and the first broadband spectral observation of the photoproduct conformational relaxation.

Results

Steady state photolysis of CHD and α-PH electronic spectroscopy of CHD:

The steady state photolysis of CHD to form a mixture of HT isomers is shown in Figure 4.2. For the earliest irradiation times, most of the HT population is of the Z type, but as the irradiation proceeds and a substantial population of HT builds, isomerization about the double bond to E-hexatriene occurs. This is true of all of the molecules considered here, so only the lowest irradiation time is used for calculating the steady state difference spectra.

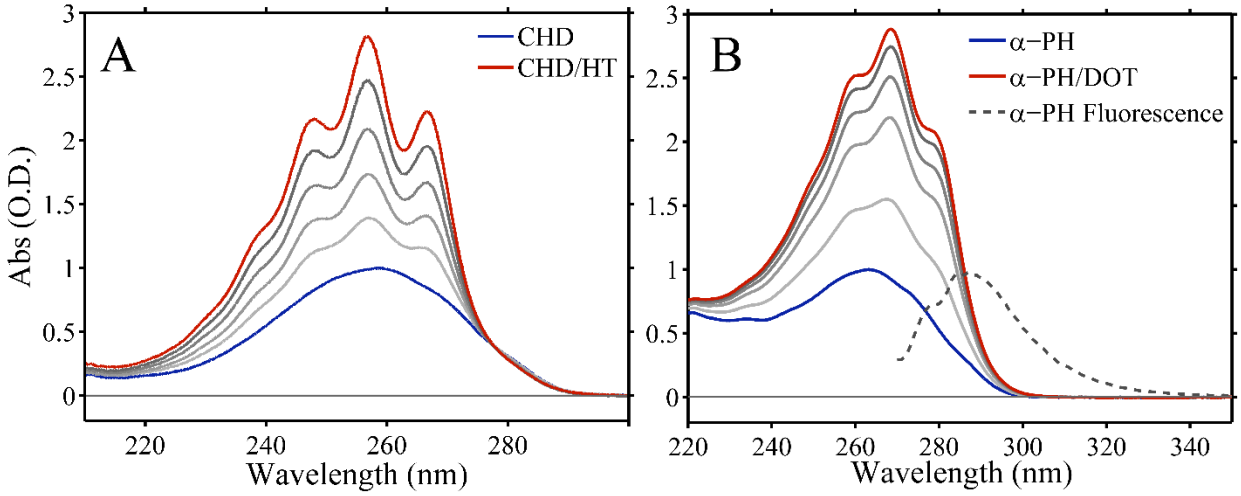

Figure 4.2: Steady state photolysis of CHD and α-PH in 10 s increment. At long irradiation times, an increasingly large population of the HT photoproduct forms, and triene photochemistry begins to contribute to the spectral shape. The final spectrum (50 s) contains a mixture of the diene along with the Z- and E- isomers of the HT product.

The steady state UV-Vis absorption spectra of α-phellandrene and its photoproducts in heptane for various UV irradiation times are shown above as well. The spectrum evolves from a broad unstructured peak with a maximum at 263.2 nm into a more intense and vibronically structured spectrum characteristic of planar conjugated hexatrienes. The vibronic bands peak at 279.0 nm, 267.6 nm, and 260.2 nm. Further irradiation results in continued growth of the triene photoproduct, until at exceptionally long times (> 3 mins.) the peak decreases in intensity as the Z-DOT form begins to convert to E-DOT. Spectra of α-PH and its photoproducts in all solvents used here were identical with only minor (~1-2 nm) shifts in the peak positions. The

fluorescence spectrum of α-PH is also shown in Figure 2, although the presence of fluorescent impurities in the sample and solvent deter a precise measurement of the fluorescence lifetime.

UV-Vis transient absorption spectroscopy of CHD:

Ultrafast transient absorption spectra taken after excitation of CHD in heptane and 1-butanol are shown in Figure 4.3. The initial spectrum is a broad peak with a maximum at 286 nm in heptane and 287.5 nm in 1-butanol. At longer time delays, the peak shifts to the blue, and eventually out of the spectral window for our experiments. These results are consistent with those reported earlier, but the quality of the data is much improved.[16,23,24] The temporal behaviour across the UV spectrum required two exponentials, along with a constant amplitude for the permanent photoproduct, to properly fit the data at each wavelength.

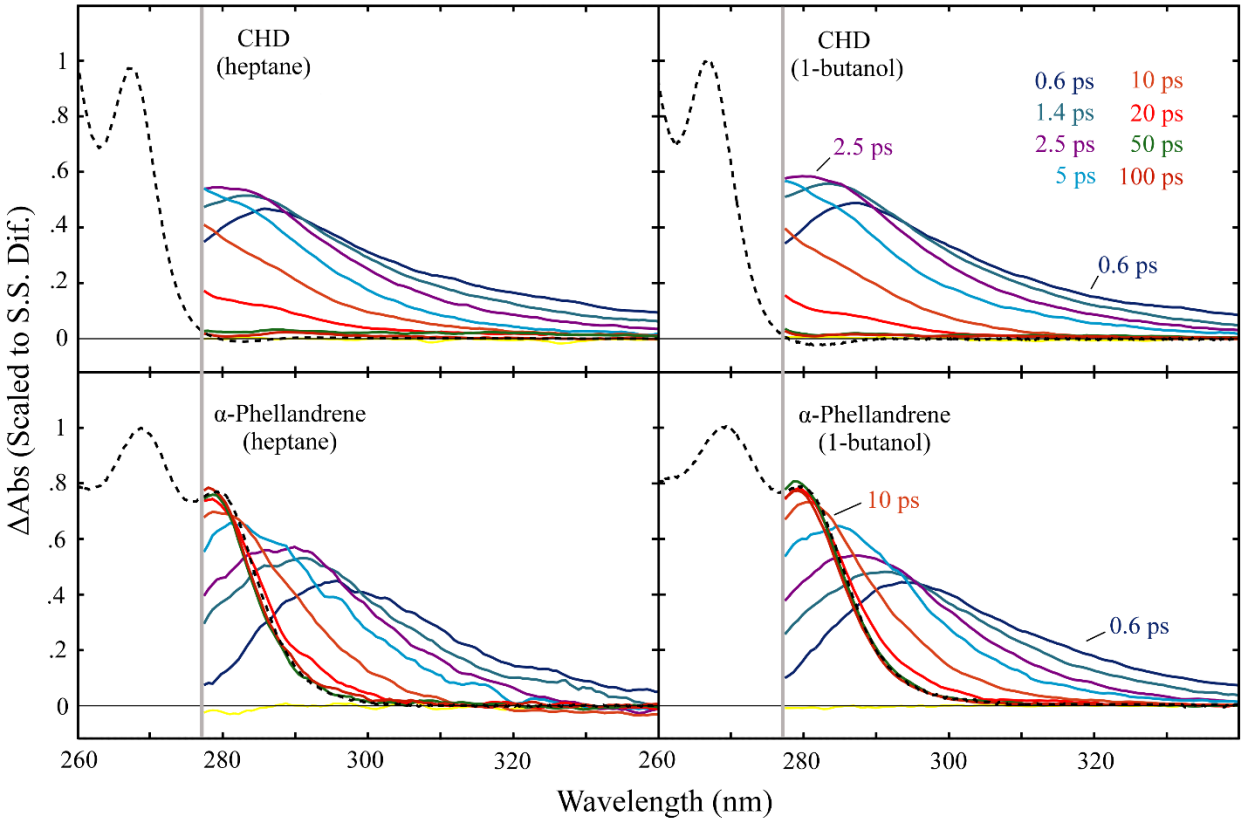

Figure 4.3: Transient absorption spectra at various time delays of CHD and α-phellandrene. For ease of comparison the same time delays are presented in all four spectra. Note that the traces for CHD shift to the blue out of our spectral window, and appear to decay to 0. The black dashed lines are the steady state photolysis difference spectra (S.S. Dif.) and the trace around zero in α-phellandrene is for the time delay -1 ps. There is uncertainty in the

intensity of the HT steady state spectrum relative to the transient absorption data due to the extent of the continuum in these measurements. The intensity shown is adapted from data reported earlier.[16,19]

A strong wavelength dependence was found for all of the fitting parameters due to the competing processes of conformational relaxation and thermalization from the initial high internal molecular temperature. This wavelength dependent relaxation is in agreement with earlier observations.[16,24] Although a complete description of the dynamics requires a more complex model, the spectral evolution can be characterized with a fast rise component and a slower decay component. The values shown in Table 4.2 are provided for comparison with α-PH and represent the average single wavelength fitting parameters in the 280 – 290 nm range where a clear rise and decay is seen.

Table 4.2: Average fitting parameters for the ultrafast dynamics of CHD and α-PH.

Sample	Solvent	η (mPa s)[a]	τ_1	τ_2
CHD	Heptane	0.387	1.4 ±0.4	10.1 ±0.4
	Hexadecane	3.03	1.4 ±0.55	9.4 ±0.55
	Methanol	0.544	1.0 ±0.5	7.8 ±0.5
	1-Butanol	2.54	1.4 ±0.55	8.4 ±0.55
α-Phellandrene	Heptane	0.387	2.5 ±0.3	9.2 ±0.3
	Hexadecane	3.03	2.9 ±0.4	7.7 ±0.4
	Methanol	0.544	2.8 ±0.45	6.6 ±0.45
	1-Butanol	2.54	2.6 ±0.4	7.5 ±0.4

[a] Viscosities are reported at 298 K.[27]

UV-Vis transient absorption spectroscopy of α-phellandrene:

Early measurements on α-PH in hexane provided no evidence for a visible excited state absorption, in contrast to the strong absorption observed for α-TP and DHC (Chapter 3).[9] However with the improved sensitivity of an upgraded spectrometer, a weak excited state absorption is observed. Transient absorption data obtained in ethanol are plotted in Figure 4.

The peak of the ESA is centered around 500 nm, and is about a factor of 12 weaker relative to α-TP. The ESA spectrum of α-TP is also shown for comparison, as well as the decay associated spectra from a global fit of the kinetics.

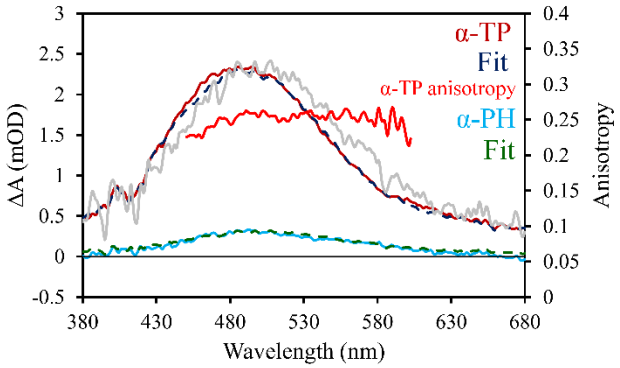

Figure 4.4: ESA in α-PH with comparison to α-TP. The gray trace is the spectrum of α-PH scaled by a factor of 12 for comparison.

A single exponential global fit of the excited state absorption returns a time constant of 190 fs for α-TP and 370 fs for α-PH in ethanol. Fits of α-TP and α-PH ESA are shown in Figure 4.5 A and B. The lifetime of a-TP is consistent with the lifetimes reported in Chapter 3 for heptane, propanol and butanol solvents, and the longer ESA lifetime in a-PH is consistent with integrated fluorescence measurements which routinely yield a longer lifetime for a-PH compared with a-TP (see below).

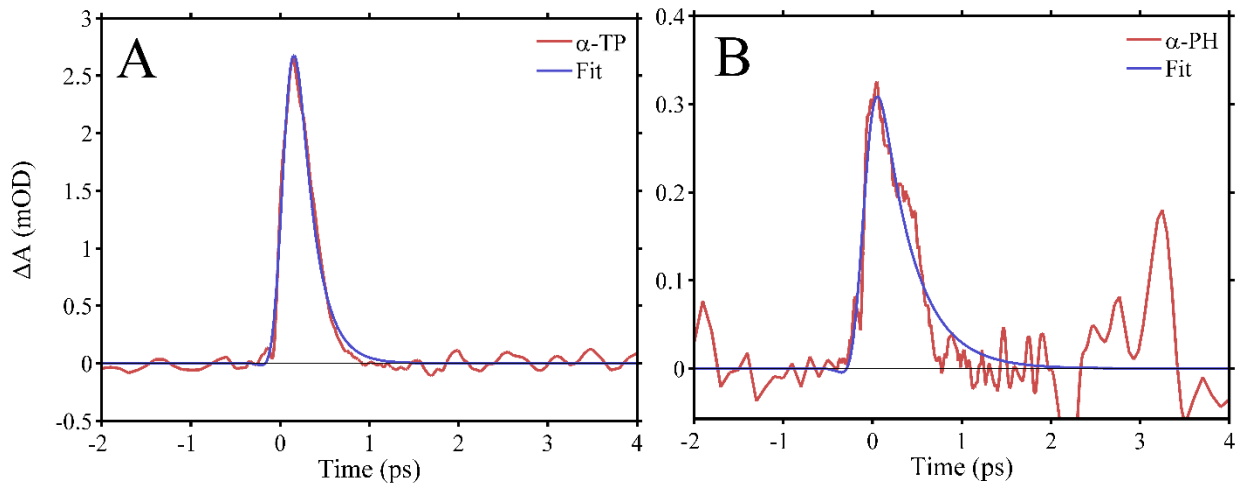

Figure 4.5: A and B: Fits over the excited state absorption integrated from 470 – 530 nm of α-TP (A) and α-PH (B). The higher noise in the α-PH measurement is a result of the extremely weak oscillator strength of the absorption.

The ultrafast spectral dynamics of the α-PH photoproduct, DOT, were studied in four solvents of varying polarities and bulk viscosities: heptane, hexadecane, methanol and 1-butanol. The early time spectra of α-phellandrene show a peak at $\lambda \sim 294$ nm. At longer time delays, the peak shifts to the blue, resulting in a difference spectrum consistent with the formation of tZt-DOT in thermal equilibrium with the surrounding solvent within 50-100 ps. Figure 4.3 shows the transient absorption spectra in n-heptane and 1-butanol compared with the corresponding measurements of hexatriene formed from CHD.

Kinetic traces of DOT in 1-butanol at select wavelengths are shown in Figure 4.6. The time domain behaviour was modelled using a biexponential model plus a constant amplitude to account for the formation of a permanent photoproduct. The necessity for a model consisting of at least two exponential components is clear from the rise and decay seen in the wavelength region of 282 – 300 nm. For most solvents two exponential components were sufficient to fully characterize the behaviour within the signal to noise of the data.

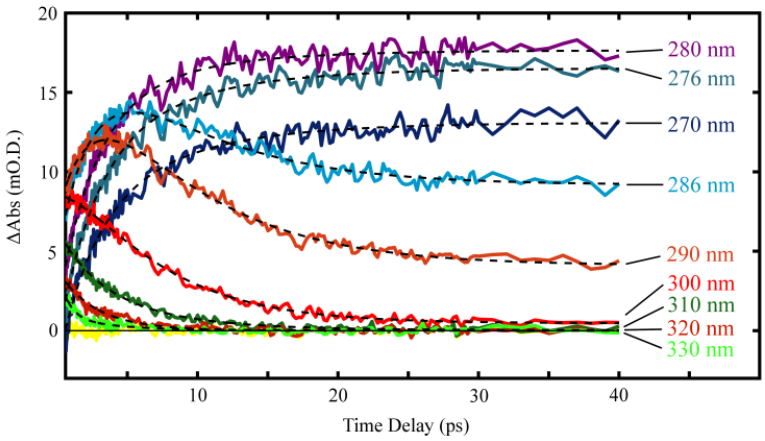

Figure 4.6: Kinetic traces across the transient absorption spectrum of α-phellandrene. The yellow curve is the residual for the fits. There is uncertainty in the intensity of the 270 and 276 nm traces due to low white light intensity to the blue of 277 nm.

The two components account for the decay of the initial peak and the rise of the steady state photoproduct difference spectrum. The time constant associated with the decay of the initial spectrum is fast relative to the rise component, with a decay constant of 2.5 – 3 ps depending on the solvent, while the slower component ranges from 6.5 – 9 ps. The decay components are free fitting parameters at each wavelength, and the overall decay becomes somewhat faster at the reddest wavelengths. Between 300 nm and 270 nm the rate constants are essentially wavelength independent. The faster rate of decay observed on the red side of the spectrum reflects thermal cooling of the initial hot photoproduct that accompanies conformational relaxation. Table 4.2 shows the average time constant obtained from the blue portion of the spectrum where the fitting parameters were constant. The data in methanol had significantly better signal to noise, and required a third sub-picosecond time constant to fit the data well. This time constant ranged from 0.6 ±0.2 ps at $\lambda < 280$ nm to 0.4 ±0.2 ps at redder wavelengths. The timescale of this component indicates that it may be associated with decay of the excited state, given its similarity to the timescale of the excited state absorption. The spectral behavior is also consistent with this assignment. The methanol data will be discussed in more detail below.

Quantum chemical calculations on CHD, α-PH, and photoproducts

TDDFT calculations were performed for CHD, a-PH and their photoproducts. The purpose of this calculation was to aid in the qualitative assignment of the ultrafast and steady state UV-Vis absorption measurements. Quantitative predictions cannot be expected within the limitations of the TD-DFT method and the level of theory employed. Nevertheless, relatively good agreement is found in the predicted absorption pattern and the spectral evolution observed in experiment.

DFT calculations were performed for CHD and for the gZg, cZt, and tZt rotamers of HT at the B3LYP level of theory with the 6-311++G(d,p) basis set. TD-DFT calculations predict a spectral pattern for the first singlet transitions which are qualitatively consistent with the observed spectral shifts for CHD and the relaxation from gZg-HT to tZt-HT observed in the ultrafast experiments and with earlier calculations.[16,24,28,29] The cZc photoproduct is predicted to absorb to the red of CHD. Conformer interconversion leads to a blue shift with the tZt rotamer having a higher frequency transition than CHD. Isomerization on the ground state proceeds through the cZc → cZt barrier of 5.4 kJ/mol and the cZt → tZt barrier of 10.5 kJ/mol.

Similar calculations were performed on α-PH and DOT with the same basis set mentioned above. The conformational minima and transition states of the α-PH photoproduct are depicted graphically in Figure 4.7. These structures were used for ground and excited state calculations. TD-DFT calculations were used to predict the spectral pattern expected for the formation of an all-cis triene photoproduct (gZg-DOT) and the shifts expected from its subsequent relaxation to the steady state photoproduct (tZt-DOT).

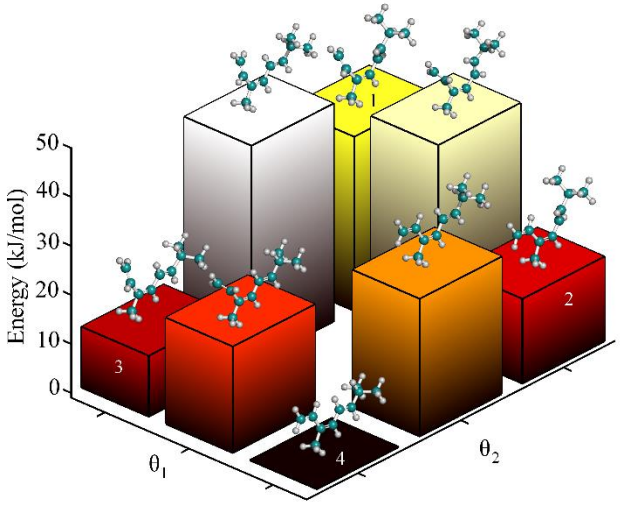

Figure 4.7: Transition states and barriers for the conformational relaxation of DOT. (1) gZg-DOT, (2) tZg-DOT, (3) gZt-DOT, (4) tZt-DOT

The TD-DFT results predict that the initial gZg-DOT photoproduct will absorb at a longer wavelength than α-PH. Isomerization through the spectrally overlapping gZt- and tZg-DOT conformers is predicted to result in a blue shift relative to gZg-DOT, and further isomerization to the steady state tZt-DOT rotamer should shift the spectrum bluer still. The tZt rotamer is predicted to absorb at the highest frequency of the DOT rotamers, though the center wavelength is still red-shifted with respect to α-PH. These predictions are completely consistent with the observed spectral shifts in the ultrafast and steady state UV-Vis absorption experiments. The predicted singlet transitions are given in Table 4.3.

Table 4.3: First singlet transition energies and the relative ground state free energies of the various conformations of HT and DOT. The ground state free energies for the HT and DOT conformers are given relative to the lowest energy tZt conformations respectively. Entries labelled 'a-b TS' are the transition states between conformer a and b.

Conformer	Calculated Oscillator Strength	Singlet Transition (nm)	ΔG (kJ/mol)
CHD	0.1186	268.57	-35.9
gZg-HT	0.1455	292.75	38.9
gZg-cZt TS	-	-	44.3
cZt-HT	0.4186	274.71	16.8
cZt-tZt TS	-	-	27.4
tZt-HT	0.8855	267.41	0
α-Phellandrene	0.0862	272.28	-20.6
gZg-DOT	0.1717	290.13	35.5
gZg-tZg TS	-	-	41.3
gZg-gZt TS	-	-	44.5
tZg	0.4888	283.36	17.3
gZt	0.3906	284.23	12.4
tZg-tZt TS	-	-	28.1
gZt-tZt TS	-	-	21.7
tZt-DOT	0.9755	280.27	0

Vibrational frequency calculations were used to predict the barrier height for isomerization between the various conformers of DOT by optimizing to energy minima and transition state geometries. These calculations show that the gZg conformation has the highest energy, while interconversion between the conformers proceeds through two decay channels (see Figure 4.1B), resulting in an overall decrease in free energy of ~38 kJ/mol for tZt relative to gZg. The two pathways have similar, but not identical energy barriers (Table 4.3). The calculated barriers are in good agreement with calculations previously reported by Marzec et al. The gZg-

DOT conformation relaxes through two barriers of 5.8 and 9 kJ/mol to tZg-DOT and gZt-DOT. These two conformations then further relax through barriers of 10.8 kJ/mol and 4.4 kJ/mol respectively to arrive at the steady state tZt form.

Discussion

Global comparison of excited state dynamics

The influence of steric substitution on the excited state dynamics of the CHD backbone was investigated by Garavelli *et al*. using *ab initio* calculations and transient ionization measurements.[18] It was found that the lifetime of the optically excited state was shortest for CHD and α-phellandrene and markedly longer for α-terpinene. These results led to the conclusion that the difference in the lifetime of the Franck-Condon wavepacket arose because of a mass effect on C1 and C4 (see numbering scheme in Figure 4.1), which decreases the momentum in the reactive ethylenic-stretch coordinate for α-terpinene. Our measurements on α-TP and DHC are consistent with this mechanism, though the measured lifetime for the α-PH ESA is not. α-TP and DHC both have C1 and C4 substitution, and appear to traverse the Franck-Condon region on a time scale of ~150 fs for α-terpinene and ~1 ps for DHC as evidenced by fluorescence measurements and ESA in ultrafast TA experiments (see Chapter 3).[26] Conversely, CHD leaves the Franck-Condon region in <50 fs, resulting in a very low fluorescence quantum yield and no excited state absorption. The lack of ESA may also be attributed to low oscillator strength for the $S_1 \rightarrow S_n$ transition.

The UV-visible transient absorption measurements of α-PH show an excited state absorption with very low oscillator strength relative to α-TP and DHC. We measured the fluorescence of a-PH on several occasions to determine the excited state lifetime. Although the data are insufficient for quantitative analysis, the lifetime of the a-PH excited state was

consistently estimated to be longer than the excited state lifetime of a-TP. The photoproduct appears in the TA on a time scale of ~350 fs as described below, but is limited by the time resolution in this wavelength range. Femtosecond time-resolved fluorescence measurements may be required to determine the excited state lifetime with the necessary accuracy to fully characterize the excited state decay, but would be extremely difficult given the low fluorescence quantum yield. Although the fluorescence lifetime in α-PH is undetermined, the visible excited state absorption signal provides another means of estimating the excited state lifetime. The single exponential fits shown in Figure 4.5 represent the global excited state lifetime for each molecule.

These ultrafast measurements combined with observations from integrated fluorescence present a picture that is in contrast to the mechanism proposed by Garavelli et al.[18] Gas phase measurements show a slowdown in the excited state for the 1,4- substituted α-TP relative to α-PH, but in solution the trend is reversed. It remains unclear why this might be, although few aspects of the solvent have been tested so far. It seems unlikely that solvent viscosity would have any effect on the minor structural rearrangement that occurs on the excited state, but polarity could be a factor.

The very low oscillator strength for the $S_1 \rightarrow S_n$ ESA of α-PH relative to α-TP is interesting considering the minor differences between the molecules. In a molecular orbital picture, the alkyl substitution is not significantly coupled to the pi bonding network that dominates the electronic transitions.[8] Since the mixing of the sigma orbitals from the alkyl groups with the pi orbitals is small, it is unlikely to perturb the electronic structure of the chromophore significantly. Nevertheless, it seems that the 1,4-substitution in α-TP allows for a large transition dipole moment for ESA, while the chiral 2,5-substitution in α-PH greatly

decreases the absorption to higher excited states. The ESA in α-TP is strong enough to measure an anisotropy value that is fairly constant around 0.25 (Figure 4). This is very similar to the value of 0.26 measured across the ESA of DHC.[7,30]

As a further note, the $S_0 \rightarrow S_1$ transition is also weakest for α-PH when compared with the 3 other dienes under consideration (see Figure 1.3). Symmetry considerations are likely at play, although detailed electronic structure calculations on the higher excited states are not available for these compounds at the time of writing. Clearly the location of unconjugated substitution on the ring can have a significant effect on the electronic structure of the CHD chromophore; an observation that has relevance for the design of functional molecules that rely on the CHD switching mechanism.

Global comparison of ground state dynamics

The conformational relaxation in HT has been studied extensively as a function of solvent and initial conformation.[16,19,23] The data presented here are in general agreement with the trends observed previously. The initial peak at 286 nm (Figure 4.3, top panels) represents the difference spectrum between gZg-HT and CHD. This assignment is supported by the TD-DFT calculations, which place the absorption spectrum of the initial photoproduct to the red of the more stable conformations. It is also consistent with earlier measurements that allowed for the formulation of basis spectra corresponding to both gZg-HT and cZt-HT.[16,24,29] The relaxation from gZg-HT to cZt-HT and tZt-HT is faster in alcohols than in alkanes (Table 4.2 and Figure 4.3) although the differences are smaller than deduced from measurements using single-wavelength probes.[16,19] A small residual peak at 290 nm in the transient difference spectra in alkanes (heptane shown in figure 4.8) is evidence for trapping of a small population of the cZt-HT rotamer as discussed by Harris *et al*.[19]

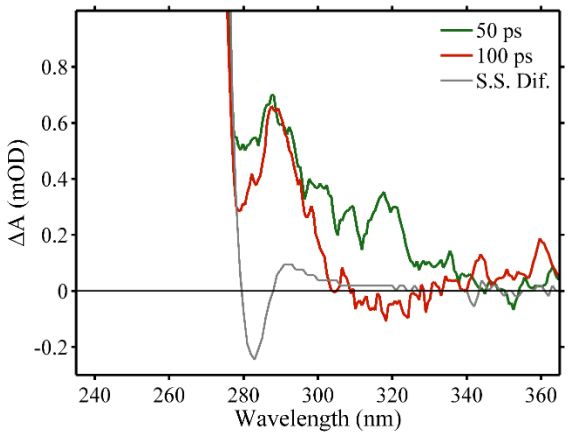

Figure 4.8: TA spectra of CHD in heptane at 50 ps and 100 ps. The peak is assigned to residual cZt-HT trapped as the molecule thermalizes. This population undergoes much slower relaxation to the ground state tZt-HT conformation.

The rotamer interconversion in DOT is qualitatively different than for HT, although it occurs on a similar time scale. Though the differences are slight, the interconversion proceeds faster in alcohols than in alkanes (Table 4.2). The initial peak in the TA spectra at 294 nm is assigned to the difference spectrum between gZg-DOT and α-phellandrene (Figure 4.3, bottom panels). The shift of the spectrum to shorter wavelengths is consistent with the spectral changes predicted by the TD-DFT calculations for isomerization to the tZt-DOT rotamer.

Despite the steric groups and comparable barriers for conformational isomerization, the overall relaxation of DOT is faster than that of HT. While one might expect that solvent interactions with the steric groups on DOT should lead to substantially more trapping of intermediate conformations, this is not observed. Notably, there is no spectral evidence for trapping of any residual gZt-DOT or tZg-DOT intermediate on short time scales or on longer time scales following excitation of α-PH. Comparison of the 20 ps difference spectra in Figure 4.3 (red lines) highlights these differences. The shoulder at 290 nm in HT requires substantial persistent population of the cZt conformer. The data for DOT shows a smooth transition from the initial photoproduct at 0.6 ps to the relaxed product at 50 ps. The calculations reported in

Table 4.3 provide no clear explanation for the observed differences. The barriers for conformational isomerization are comparable for HT and DOT (~10 kJ/mol), and the oscillator strengths of the gZt/tZg-DOT and cZt-HT conformations are similar suggesting that gZt/tZg-DOT should be apparent in the spectrum if populated at a significant level.

An earlier study by Harris *et al*. investigated the cZt-HT → tZt-HT reaction as a function of solvent using excitation of tZt-HT to produce a small residual population of cZt-HT.[19] The decay of this trapped population was measured as a function of temperature and a barrier and Arrhenius prefactor for isomerization deduced. The barrier is higher than calculated and is dependent on the nature of the solvent, 17.4 kJ/mol in alcohols and 23.5 kJ/mol in alkanes. The data obtained for the isomerization of cZt-HT is not easily explained by simple models for condensed phase reaction dynamics.[19] The current study of DOT again points to an anomaly in the behaviour of cZt-HT. The smooth relaxation of DOT and the absence of trapped population in the gZt-DOT or tZg-DOT conformations are consistent with the calculated barriers and with simple theories for condensed phase reaction dynamics. Sophisticated molecular dynamics simulations have identified specific aspects of the solvent that explain the trends in the HT rates, but have not been implemented on the bulkier HT derivatives.[31]

It is also informative to examine the similarities between the TA of α-PH and α-TP. A comparison of the UV transient absorption signals following excitation of α-PH and α-TP in methanol demonstrates that the transient spectra outside the region of the ground state absorption are essentially identical within a few hundred femtoseconds (Figure 4.9). The spectra were taken back to back under the same conditions with the concentrations adjusted to achieve the same absorbance at the excitation wavelength (266 nm). These data suggest that the spectrum of the

ground state gZg conformation is extremely similar for both compounds and that the ground state appears within 350 fs, the apparent upper limit for the excited state lifetime of α-PH.

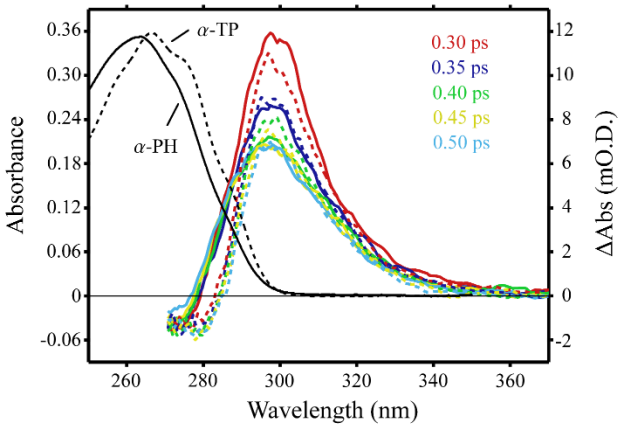

Figure 4.9: TA spectra obtained following excitation of α-PH (solid lines) and α-TP (dashed lines) in methanol. The experiments were run consecutively on samples with similar absorbance and the data are not scaled. The black curves are the steady state UV-Vis spectra.

The dynamics of each photoproduct also appear very similar. The gZg conformation returns to the ground state with a large excess of vibrational energy in both cases, resulting in a broad red edge in the TA. In the same methanol data set, the red tail in the spectrum of each molecule (gZg-DOT and gZg-IPMHT) match remarkably well, even after tens of picoseconds (Figure 4.10). This appears to be a strong indication of nearly identical cooling dynamics, as the narrowing of the spectrum over time is indicative of species in higher vibrational states cooling down or converting into other photoproduct conformations.

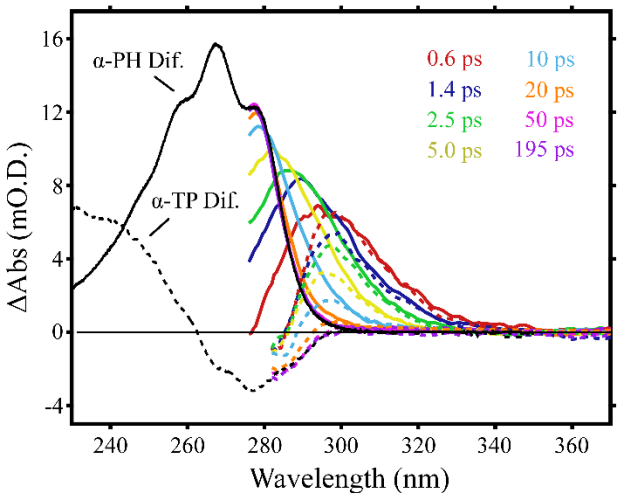

Figure 4.10: Steady state and ultrafast UV-Vis difference spectra following 266 nm excitation of α-PH (solid lines) and α-TP (dashed lines) in methanol. The steady state difference spectra are scaled to show the final photoproduct, athough the ultrafast probe does not cover the deeper UV wavelengths.

Conclusion

The aim of this study was to characterize the excited and ground state dynamics of α-phellandrene in solution and present this data in the broader context of the CHD chromophore and HT backbone dynamics. The excited state properties of the various dienes are discussed using fluorescence and ultrafast excited state absorption measurements. After the photoreaction, the conformational relaxation of the DOT photoproduct of α-PH was studied in multiple solvents with varying viscosity and hydrogen bonding capacity using UV transient absorption measurements and compared with the relaxation of similar HT derivatives. Quantum chemical calculations were used to predict the shifts in the UV-Vis spectra of the photoproducts to help in assignment of ultrafast TA and steady state photolysis measurements.

Unlike the substituted dienes, no visible excited state absorption was detected in TA experiments conducted on CHD. The very rapid relaxation out of the 1B potential surface to the 2A dark state or low oscillator strength could explain this. Previous studies have attributed the longer lifetime of the Franck-Condon region of electronically excited α-TP to a mass effect due

to the 1,4 substitution pattern.[18] Our comparison of α-TP and α-PH in solution appear to contradict this, although the prediction was made on the basis of gas phase calculations and experiments. Perturbation of the symmetry of the upper electronic states by the chiral substitution in α-PH could explain the 12-fold smaller ESA in the ultrafast experiments compared with α-TP. This is also likely given the similarity in the spectral profile when compared with that of α-TP.

The ground state conformational relaxation of IPMHT and Pre formed following excitation of α-TP and DHC respectively is confined to the gZg → tZg isomers (see discussion in Chapter 3). The gZg-IPMHT → tZg-IPMHT transition occurs on a time scale independent of bulk solvent properties like viscosity and polarity.[26] Similarly, the gZg → tZg isomerization of Pre shows a very weak dependence on bulk solvent viscosity despite its size and the presence of a hydroxyl group.[26] For both of these compounds, the conformational relaxation occurs on a ca. 5 – 8 ps timescale. In contrast HT and DOT approach an equilibrium population dominated by the tZt conformer, with the relaxation gZg → tZg → tZt on a ca. 6 – 10 ps timescale. The overall relaxation is somewhat faster in alcohols compared with alkanes. The similarity in the relaxation timescale is surprising given the difference in size of the four trienes studied as well as the difference in the conformational minima available to the molecules. The contrast between the relaxation of cZt-HT and gZt/tZg-DOT again points to an anomaly in the behaviour of hexatriene. Comparison of the gZg-IPMHT and gZg-DOT spectra indicate that the ground state spectrum of this hot HT moiety is not strongly dependent on the substitution on the ring. In addition, the redistribution of vibrational energy from the hot vibrational states and depletion of population of the gZg conformation match remarkably well between these two molecules. Drawing comparison between the bare CHD chromophore and chiral and achiral substituted

CHD derivatives allows for the development of an overall picture of what different alkyl substitution patterns will have on the excited and ground state dynamics.

Acknowledgements

This work has been supported by the National Science Foundation through Grant No. CHE-0718219 and CHE-1150660.

References

(1) Geppert, D.; Seyfarth, L.; de Vivie-Riedle, R. *Appl*. *Phys*. *B* **2004**, *79*, 987-992.

(2) Rangel, N. L.; Williams, K. S.; Seminario, J. M. *J*. *Phys*.*Chem*. *A* **2009**, *113*, 6740-6744.

(3) Conyard, J.; Addison, K.; Heisler, I. A.; Cnossen, A.; Browne, W. R.; Feringa, B. L.; Meech, S. R. *Nat*. *Chem*. **2012**, *4*, 547-551.

(4) Wang, J. B.; Feringa, B. L. *Science* **2011**, *331*, 1429-1432.

(5) Anderson, N. A.; Shiang, J. J.; Sension, R. J. *J*. *Phys*.*Chem*. *A* **1999**, *103*, 10730-10736.

(6) Fuss, W.; Hofer, T.; Hering, P.; Kompa, K. L.; Lochbrunner, S.; Schikarski, T.; Schmid, W. E. *J*. *Phys*.*Chem*. **1996**, *100*, 921-927.

(7) Tang, K.-C.; Rury, A.; Orozco, M. B.; Egendorf, J.; Spears, K. G.; Sension, R. J. *J*. *Chem*. *Phys*. **2011**, *134*, 104503.

(8) Deb, S.; Weber, P. M. *Ann*. *Rev*. *Phys*.*Chem*. **2011**, *62*, 19-39.

(9) Arruda, B. C.; Sension, R. J. *Phys*. *Chem*. *Chem*. *Phys*. **2014**, *16*, 4439-4455.

(10) Hofmann, A.; de Vivie-Riedle, R. *J*. *Chem*. *Phys*. **2000**, *112*, 5054-5059.

(11) Nenov, A.; Kolle, P.; Robb, M. A.; de Vivie-Riedle, R. *J*. *Org*. *Chem*. **2010**, *75*, 123-129.

(12) Schonborn, J. B.; Sielk, J.; Hartke, B. *J*. *Phys*.*Chem*. *A* **2010**, *114*, 4036-4044.

(13) Tapavicza, E.; Meyer, A. M.; Furche, F. *Phys*. *Chem*. *Chem*. *Phys*. **2011**, *13*, 20986-20998.

(14) Reid, P. J.; Doig, S. J.; Wickham, S. D.; Mathies, R. A. *J*. *Am*. *Chem*. *Soc*. **1993**, *115*, 4754-4763.

(15) Trulson, M. O.; Dollinger, G. D.; Mathies, R. A. *J*. *Chem*. *Phys*. **1989**, *90*, 4274-4281.

(16) Anderson, N. A.; Pullen, S. H.; Walker, L. A.; Shiang, J. J.; Sension, R. J. *J*. *Phys*.*Chem*. *A* **1998**, *102*, 10588-10598.

(17) Carroll, E. C.; Pearson, B. J.; Florean, A. C.; Bucksbaum, P. H.; Sension, R. J. *J*. *Chem*. *Phys*. **2006**, *124*, 114506.

(18) Garavelli, M.; Page, C. S.; Celani, P.; Olivucci, M.; Schmid, W. E.; Trushin, S. A.; Fuss, W. *J*. *Phys*.*Chem*. *A* **2001**, *105*, 4458-4469.

(19) Harris, D. A.; Orozco, M. B.; Sension, R. J. *J*. *Phys*.*Chem*. *A* **2006**, *110*, 9325-9333.

(20) Carroll, E. C.; White, J. L.; Florean, A. C.; Bucksbaum, P. H.; Sension, R. J. *J*. *Phys*.*Chem*. *A* **2008**, *112*, 6811-6822.

(21) Kim, J.; Tao, H. L.; White, J. L.; Petrovic, V. S.; Martinez, T. J.; Bucksbaum, P. H. *J*. *Phys*.*Chem*. *A* **2012**, *116*, 2758-2763.

(22) Kosma, K.; Trushin, S. A.; Fuss, W.; Schmid, W. E. *Phys*. *Chem*. *Chem*. *Phys*. **2009**, *11*, 172-181.

(23) Lochbrunner, S.; Fuss, W.; Schmid, W. E.; Kompa, K. L. *J*. *Phys*.*Chem*. *A* **1998**, *102*, 9334-9344.

(24) Pullen, S. H.; Anderson, N. A.; Walker, L. A.; Sension, R. J. *J*. *Chem*. *Phys*. **1998**, *108*, 556-563.

(25) Marzec, K. M.; Reva, I.; Fausto, R.; Proniewicz, L. M. *J*. *Phys*.*Chem*. *A* **2011**, *115*, 4342-4353.

(26) Arruda, B. C.; Peng, J.; Smith, B.; Spears, K. G.; Sension, R. J. *J*. *Phys*.*Chem*. *B* **2013**, *117*, 4696-4704.

(27) In *CRC Handbook of Chemistry and Physics*; 91st Edition (Internet Version 2011) ed.; Haynes, W. M., Ed.; CRC Press/Taylor and Francis: Boca Raton, FL.

(28) Pullen, S.; Walker, L. A.; Donovan, B.; Sension, R. J. *Chem*. *Phys*. *Lett*. **1995**, *242*, 415-420.

(29) Pullen, S. H.; Anderson, N. A.; Walker, L. A.; Sension, R. J. *J*. *Chem*. *Phys*. **1997**, *107*, 4985-4993.

(30) Tang, K. C.; Sension, R. J. *Farad*. *Disc*. **2011**, *153*, 117-129.

(31) Vazquez, F. X.; Talapatra, S.; Sension, R. J.; Geva, E. *J*. *Phys*.*Chem*. *B* **2014**, *118*, 7869-7877.

Chapter 5

Photochemistry of 7-dehydrocholesterol in liposomal models of biological membranes

Introduction

Vitamin D_3 (VitD) is a hormone crucial for regulation of calcium metabolism in many organisms, a mechanism that dates back at least 750 million years to marine phytoplankton.[1] Biological VitD photosynthesis can be simplified into a process with a photochemical activation step followed by thermal formation of the vitamin. The photosynthetic step takes advantage of the 1,3-cyclohexadiene (CHD) chromophore embedded within the rigid steroid skeleton of 7-dehydrocholesterol (DHC). DHC resides in the cutaneous tissue of mammals, as a component of the cell membrane. Exposure of DHC to UVB radiation from the sun results in an electrocyclic ring-opening of the CHD chromophore to form a 1,3,5-hexatriene photoproduct, previtamin D_3 (Pre). The previtamin is vibrationally hot on return to the ground state, and forms in the relatively unstable gauche-Z-gauche (gZg) conformation. In solution, Pre can undergo rotational isomerization and thermalization on a 10 ps timescale to reach the tZg-Pre minimum, which dominates the population of Pre at equilibrium (Figure 5.1).[2] This process has been extensively discussed in chapters 1, 3, and 4.

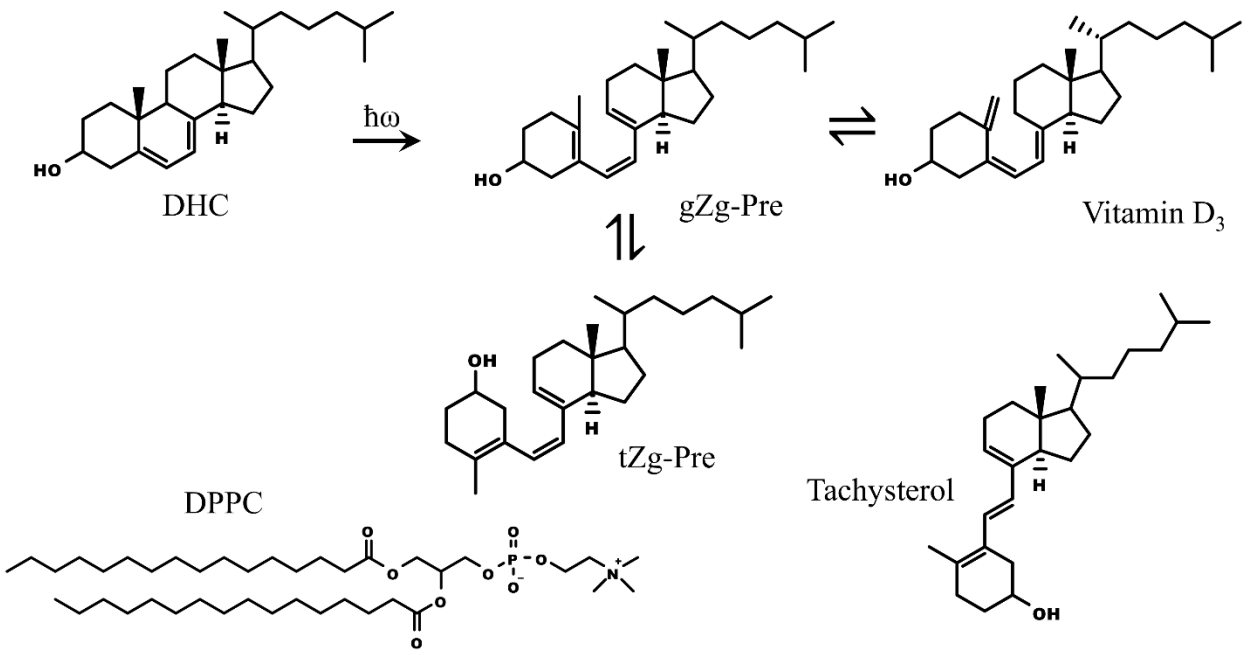

Figure 5.1: Structures of the major conformers involved in the synthesis of Vitamin D_3. The ultrafast measurements probe only DHC and the conformations of Pre. Tachysterol is a secondary photoproduct produced after irradiation of Pre in steady state measurements (Figure 5.3 B Inset). DPPC is the phospholipid used to make the liposomes in these experiments.

The complex interaction between sterols such as cholesterol or DHC and lipid bilayers is a well-documented area of intense research. The observation of strong influences on the properties of lipid bilayers as a result of sterol content has led to the refinement of the fluid mosaic model of the cell membrane.[3-9] It is now recognized that the formation of so-called lipid rafts, domains with specific lipid, protein, and sterol composition, must be taken into account. These domains serve to restrict lateral diffusion within the bilayer, and maintain order in the complex chemical machinery at the cell membrane–cytoplasm interface.

Incorporation of Cholesterol (Chl), DHC, and other loads into lipid bilayers is known to impact both the structural and dynamic properties of the membrane and surrounding hydrophobic hydration layer as observed through anisotropy measurements of fluorescent probes[10,11], melting point analysis, solubility experiments[12], microscopy, ultrafast methods[13-15], molecular

dynamics[16,17] and single-molecule techniques[18]. The observed changes in the membrane's physical properties are a function of the sterol and lipid identity and their relative concentrations.

C. Bernsdorf and R. Winter used the fluorescence anisotropy of a reporter molecule to investigate the trends in the membrane ordering at a range of temperatures and increasing sterol concentration.[11] In the gel phase of DPPC ($T < T_m \approx 41.5$ °C), addition of 10 mol% Chl to the liposome decreases the anisotropy of the probe, which correlates with a decrease in structural order. Higher concentrations of Chl (up to 50%) serve to increase the structural order, but the anisotropy is never restored to the original value. Addition of DHC to a DPPC liposome monotonically decreases the ordering of the lipids for concentrations of 10 – 50 mol%.[11] For temperatures greater than the gel to liquid crystalline phase transition (chain melting point) of 41.5 °C, addition of sterols has a significant effect on the bilayer, nearly always increasing the anisotropy of the reporter molecule and the structural order by a significant amount with respect to the changes observed in the gel phase. While many reports show similar effects on different bilayer systems, an area of relatively little exploration is the impact these rigid and structurally ordered domains have on the photochemistry of DHC, and the subsequent conformational changes that the photoproduct undergoes.

The thermal conversion of Pre into VitD occurs exclusively from gZg-Pre (Figure 5.1). This conformation sensitive process involves a hydride shift within the hexatriene backbone to form the vitamin. Investigation of the thermal process has yielded interesting results relating to the stabilization of the thermally active gZg conformation in rigid environments. X. Q. Tian et al. characterized the environmental dependence of the rate of VitD formation from gZg-Pre.[19,20] It was found that when Pre was photochemically formed, the rate of gZg-Pre ⇌ VitD thermal isomerization was enhanced by an order of magnitude in human skin ($t_{1/2}$ = 2.5 h) with respect to

bulk hexane or disordered lipid solution ($t_{1/2}$ = 30 h). A mechanism was proposed whereby hydrogen bonding between the –OH group on Pre and the ester portion of the lipid molecule stabilized the gZg-Pre conformation as well as the transition states between Pre and VitD (Figure 5.2). While this hypothesis is consistent with the experiments, no structural data has been obtained on gZg-Pre embedded in a lipid membrane to confirm. While investigating different rigid environments, the same group found that β-cyclodextrin complexation of Pre can also lower the gZg-Pre ⇌ VitD equilibrium constant by a factor of 12, as well as increase the rates of both the forward and reverse reaction.[21]

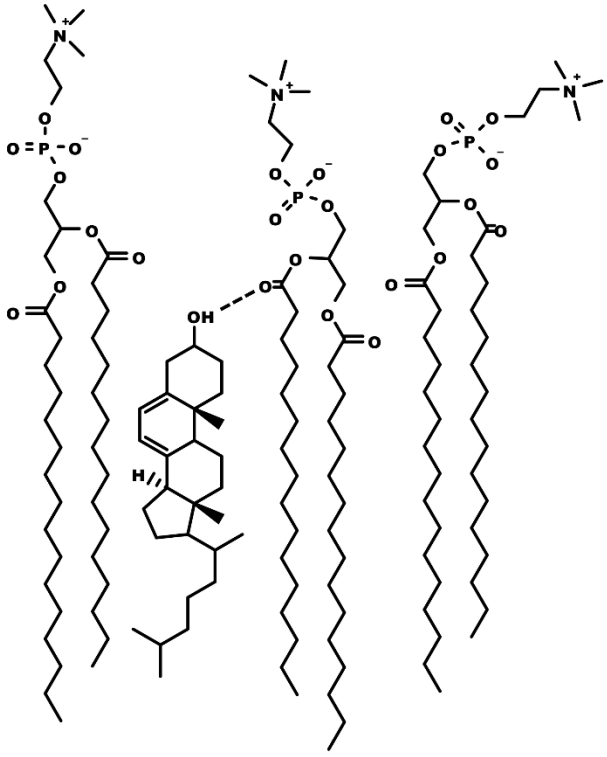

Figure 5.2: Interaction proposed by X. Q. Tian et al. to explain the 10-fold increase in rate of VitD formation in DPPC liposomes.[20] Hydrogen bonding from DHC, and the ring-open Pre photoproduct keeps the orientation of the OH group facing the headgroups of the lipids.

Here we present the first experiments on the dynamics and photochemistry of DHC in a liposome model for the biological cell membrane using ultrafast broadband transient absorption (TA) spectroscopy in the UV-visible spectral region. We use a 1,2-dipalmitoyl-sn-glycero-3-

phosphocholine (DPPC – see Figure 5.1) liposomal model of the cell membrane; a small unilamellar vesicle selected for ease of implementation with the ultrafast laser system. The spherical bilayer vesicles are single walled liposomes on the order of 100 nm in diameter, and contain an enclosed aqueous region. DPPC lipids (16 carbons on the lipid chain) are used as the liposome formers to be directly comparable to past experiments probing the Pre ⇌ VitD reaction mentioned.[19,20] Liposomes hold specific advantages over other membrane models for integration into the TA instrument. Since DHC is insoluble in aqueous solution, when the vesicles are suspended in H_2O, all of the DHC is incorporated into the bilayer of the vesicles. In addition, the relatively small size of the liposomes helps to reduce scattering that increases background and reduces signal to noise, especially in the UV spectral region. Finally, the liposomes suspended in water are amenable to a flow cell sample scheme, eliminating contributions from photoproduct buildup in the probed volume.

Results

Steady state UV-visible absorption and photolysis

All of the experiments presented here are conducted at room temperature, below the gel to liquid-crystal phase transition for DPPC. The spectrum of DHC in a DPPC liposome is shown in Figure 5.3 A. The DHC spectrum sits on top of a background that closely resembles a λ^{-4} Rayleigh scattering spectrum. The distribution of liposome sizes causes slight deviation from the ideal Rayleigh spectrum (gray curve in figure). Photolysis measurements produce a difference spectrum similar to those obtained in bulk (Chapter 3), but with a small negative deviation in the baseline around 325 nm (Figure 5.3 B). This negative signal is also seen in the transient difference spectrum and will be discussed below. The steady state difference spectrum is generated after 15 seconds of irradiation. Other photoproduct pathways such as cis-trans

isomerization of the central double bond in Pre to form tachysterol (Figure 5.1) begin to contribute after longer irradiation periods (Figure 5.3 B Inset).[22]

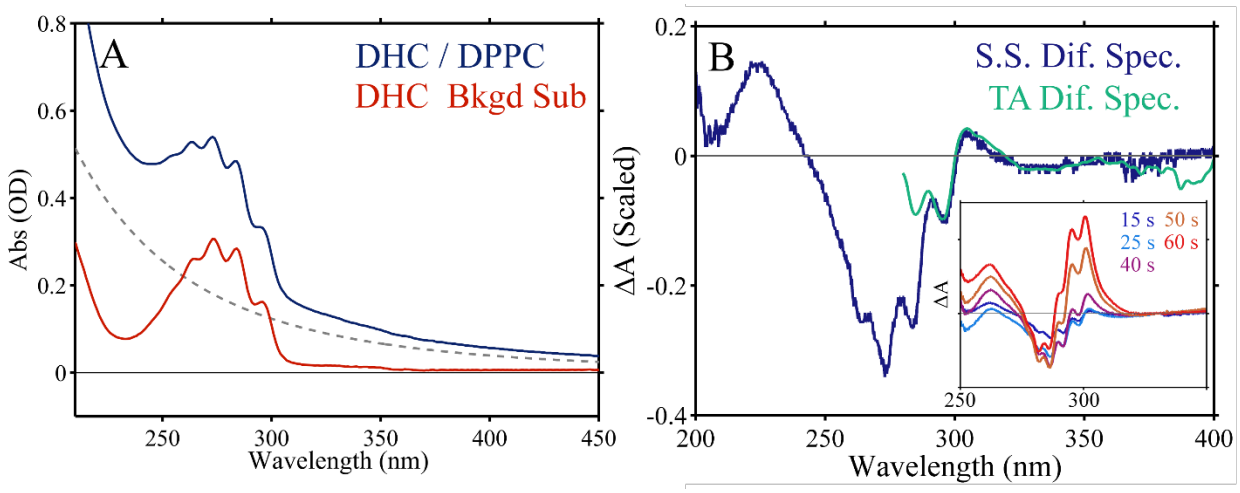

Figure 5.3: A: UV-Vis absorption of DHC in a DPPC liposome. The gray line is a scaled λ^{-4} Rayleigh scattering background, and the red curve is the spectrum with the background subtracted. B: Steady state difference spectrum between DHC and the Pre photoproduct following 15 s of UV photolysis. At long times in the TA, all features in the difference spectra are in agreement. Inset: Buildup of other photochemical products as the mixture of DHC and Pre is irradiated.

Visible continuum transient absorption of 40 mol% DHC in DPPC liposomes

The first experiments utilized an 800 nm white light probe to take advantage of the stability of the continuum and minimize the contribution of scattering to the noise. This probe covers the excited state absorption (ESA) of DHC, and the time dynamics observed originate solely from the excited state. A high loading concentration was used initially (40 mol%) in order to maximize the transient signal by increasing the concentration of absorbers in the probe beam. Figure 5.4 A shows the transient absorption of the DHC excited state in a DPPC liposome.

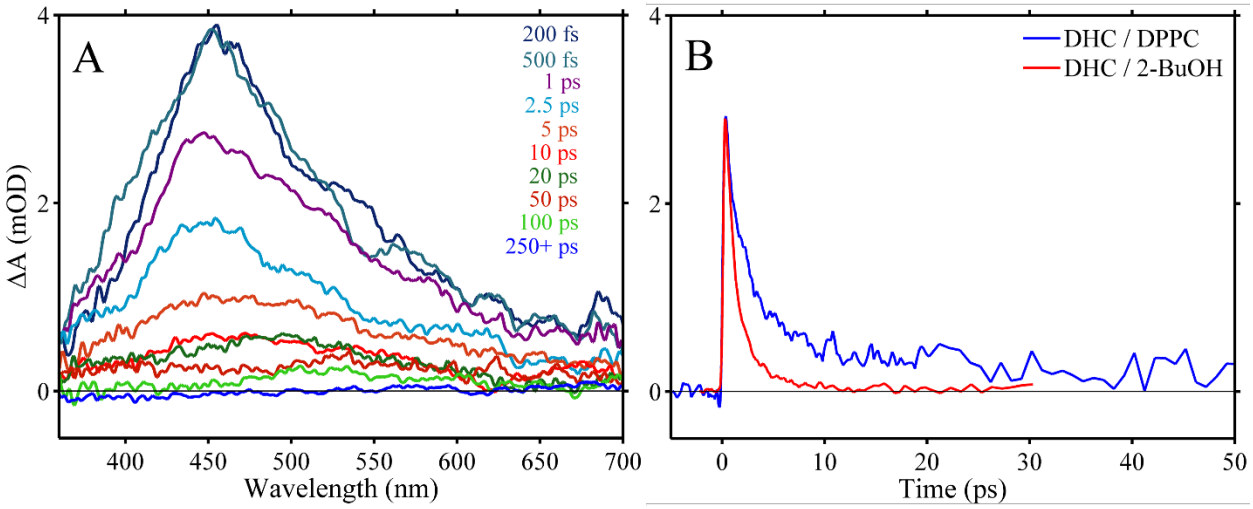

Figure 5.4: A: Transient absorption of 40 mol% DHC in a DPPC liposome. B: Kinetic lineouts of the integrated ESA comparing the excited state lifetime in bulk 2-butanol solution with that in a liposome.

The shape of the spectrum is similar to previous measurements in bulk solution discussed in chapters 1, 3, and 4. However, the time dynamics are significantly lengthened relative to the bulk measurements. The kinetic trace in Figure 5.4 B shows a comparison between the integrated lineouts of the ESA in DPPC liposome vs bulk 2-butanol solution. In this liposome measurement, care was taken to reduce the power of the pump enough to obtain a TA with minimal solvent background signal. This reduces the magnitude of the sample signal and decreases signal to noise, but shows conclusively that all of the transient signals and their dynamics originate from the DHC rather than a background associated with the vesicle.

UV continuum TA of DHC / Cholesterol mixtures in DPPC liposomes

Liposomes with three different loading concentrations were used to probe the effect of membrane structure on the DHC and Pre dynamics. The overall spectral shapes are similar, but the background (constant offset in the TA) at long time delays is very sensitive to the laser characteristics such as pump spot size and energy. A solvent background is not unusual for experiments utilizing the 266 nm pump and UV white light probe, but the background for liposomes is larger and harder to avoid than is typically observed in bulk for the same pulse

energies. Scans of Chl / DPPC liposomes were taken for each experiment to as a metric for estimating the background contributions. Differences between the spectral shapes are attributed to the changing background in each experiment. During global analysis, the background is fit at long times, and the region of the spectrum where no photoproducts absorb (ca. 450 – 600 nm) can be set to zero difference absorption. UV TA spectra of a liposome sample loaded with 30 mol% DHC, 50 mol% DHC, and mixed 30/20 mol% of DHC/Chl are shown in Figure 5.5 A, B, and C respectively.

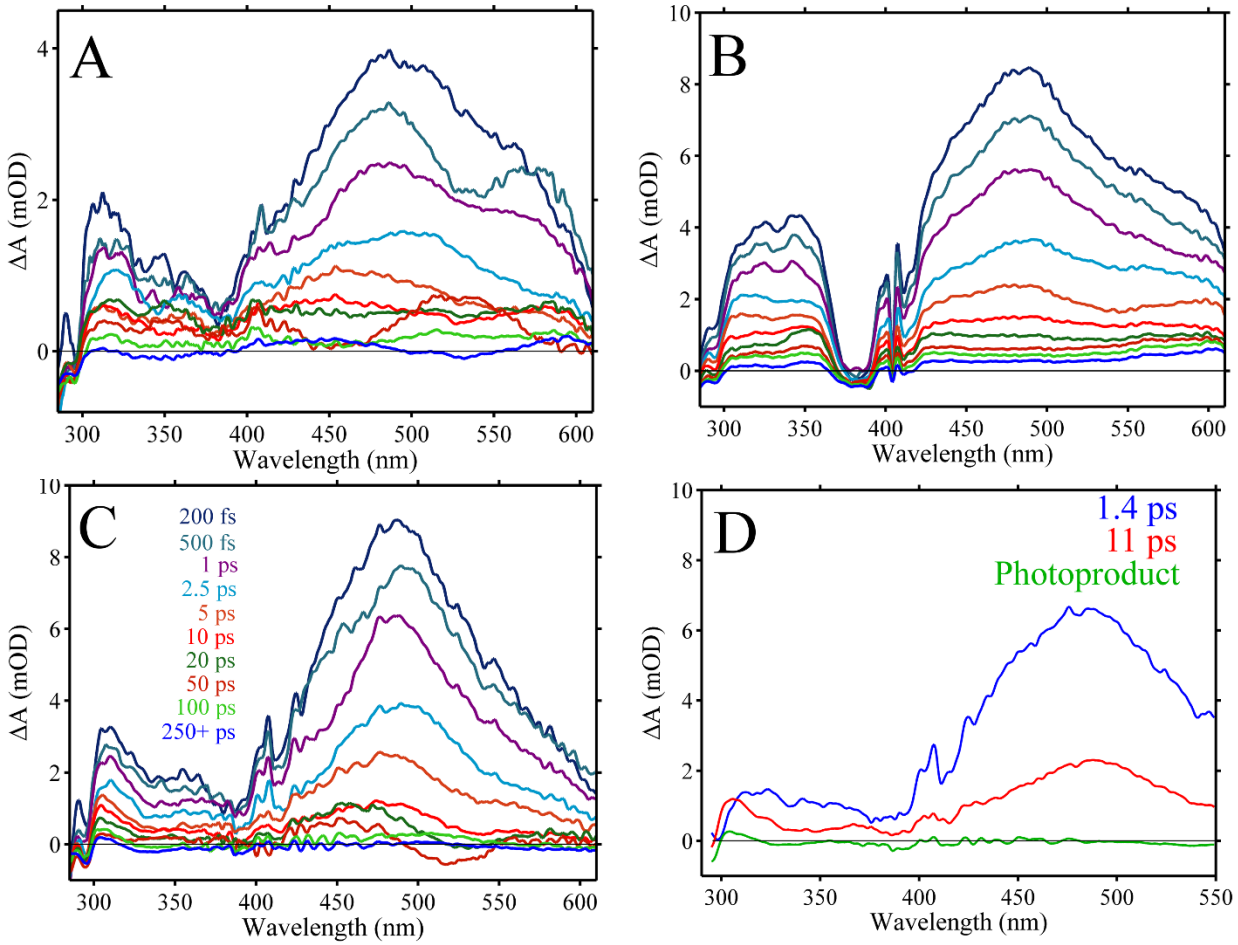

Figure 5.5: Transient difference spectra of DHC obtained with a UV continuum. The loading concentrations are A) 30% DHC, B) 50% DHC, and C) 30/20% DHC/Chl. Prominent bands for the ESA (~490 nm), photoproduct (~310 nm), and ground state bleach (< 300 nm) can be seen. D: Decay associated difference spectra obtained after globally fitting the TA in C.

The strong excited state absorption is seen clearly in the visible portion of the spectrum, and the peak at 310 nm reflects the initial gZg-Pre photoproduct as discussed in chapters 3 and 4. The time dynamics of the spectral evolution were fit using the Glotaran analysis program. Consistent fits were obtained using two exponential components and a constant offset for the photoproduct. The decay associated difference spectrum (DAS) for the mixed DHC/Chl TA experiment is shown in Figure 5.5 D. Representative kinetic traces for the TA experiment in Figure 5.5C with fits are shown below in Figure 5.6. Time constants for fits of all of the data presented here are shown below in Table 5.1. In general, the time constants are significantly lengthened with respect to bulk solution (Table 3.3).

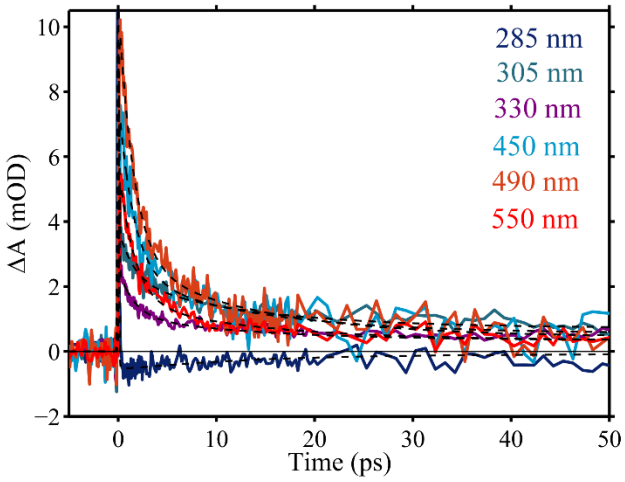

Figure 5.6: Kinetic traces of the 30/20% DHC/Chl loaded liposome. The decay is biexponential, with time constants of 1.6 and 13 ps for this experiment.

Table 5.1: Summary of time constants for the ultrafast experiments on DHC in liposomes. Each experiment also required an amplitude to account for the background offset. The continuum column indicates the fundamental laser wavelength used to generate the white light continuum probe for the particular experiment.

Sterol Loading		Time Constants			
DHC (mol%)	**Chl (mol%)**	**τ_1 (ps)**	**τ_2 (ps)**	**τ_3 (ps)**	**Continuum (nm)**
20	0	1.5	14		800
		1.0	5.0	65	800
30	0	1.7	41		400
		0.88	4.0	48	800
40	0	2.1	47		800
50	0	1.5	18.6		400
		0.91	5.0	130	800
30	20	1.6	13		400

Discussion

Excited state dynamics of DHC in the liposome environment

Previous measurements on DHC in bulk solution showed only minor changes in the kinetic components of the ESA.[23,24] The spectrum decays with two exponentials; a fast ~300 - 500 fs timescale, and a slower ~1 – 2 ps timescale, both of which depend on the solvent. The solvation microenvironment plays a role in the relative magnitudes of each component as well, with the fast piece ranging from half to equal in magnitude compared with the slower timescale. While these observations are statistically significant, the change in the kinetics is minor in comparison to the slowdown shown above for the liposome. Of the bulk solutions studied, 2-butanol presents the slowest dynamics with a timescale of 560 fs and 1.8 ps, while the liposomes give excited state lifetimes as low as 11 ps and as high as 56 ps when fit with a biexponential model.[24] Some data sets with better signal to noise require a third component to account for a

long timescale decay in the baseline, and it is unclear at this time whether this originates from the DHC absorption or a non-linear background signal from the lipid molecules. In either case, the rates accounting for the DHC excited state signal (τ_1 and τ_2) are elongated with respect to bulk solvents.

The bi-exponential nature of the excited state in bulk solution is explained by a parallel pathway forming two distinct excited state populations. These populations could correspond to ring distortions along separate coordinates as the reaction proceeds along the general reaction pathway for the CHD chromophore shown in Figure 1.3. In CHD the different torsions are degenerate, but due to the asymmetry of the DHC substitution, the degeneracy along each pathway is broken. Tapavicza et al. also propose that the parallel pathways could explain the ca. 30% quantum yield for ring opening[25], where one pathway is reactive and the other relaxes to the DHC ground state.[26] The major conformational changes in DHC as it reacts in the excited state consist of CHD ring torsions and associated movement of the steroid rings nearest the CHD chromophore. The observation of a ca. 1.5 ps component in the excited state absorption in liposomes may represent the average timescale of "bulk-like" DHC, while the longer time constant corresponds to a sub-population in a constrained environment. The fast component (1.5 to 2 ps) could be a combination of a sub-picosecond piece and a ca. 2 ps piece. Due to the highly scattering nature of the liposome samples, the signal to noise is not sufficient to distinguish between the two. It is clear that in DPPC there is a long component that is not observed in isotropic solution.

Two factors of the liposome environment could explain the long timescale for the reaction along this pathway. The hypothesis mentioned above that hydrogen bonding with the lipid head group restrains or otherwise stabilizes some conformations could certainly play a role

(Figure 5.2).[20] While DHC has been studied in a range of alcohol solvents capable of hydrogen bonding, the solvation structure of the bulk solution is neither rigid nor ordered. The DHC molecules in the liposome are oriented with the hydrophilic OH group facing the phosphatidylcholine head group. The hydrogen bond is proposed to form between the OH group on DHC and the ester portion of the phospholipid. Unlike bulk alcohol solution, the H-bond recipient (the lipid headgroup) is constrained in place in the self-assembled bilayer. Free diffusion plays no role in the equilibrium constant for the H-bonded complex. In this instance it is the thermodynamically favorable self-assembly of the bilayer that maintains the hydrogen bonding with DHC.

In addition, the liposome environment is not isotropic. The bulk of the hydrophobic portion of DHC is oriented collinearly with the alkyl tails in the bilayer. In the gel phase, DHC content has the effect of disordering the tails, but nevertheless, the interior of the liposome must conform to more stringent requirements for the orientation and packing of the tails compared with bulk solvents.[11,20] It is possible that the contortions of the diene system that DHC undergoes on the excited state surface are hindered by the relatively rigid packing of the lipid tails. This would have the effect of slowing down the excited state trajectory as it approaches the conical intersection with the ground state.

Loading of the liposome with different sterol concentrations has a dramatic effect on the order and rigidity of the lipid environment around the DHC molecule, which appear to affect the rate of relaxation in turn. The slowest timescale for relaxation is found in the 30 mol% DHC liposome (Table 5.1). This loading concentration adds the least disorder to the lipid chains, allowing the membrane to remain relatively rigid.[11] The higher loading concentrations are thought to be more disordered, and the observed rate of relaxation is lower. The difference

between the mixed 50% loading and the pure DHC 50 mol% can be explained by the difference in the structural perturbations to the membrane between these sterols.[11,16] Relaxation is slowest in the 30 mol% DHC liposome, faster with 50mol% DHC, and faster still when Chl is co-dissolved with DHC at a total of 50 mol%. The general trend of increasing rate of relaxation with increased loading roughly correlates with the trend of decreasing structural order in DPPC liposomes observed by Bernsdorf and Winter.[11] Clearly the relaxation process of DHC is sensitive to the local structure of the liposome.

Photoproduct conformational dynamics and equilibrium in the liposome environment

In a biological system, the important constraint in the synthesis of VitD is the equilibrium constant for gZg-Pre ⇌ tZg-Pre as VitD is formed strictly from the gZg isomer. In bulk solution this equilibrium constant is quite large, with nearly all of the Pre relaxing to tZg.[22,26] In the ultrafast regime, we observe the depletion of the gZg population (correlated with the depletion of the peak around 310 nm) and the establishment of the conformational equilibrium. At early time delays, this photoproduct peak likely corresponds to pure gZg isomer, as the excited molecule returns to the ground state in this conformation. At equilibrium, the residual peak around 310 nm seen in the stead state photolysis in bulk (Figure 3.8), and in the liposome (Figure 5.3 B), contains contribution from both gZg-Pre as well as overlapping absorption from tZg-Pre. The spectra of each isomer are broad and overlap significantly with each other and the DHC absorption.[22] High level computational techniques as well as quantitative fluorescence analysis suggest that the absorption spectrum of equilibrated Pre contains overlapping contribution from both isomers at all wavelengths, although gZg-Pre has a higher extinction coefficient with respect to tZg-Pre at low frequencies.[26]

X. Q. Tian et al., used both a kinetic and thermodynamic analysis to show that the rate of forward reaction from gZg-Pre to VitD increases by an order of magnitude in liposomes and human skin when compared to bulk hexane solvent.[19,20] Hydrogen bonding with the head groups as a means of stabilizing the "cholesterol-like" gZg-Pre conformation (shifting the gZg-Pre ⇌ tZg-Pre equilibrium) was used to explain this observation. Based on a unimolecular rate law that is first order in [gZg-Pre], a 10 fold increase in the rate of gZg-Pre → VitD implies a 10-fold increase in the equilibrium population of gZg-Pre. In solution, the equilibrium constant for the gZg-Pre ⇌ tZg-Pre equilibrium is extremely high, approaching complete conversion to the tZg-Pre conformation. If the equilibrium fraction of gZg in solution were on the order of 1%, a shift to 10% in the liposome should be detectable in steady state UV-Vis and TA. However, an increase from 0.1% to 1% would not be detectable in either case. Our results suggest then that if there is a change in population of the gZg conformation in the liposome, then the change in the photoproduct peak is below the noise threshold of these measurements.

The residual negative signal seen in the steady state difference spectrum and at long time delay in TA around ~325 nm is an important point. The sign of the signal indicates a permanent decrease in the sample absorption after the photochemical reaction. This could originate from a new lower lying electronic absorption appears when DHC is packed closely with the lipids or stacked with other DHC molecules. In this case, the negative signal would originate from a ground state bleach that remains at long time delay because of the formation of photoproduct. The spectral position is outside of the absorption range of both DHC and Pre in bulk solution. An alternative hypothesis is that its origin may be from a permanent change in the scattering background induced by the ring-opening of DHC. A decrease in the scattering background would correspond to loss of scattering species, and raises the possibility that some liposomes are

destroyed, split apart, or permanently structurally perturbed as a result of the photoexcitation, although the peak-like shape of the spectrum casts some doubt on this hypothesis. A change in the scattering background would most likely be observed to occur across the entire spectral range (see figure 5.3A), not just an isolated region near the DHC absorption.

Conclusion

The goal of these experiments was to understand how the photochemical process of formation of Previtamin D_3 occurs in a DPPC liposome model for the cell membrane. While spectroscopic methods in bulk solution provide an excellent starting point for understand biologically relevant processes, it is well known that the unique and crowded environments in biological systems can often have dramatic effects on various aspects of a reaction. We used ultrafast transient absorption to characterize the excited and ground state dynamics of DHC and its photoproducts in liposomes loaded with different concentrations of DHC and Chl. These experiments tested both the dependence of the excited state lifetime and the ground state conformational equilibrium on the internal structure of the liposome.

The longest component in the excited state decay in DHC is more than an order of magnitude longer in liposomes when compared with bulk solution. The rigid structure of the liposome likely leads to hydrogen bonding with the lipid headgroups, as well as tight packing with the alkyl chains that slow the approach to the S_1 / S_0 conical intersection. Movement towards this intersection involves motion along coordinates that would perturb the hydrogen bonding as well as the bulky steroid skeleton of the DHC molecule. The excited state dynamics appear to be longest in liposomes that are less loaded with sterol (30 and 40 mol% DHC) than in the higher concentrations (50 mol% loading). This correlates with previous experiments that showed that the structural order of the liposome is decreased at higher sterol concentrations.[11]

On return to the ground state, the gZg-Pre conformation relaxes to more stable conformations, dominated by tZg-Pre. While we observe no change in the long-time spectrum of the equilibrated Pre ensemble, we argue that this does not necessarily indicate that no change in the equilibrium amounts of each isomer has occurred. The peak in the difference spectrum that reports on the steady state ensemble is weak in these experiments, and a change in the relative concentrations of the spectrally overlapping gZg- and tZg-Pre conformations may not be observable. The kinetic component corresponding to the photoproduct peak appears to be limited by the decay of the overlapping ESA in this region. Previous experiments by other groups have shown that the thermal step in the synthesis of Vitamin D_3 is highly influenced by the rigid environment imposed by a liposome or cell membrane. Our experiments report the first observations that the photochemistry is also affected by the structure of the lipid membrane. These experiments point toward many new avenues of research that may answer important questions about how Vitamin D_3 precursors in biological systems behave, which will be discussed in Chapter 6.

References

(1) Holick, M. F. *Journal of Cellular Biochemistry* **2003**, *88*, 296-307.

(2) Arruda, B. C.; Peng, J.; Smith, B.; Spears, K. G.; Sension, R. J. *J. Phys.Chem. B* **2013**, *117*, 4696-4704.

(3) Singer, S. J.; Nicolson, G. L. *Science* **1972**, *175*, 720-&.

(4) Ahmed, S. N.; Brown, D. A.; London, E. *Biochemistry* **1997**, *36*, 10944-10953.

(5) Simons, K.; Ikonen, E. *Nature* **1997**, *387*, 569-572.

(6) Xu, X. L.; London, E. *Biochemistry* **2000**, *39*, 843-849.

(7) Xu, X. L.; Bittman, R.; Duportail, G.; Heissler, D.; Vilcheze, C.; London, E. *Journal of Biological Chemistry* **2001**, *276*, 33540-33546.

(8) Engelman, D. M. *Nature* **2005**, *438*, 578-580.

(9) Lingwood, D.; Simons, K. *Science* **2010**, *327*, 46-50.

(10) Bernsdorff, C.; Wolf, A.; Winter, R. *Zeitschrift Fur Physikalische Chemie-International Journal of Research in Physical Chemistry & Chemical Physics* **1996**, *193*, 151-173.

(11) Bernsdorff, C.; Winter, R. *J. Phys.Chem. B* **2003**, *107*, 10658-10664.

(12) Chen, C.; Tripp, C. P. *Biochimica Et Biophysica Acta-Biomembranes* **2012**, *1818*, 1673-1681.

(13) Kel, O.; Tamimi, A.; Thielges, M. C.; Fayer, M. D. *J. Am. Chem. Soc.* **2013**, *135*, 11063-11074.

(14) Osborne, D. G.; Dunbar, J. A.; Lapping, J. G.; White, A. M.; Kubarych, K. J. *J. Phys.Chem. B* **2013**, *117*, 15407-15414.

(15) Kel, O.; Tamimi, A.; Fayer, M. D. *Proc. Natl. Acad. Sci.* **2014**, *111*, 918-923.

(16) Rog, T.; Vattulainen, I.; Jansen, M.; Ikonen, E.; Karttunen, M. *J. Chem. Phys.* **2008**, *129*.

(17) Khelashvili, G.; Rappolt, M.; Chiu, S.-W.; Pabst, G.; Harries, D. *Soft Matter* **2011**, *7*, 10299-10312.

(18) Eggeling, C.; Ringemann, C.; Medda, R.; Schwarzmann, G.; Sandhoff, K.; Polyakova, S.; Belov, V. N.; Hein, B.; von Middendorff, C.; Schoenle, A.; Hell, S. W. *Nature* **2009**, *457*, 1159-U1121.

(19) Tian, X. Q.; Holick, M. F. *Journal of Bone and Mineral Research* **1996**, *11*, T480-T480.

(20) Tian, X. Q.; Holick, M. F. *Journal of Biological Chemistry* **1999**, *274*, 4174-4179.

(21) Tian, X. Q.; Holick, M. F. *Journal of Biological Chemistry* **1995**, *270*, 8706-8711.

(22) Redwood, C.; Bayda, M.; Saltiel, J. *J. Phys. Chem. Lett.* **2013**, *4*, 716-721.

(23) Tang, K. C.; Sension, R. J. *Farad. Disc.* **2011**, *153*, 117-129.

(24) Tang, K.-C.; Rury, A.; Orozco, M. B.; Egendorf, J.; Spears, K. G.; Sension, R. J. *J. Chem. Phys.* **2011**, *134*, 104503.

(25) Havinga, E.; Dekock, R. J.; Rappoldt, M. P. *Tetrahedron* **1960**, *11*, 276-284.

(26) Tapavicza, E.; Meyer, A. M.; Furche, F. *Phys. Chem. Chem. Phys.* **2011**, *13*, 20986-20998.

Chapter 6

Conclusions and outlook

The goal of understanding photochemistry in model systems and using environmental and optical stimuli to change the outcome of photochemical events is a field with a great breadth of research. The projects described here have largely focused on the variables of chemical substitution around a chromophore and the solvation environment around the whole molecule. Understanding how steric substitution affects the photochemistry of this highly relevant chromophore will guide the design of future molecular switching motifs. In addition, development of experimental methods that probe molecular processes in biologically relevant environmental conditions serve to more accurately inform how photobiological processes occur in organisms where the molecular environment can be crowded and anisotropic.

The earliest experiments I conducted are presented in chapters 3 and 4. These experiments tested a variety of factors that contribute to the understanding of the 1,3-cyclohexadiene (CHD) ring-opening reaction. First, the role of chemical substitution on the CHD ring was explored by using ultrafast spectroscopy to determine the electronic states, conformations, and associated timescales in the ring opening of the 1,4- substituted α-terpinene (α-TP) and the 2,5- substituted α-phellandrene (α-PH). By comparison with the transient absorption of CHD and 7-dehydrocholesterol (DHC), these experiments showed that the relative energies and stable conformations are greatly affected by this small change in substitution pattern on the CHD ring.

α-TP appears to behave very similarly to 7-dehydrocholesterol in terms of the strong excited state absorption (ESA) and conformational relaxation of the photoproduct. Conversely, α-PH and CHD behave significantly differently. While α-PH has an ESA similar in shape to α-TP, it is roughly 12 times weaker in strength. This observation points to a change in the symmetry of the upper electronic state participating in the absorption resulting from the change in the position of the alkyl substitution. Computational methods capable of probing the structure of higher electronic states for these molecules may provide insight into the origin of the observed changes. CHD appears to be the outlier from these experiments, exhibiting no excited state absorption. This may result from the higher symmetry, the ultrashort excited state lifetime (<50 fs), or both.

A second variable that was examined was how the relaxation of the photoproducts depended on the solvent environment. While HT itself has been studied before with ultrafast[1-4] and computational methods[5], the data presented on the α-PH and α-TP photoproducts as well as the UV measurement of Pre are new. All of the molecules behave slightly differently in a range of alcohols and alkanes, with only minor changes between solvents. This is surprising given the size distribution and different conformations of the different photoproducts. In addition, the 1,3,5-hexatriene (HT) photoproduct has a very broad spectrum in the ground state, and we directly observe trapped cZt-HT isomers. This behavior has not been observed in any of the other compounds mentioned.

These experiments utilized a UV continuum that extended to ~270 nm, which allowed for observation of the depletion of the photoproduct as it relaxes. Future experiments that utilize deeper UV continuum will be necessary to observe the formation of the equilibrium distribution of photoproduct. This could be obtained using a 266 nm beam to generate the whitelight, or by

doubling a broadband non-collinear optical parametric amplifier (NOPA). The deeper UV spectrum will also be very important for understanding the conformational equilibrium of Previtamin D_3 (Pre) in solution as discussed in Chapter 5.

Looking ahead, these basic studies can inform the design of molecules for specific functions such as diarylethenes[6-8] and fulgides[9-11]. Both of these motifs utilize the reversible CHD ring-opening reaction, and are thought to be of potential use for memory devices and switches for molecular circuits. An understanding of both the design of the molecule as well as how it responds to changes in its environment will be important for the advancement of the field. Many researchers are interested in the photochemistry of these more complicated and useful systems, so a push towards synthesis of some of these compounds is an area of potential future research.

The isotropic small molecule alkane and alcohol solvents are poor models for the confined anisotropic environment of a cell membrane. Towards addressing this issue, my final project involved synthesizing liposomes incorporated with DHC as a model of the cell membrane where DHC exists *in vivo*. Here, we found the result that the excited state dynamics of DHC are significantly slowed in the bilayer of the vesicles. These experiments have exciting future directions that will be important for understanding the photosynthetic formation of Vitamin D_3 in many organisms.

Various properties of the lipid membrane remain to be tested for potential impact on DHC photochemistry. Chain length of the lipids in the membrane can modify how DHC and Pre pack and interact with the headgroups of the liposome. This has been shown by X. Q. Tian et al. by examining the rate of Vitamin D_3 formation from Pre.[12] The faster rates in longer chain lipids may indicate a further shift towards populating the gZg conformation of Pre. Understanding the

interactions that impact DHC and Pre will require careful testing of bilayer parameters. TA experiments in liposomes formed from lipids with varying chain lengths will affect how the head groups interact with the DHC molecules. The packing around the steroid skeleton will also change between lipids. The degree of saturation in the lipids is another factor that greatly affects the ability of the membrane to pack in cells. Doping the liposomes with unsaturated sphingolipids will change the packing around DHC while keeping the headgroups relatively unperturbed. Between the effects of different chain lengths, saturation, temperature, and even different self-assembled structures such as planar bicelles, there are many untapped areas of research that can expand the horizons of this project.

The experiments on DHC in liposomes presented in chapter 5 lay the foundation for many more avenues of research. While ultrafast measurements and careful selection of variables to change can provide observational results about these bilayer systems, they provide no complementary structural information. It is crucial in moving the project forward that collaboration with groups capable of molecular dynamics (MD) experiments on these systems be sought out. A number of questions that remain are best answered by computational simulations.

The equilibrium between the gZg-Pre ⇌ tZg-Pre conformations in bulk solution vs liposome is a critical factor for understanding how our ultrafast results relate to biological systems. An equilibrium MD experiment monitoring the bond dihedrals that define the different conformations in a generic solvent such as hexane or methanol compared with a similar simulation in a bilayer could determine the magnitude of change in equilibrium constant between these two environments. In addition to a quantitative measure of the change in equilibrium constant, the mechanism of this change is important in guiding future experiments. Tools developed for the purpose of investigating chemical dynamics in bilayers are available in the

CHARMM simulation package.[13-17] Experiments that probe this dynamic equilibrium are difficult because the rate of forward and reverse reaction is rapid, and obtaining pure standards of each isomer has thus far been impossible.

The field of photochemistry will continue to advance as new spectroscopic tools are developed. The technology continues to improve on the front of hardware and software, and new capabilities will allow for the treatment of ever more challenging problems. Combined with new computational tools, there is a great wealth of information that remains to be uncovered. The experiments presented in this thesis represent the establishment of a strong foundation for future experiments conducted in models for biological systems. The development of an experimental protocol to study DHC in a liposomal model for the cell membrane is a significant step towards understanding how variables in a biological setting can project onto the photochemical synthesis of previtamin D_3. The experimental groundwork presented here opens up a large number of experiments and simulations that will shed light on this question.

References

(1) Harris, D. A.; Orozco, M. B.; Sension, R. J. *J*. *Phys*.*Chem*. *A* **2006**, *110*, 9325-9333.

(2) Pullen, S. H.; Anderson, N. A.; Walker, L. A.; Sension, R. J. *J*. *Chem*. *Phys*. **1997**, *107*, 4985-4993.

(3) Anderson, N. A.; Shiang, J. J.; Sension, R. J. *J*. *Phys*.*Chem*. *A* **1999**, *103*, 10730-10736.

(4) Anderson, N. A.; Durfee, C. G.; Murnane, M. M.; Kapteyn, H. C.; Sension, R. J. *Chem*. *Phys*. *Lett*. **2000**, *323*, 365-371.

(5) Vazquez, F. X.; Talapatra, S.; Sension, R. J.; Geva, E. *J*. *Phys*.*Chem*. *B* **2014**, *118*, 7869-7877.

(6) Irie, M.; Kobatake, S.; Horichi, M. *Science* **2001**, *291*, 1769-1772.

(7) Kobatake, S.; Takami, S.; Muto, H.; Ishikawa, T.; Irie, M. *Nature* **2007**, *446*, 778-781.

(8) Ward, C. L.; Elles, C. G. *J*. *Phys*. *Chem*. *Lett*. **2012**, *3*, 2995-3000.

(9) Nenov, A.; de Vivie-Riedle, R. *J*. *Chem*. *Phys*. **2011**, *135*.

(10) Siewertsen, R.; Strube, F.; Mattay, J.; Renth, F.; Temps, F. *Phys*. *Chem*. *Chem*. *Phys*. **2011**, *13*, 3800-3808.

(11) Renth, F.; Siewertsen, R.; Temps, F. *International Reviews in Physical Chemistry* **2013**, *32*, 1-38.

(12) Tian, X. Q.; Holick, M. F. *Journal of Biological Chemistry* **1999**, *274*, 4174-4179.

(13) Jorgensen, W. L.; Chandrasekhar, J.; Madura, J. D.; Impey, R. W.; Klein, M. L. *J*. *Chem*. *Phys*. **1983**, *79*, 926-935.

(14) Jo, S.; Kim, T.; Im, W. *Plos One* **2007**, *2*.

(15) Brooks, B. R.; Brooks, C. L., III; Mackerell, A. D., Jr.; Nilsson, L.; Petrella, R. J.; Roux, B.; Won, Y.; Archontis, G.; Bartels, C.; Boresch, S.; Caflisch, A.; Caves, L.; Cui, Q.; Dinner, A. R.; Feig, M.; Fischer, S.; Gao, J.; Hodoscek, M.; Im, W.; Kuczera, K.; Lazaridis, T.; Ma, J.; Ovchinnikov, V.; Paci, E.; Pastor, R. W.; Post, C. B.; Pu, J. Z.; Schaefer, M.; Tidor, B.; Venable, R. M.; Woodcock, H. L.; Wu, X.; Yang, W.; York, D. M.; Karplus, M. *Journal of Computational Chemistry* **2009**, *30*, 1545-1614.

(16) Klauda, J. B.; Venable, R. M.; Freites, J. A.; O'Connor, J. W.; Tobias, D. J.; Mondragon-Ramirez, C.; Vorobyov, I.; MacKerell, A. D., Jr.; Pastor, R. W. *J. Phys.Chem. B* **2010**, *114*, 7830-7843.

(17) Klauda, J. B.; Venable, R. M.; Pastor, R. W. *Biophysical Journal* **2010**, *98*, 282A-282A.